Growth, Motility and Metabolism of Harmful Cyanobacteria and Lipid-Producing Microalgae in Fluid Environments: From Laboratory to Field Study

A THESIS

SUBMITTED TO THE FACULTY OF THE GRADUATE SCHOOL

OF THE UNIVERSITY OF MINNESOTA

BY

Jiaqi You

IN PARTIAL FULFILLMENT OF THE REQUIREMENTS

FOR THE DEGREE OF

DOCTOR OF PHILOSOPHY

Professor Miki Hondzo, *advisor*

August 2020

Acknowledgements

The work presented in this dissertation involves input and efforts from many scientists, engineers, agencies and fellows. This dissertation could not have been completed without any of these supports. First of all, I would like to thank my advisor Prof. Miki Hondzo, who has guided me to achieve each milestone in the journey of my PhD study. I am so grateful to him for not only being an academic advisor passing knowledge and research experience to me, but being a mentor encouraging me and leading me all the time in my personal and professional development as well.

I am grateful to Prof. Jiarong Hong and Dr. Kevin Mallery for the long-term collaboration and the participation in many studies present in this dissertation. Their strong support of holographic technology aids our exploration of microorganisms in such a new way. I am also grateful to Prof. Douglas Mashek and Dr. Mark Sanders for their contributions to the lipid-producing algae studies. The research goals would not have been achieved smoothly without the efforts of these professional researchers.

St. Anthony Falls Laboratory is a wonderful and magic place. I am grateful to everyone in the SAFL family. I would like to thank Dr. Chris Ellis for the development of the "David Buoy" research station, which is an excellent helper for our field studies. I would also like to thank Ben Erikson who is always ready to help in any situations I met and thank all the technical team members who have provided so many more possibilities for the research work. Special thank you to Dr. Anne Wilkinson, who helped me from my first day in the Ecolab. I was lucky to have you by my side as a friend and a labmate in

the first few years of my PhD life and my exploration of algae world. I am also grateful to Jacqueline Taylor and Abbigail Tomasek for the friendship and the help with the lab and field works. I would also like to express my appreciation to all the SAFL faculties and fellow labmates, for all the support and inspirations in my journey.

I am also grateful to the faculty, staff and students from the Department of Civil, Environmental and Geo- Engineering who have taught me, helped me and supported me in my PhD study. Special thanks to Kathy Wabner, for the help and encouragement in my teaching work and for the friendship.

I would like to acknowledge the assistance of Guillermo Marques and John Oja at the University of Minnesota – University Imaging Centers in the cell imaging. I would like to thank Dr. Wenqi Cui and Dr. Enxiang Zhang for the technical support in neutral lipid determination, Dr. Dan Troolin for technical support in micro-PTV measurements, Jaewoo Jeong for part of the holography image processing, and Dr. Christine Salomon, Dr. Yudi Rusman and Dr. Xun Song for the assistance in ELISA analyses. I am also grateful for the support from Dr. Shahram Missaghi, City of Minneapolis, Mr. Scott Dumphy, the Ramsey Lake Association, and the Minnesota Pollution Control Agency in the deployment of research station and the public outreach.

Funding was partially provided by the Legislative-Citizen Commission on Minnesota Resources (LCCMR), Environment and Natural Resources Trust Fund 2015-2016 [Assessing the Increasing Harmful Algal Blooms in Minnesota Lakes, ID:038-B]. I am also grateful for the support from the National Science Foundation National Robotics Initiative award [NSF-IIS-1427014].

Dedication

This dissertation is dedicated with love and appreciation:

To my dad and mom, who have given me the deepest love and strongest support ever in my life. Your protection, education and love made me grow into a person with health, thoughts and hope. Thank you for inspiring me to pursue my life and career independently. I would not have the chance to explore the world as I had in the past ten year without your support. I know you are always there standing behind me and I am proud to complete the journey having you watching over me, even if overseas.

To my other family members, who have taken care of me and provided strong support in my life. Thank you to the family for supporting my overseas study plan when many other people did not understand this decision. I hope you will be proud of the better me.

To my friends, a primary source of my energy and inspiration. To Xiaocui, the most important friend I met during my PhD journey. The cheerful time we shared and the inspiring conversations about our research or even about the world will always be stored in my memory. To Lijun, Yinfei, Xiaohei and everyone in the ILDC family, the outstanding individuals sharing the love of dance and becoming my reliable friends and family. To Hanlin, Fangfang, Yueyue and all the friends who have been standing by my side during the journey. To the SAFL family, who provide the solid support and warmest welcome when I entered the door of scientific research.

To all the girls/women who are pursuing your professional career and independent life, believe yourselves! You can make it! Please don’t let anything block your steps towards your destination, but also remember to enjoy every scene in the journey.

Abstract

Microorganisms have been playing important roles in aquatic environments, including the beneficial roles in ecosystem functioning and metabolites production as potential nutrient and energy sources, and the harmful roles in water quality such as harmful algal blooms (HABs). Cyanobacteria blooms have been a worldwide threat to the ecological integrity and environmental health of the freshwater bodies due to the progressive anthropogenic activities and climate change. The complex and combined interactions of environmental variables on the growth, buoyancy and metabolism (e.g., toxin production) make the prediction and management of cyanobacteria blooms and their toxicity difficult. On the other hand, microalgae have been shown as a potential bioresource for food, biofuel, and pharmaceutical products. During the growth phases with corresponding environmental conditions, microalgae accumulate different amounts of various metabolites. The neutral lipid content accumulated in the lipid-producing microalgae cells, which can be transferred to biodiesel, varies with growth conditions. This dissertation improves the understanding of growth, motility (swimming or buoyancy regulations) and metabolism of cyanobacteria and lipid-producing algae in fluids with influences of various environmental variables, in order to maximize the efficieney of microalgal biofuel production and to minimize the harmful effects of cyanobacteria HABs.

In the laboratory study of cyanobacteria, batch cultures of *Microcystis aeruginosa* (*M. aeruginosa*) were cultivated at seven different temperatures to measure the specific growth rate at each temperature. A relationship between temperature and specific growth rate was established. We propose a cardinal temperature model for *M. aeruginosa* with the

inflection point (optimal temperature) located at 27.5˚C. The model describes 98% of the variability of experimental data from 5˚C to 35˚C. A digital inline holographic microscope was employed to visualize and analyze the buoyancy of the *M. aeruginosa* colonies at two different temperatures. The results demonstrated a five times difference in buoyant velocities of *M. aeruginosa* colonies at 17.5˚C and 28˚C. A model was derived to calculate the density of a colony using the buoyant velocity and colony size. The findings provide a better understanding of temperature effects on the growth and buoyancy of *M. aeruginosa*. The results could facilitate the prediction of cyanobacteria blooms and the development of water quality models for freshwater ecosystems.

In the laboratory study of lipid-producing microalgae, the neutral lipid accumulation was quantified and the swimming signatures (speed and trajectories) were analyzed for the motile green alga, *Dunaliella primolecta*, during the lag-exponential-stationary growth cycle at different nutrient concentrations. We discovered significant changes in the neutral lipid content and swimming signatures of microalgae across growth phases. The timing of the maximum swimming speed coincided with the maximum lipid content and both maxima occurred under nutrient stress at the stationary growth phase. Furthermore, the swimming trajectories suggested statistically significant changes in swimming modes at the stationary growth phase when the maximum intracellular neutral lipid content was observed. The results provide the potential exploitation of microalgal swimming signatures as possible indicators of the cultivation conditions and the timing of microalgal harvest to maximize the lipid yield for biofuel production. The findings can also be implemented to explore the production of food and antibiotics from other microalgal metabolites with low energy costs.

In the field study of cyanobacteria blooms, we investigated the concentrations of cyanobacteria and microcystins in a small stratified lake and examined the influence of the abiotic environmental factors on the vertical and temporal heterogeneities. The results demonstrated the similarities in the vertical heterogeneities of cyanobacteria biovolume and total microcystin concentration. Similar patterns were discovered in vertical variations of macronutrient ratio of nitrogen over phosphorus (N:P) and biovolume ratio of non-N-fixing over N-fixing cyanobacteria. Moreover, temporal lags were revealed between the maxima of cyanobacteria biovolume, total microcystin level and *Microcystis* colony size. The stability of water column significantly affected the maximum *Microcystis* colony size, the surface cyanobacteria biovolume and the surface microcystin concentration. Correlations were established between the temporal heterogeneities of cyanobacteria community composition and the macronutrient dynamics. The findings and their implications on the environmental health will facilitate the development of prediction models and management strategies in the effort to control the impacts of cyanobacteria and cyanotoxins in small to medium size stratified lakes.

Table of Contents

List of Tables

List of Figures

List of Abbreviations

A	Area
ANOVA	Analysis of variance
BV	Biovolume
C_D	Drag coefficient
CTMI	Cardinal temperature model with inflection
D	Colony diameter
D_{NO3}	Molecular diffusion coefficient
D. primolecta	*Dunaliella primolecta*
DIHM	Digital inline holographic microscope
DIH-PTV velocimetry	Digital inline holographic particle tracking
EPA	Environmental protection agency
g	Gravitational acceleration
GV	Gas vesicle
HAB	Harmful algal bloom
k	Specific growth rate
L_C	Average cell diameter
LN	Lake number
MC	Microcystin
MC-LR	Microcystin-leucine arginine
Micro-PTV	Micro-particle tracking velocimetry
MPCA	Minnesota Pollution Control Agency
M. aeruginosa	*Microcystis aeruginosa*
N	Nitrogen
N_C	Cell concentration
NER	Net energy ratio
P	Phosphorus

PAR	Photosynthetically active radiation
PCA	Principal component analysis
PDF	Probability density function
Pe	Peclet number
Re	Reynolds number
St	Schmidt stability
T	Temperature
t	time
TAG	Triacylglycerol
U	Velocity in x-direction
u_*	Shear velocity
V	Velocity in y-direction
V	Volume
v	Average swimming speed of cell
WHO	World Health Organization
W	Vertical velocity (z-direction)
W_b	Buoyant velocity
ρ_{col}	Colony density
ρ_w	Water density
υ	Kinematic viscosity

Chapter 1

Introduction

Cyanobacteria and Harmful Algal Blooms

Harmful algal blooms (HABs) are of significant concerns worldwide due to its damage to the water quality and ecological community, including deoxygenation of water columns, mass mortalities of fish, unpleasant odors and taste, toxins production and release threatening health of humans and animals, and alterations of food web [1, 2, 3]. Although there are many species of bloom-forming phytoplankton, cyanobacteria (aka. blue-green algae) is the most well-known phylum of HAB former, since they dominate considerable HABs during summers. Because of the nutrient dependence, and high temperature and calm water preference of cyanobacterial growth, the increased eutrophication of water bodies resulting from anthropogenic activities and the global climate change are two

major reasons for the proliferation and expansion of cyanobacterial HABs [4, 5]. HABs are costly – it is estimated that the average economic effects of HABs in the U.S., including loss and expense on public health, fisheries, recreation, monitoring and management, is $82 million/year, based on data from 1987 to 2000 [6].

Cyanobacteria are an ancient but diverse group of microalgae which are the only phylum of algae that possess prokaryotic cell structures. They exist in a variety of morphologies, including unicellular coccoid, colonial or filamentous forms. The size of unicellular cyanobacteria normally ranges from smaller than 1 μm to larger than 20 μm, while many colonies or filaments are visible by naked eyes. Some planktonic species of cyanobacteria can form massive surface blooms and produce toxins [7]. The most common bloom-forming cyanobacteria genera include *Microcystis*, *Dolichospermum* (formerly named *Anabaena*), *Aphanizomenon*, and *Planktothrix*. The planktonic species of the common bloom-forming cyanobacteria possess eco-physiological features that contribute to their dominance in eutrophic, warm and calm water conditions.

One common feature is the formation of colonies or filaments as an anti-grazing strategy [8]. For example, *Microcystis* form colonies to protect themselves from flagellate grazing. Some strains produce toxins (will introduced in the next section) as a defense strategy. However, sometimes toxins have no effects on their grazers, so colony and filament formations are an effective defense mechanism for cyanobacteria [9].

Another common feature is the intracellular inclusion of gas vesicles, the dark brownish, irregular hollow proteinaceous structures clustered in cells, which enables the buoyancy of these cyanobacteria [7]. Cyanobacteria containing gas vesicles can adjust their cell

density and the corresponding buoyancy and thereby controlling their vertical positions in the water column [10]. The calm water environment is in favor of cyanobacterial blooming because buoyant cyanobacteria can regulate their density easily in calm water, float to the water surface, obtain substantial light and oxygen, and outcompete other organisms [11, 12, 13]. There are three mechanisms of buoyancy regulation: 1) rate of gas vesicle synthesis compared to the rate of cell growth and division, 2) turgor collapse of gas vesicles under pressure, and 3) the relative content of intracellular dense carbohydrates ("ballast") [14, 15]. Buoyancy regulation can also assist the cyanobacteria cells to obtain the phosphorus in the deeper part of lakes [16].

It is difficult to observe and reproduce the features mentioned above in *Microcystis* lab cultures, since gas vesicle deficiency mutations [17], and size change and disintegration of colonies [18] occur after long-term lab cultivation. The long-term lab cultured *Microcystis* normally exist as unicellular coccoid forms and lack the gas vesicles synthesis ability and buoyancy regulation ability.

Some species of cyanobacteria (e.g., *Dolichospermum*) have heterocytes that can synthesize the enzyme nitrogenase which enables the fixation of gaseous nitrogen (N_2) from the atmosphere [7]. The growth of the nitrogen-fixing cyanobacteria is sensitive to phosphorus levels in the water, and therefore the composition of phytoplankton in a water body shifts to cyanobacteria dominance when it is enriched with phosphorus [19]. However, many bloom-forming cyanobacteria are not nitrogen fixers. For instance, *Microcystis* is not capable of fixing nitrogen, but it is a genus of cyanobacteria which dominates many cyanobacteria HABs during late summers all over the world, and it is

the primary producer of the hepatotoxin, microcystin [3, 20]. The blooming of *Microcystis* is also limited by the nitrogen level in the water. More research has been considering both N and P as co-limiting nutrients that control cyanobacterial HABs [5, 21]. There are some other features of surface bloom-forming cyanobacteria, such as toxin production and the ability to grow and develop well at high temperatures [22], will be introduced in the following sections. Another distinct physiological feature of cyanobacteria is the blue-green pigment production. In addition to chlorophyll-a, cyanobacterial cells contain phycobilin-protein complexes that produce exclusive pigments, e.g., phycocyanin [7]. This enables the remote monitoring of cyanobacteria biomass by detection of phycocyanin levels.

Many cyanobacteria produce hepatotoxins (e.g., microcystins and nodularins) or neurotoxins (e.g., anatoxins and saxitonxins). Among all the cyanotoxins, microcystins (MCs) produced by *Microcystis* is the most common. The production of MCs by *Microcystis aeruginosa* has been reported worldwide [23]. The cyanobacterial toxicity leading to animal deaths and human health risks has been documented since the 1800s in Minnesota. Based on the study of Minnesota Pollution Control Agency (MPCA) in 2006, the likelihood of detecting microcystin in pelagic and near-shore regions of eutrophic lakes in Minnesota is very high [24]. The prediction of toxic cyanobacterial blooms is difficult because the timing of a biomass bloom does not always coincide with the maximum toxin concentration in the water bodies [25]. The increase of cell abundance during bloom can trigger the up-regulation of microcystin biosynthesis [26].

Lipid-Producing Microalgae for Biofuel

Despite the negative role that harmful cyanobacteria play in the water quality deterioration, aquatic microorganisms such as microalgae can play beneficial roles in solving present energy challenges. As the available fossil fuels have become limited and carbon dioxide generated by burning fossil fuels has accumulated, the renewable and carbon-neutral energy sources become necessary. Biodiesel is one of the good alternatives to petroleum. Microalgae grow fast and many of them possess the ability to synthesize and accumulate neutral lipids in intracellular lipid droplets, which are approximately 20-50% of cell dry weight [27, 28]. The use of microalgae as a potential feedstock in renewable biofuel production has received increasing attention duet to their high lipid production exceeding the best-producing oil crops [27]. Research efforts have been devoted to overcoming challenges in commercialization of algal biofuel. Understanding the algal intracellular lipid accumulation in response to environmental conditions is essential to maximize algal biofuel production. It has been reported that the nutrient depletion/limitation can induce lipid accumulation in green algae cells [29, 30, 31] and can potentially affect the swimming velocities of the microalgal cells [32].

Microalgae capture solar energy and store a large amount of it as lipids that comprise primarily of triacylglycerols (TAG), which can be trans-esterified into biodiesel [30]. Many green algae species are chosen as candidate TAG producers in studies and industries, since their ability to accumulate large amounts of TAG under stress conditions, such as nutrient deprivation, salinity, light and turbulence [33, 34]. *Dunaliella* is a genus of green algae well-known for its halotolerance, which enables

them to live in brackish water or saltwater. The total lipid content in *Dunaliella* ranges from 15% - 40% [35]. Most of the TAG are accumulated in *Dunaliella* in the form of cytoplasmic lipid droplets, which comprises neutral lipid core surround by a phospholipid monolayer embedded with proteins [34, 36].

Potential Environmental Impacts on Growth, Motility and Metabolism

Macronutrient (e.g., N and P) availability is one of the most common environmental affectors on the growth of aquatic microorganisms, in both freshwater and marine environments [37, 38, 39, 40, 41]. Eutrophication led by excessive P has been realized earlier and better controlled, while global increasing N loadings due to expansion of agriculture, urban and industries and the associated impacts have gradually become focuses of environmental studies. Both N and P have great influence on the HABs occurrence, and the role of each individual nutrient has been investigated and debated in previous studies [41, 42]. Davis *et al*. [25] reported the enhanced growth rate of toxic *Microcystis* with elevated P levels. Mass addition of N to the site that is saturated with P can lead to replacement of N-fixing cyanobacteria by non-N-fixers such as *Microcystis* spp. [39]. Addition of both N and P has been rep1rted as a greater stimulation of primary production than a single nutrient in the water environment experiencing blooms of N-fixing or non-N-fixing cyanobacteria [40, 42]. Xu *et al*. [43] reported significantly

elevated Chl-a level and increased growth rate of cyanobacteria in response to the combined addition of N and P in Lake Taihu.

The ability of fast growth at higher temperatures also contributes to the prevailing cyanobacterial HABs during summers. The bloom-forming cyanobacteria usually achieve their optimal growth at temperatures higher than 25˚C, the temperature at which the growth rate of eukaryotic phytoplankton in the water generally stabilize or decrease [5, 44]. Thus, these cyanobacteria species can outcompete other phytoplankton and proliferate biomass in late summers. Many studies have reported large cyanobacterial HABs occurring during abnormally hot summers. Lake Erie experienced a record-breaking cyanobacterial HAB in 2011, which was caused by the increase of phosphorus nonpoint source coupled with the abnormally warm late spring and hot summer [45]. In 2000 summer, there was an extremely dense bloom of *Microcystis* in the Swan River, Australia when the water temperature is higher than average [46, 47,48]. Jöhnk *et al*. [3] presented the proliferation of *Microcystis* abundance in Lake Niewe Meer, Netherland in response to the extreme summer heatwave combined with reduced wind speed and reduced cloudiness in 2003.

The global climate change tends to favor the dominance of cyanobacteria not only due to the fast growth of cyanobacteria at elevated temperatures, but also because of the buoyancy regulation of cyanobacteria in warmer waters with increased stability. Increased temperature and reduced wind conditions can benefit the cyanobacterial HABs forming by reducing vertical mixing and intensifying and prolonging the thermal stratification, which provide the buoyant cyanobacteria with more stable environment

[19, 49]. The genera of cyanobacteria possessing gas vesicles can adapt themselves well to the water environment with stronger stratification by buoyancy regulation to migrate vertically in the water column [22, 50]. Nutrient availability may also affect the buoyancy regulation of cyanobacteria. Previous studies have reported higher rate of gas vesicle production relative to growth rate in the N-replete environment compared to the N-limited environment, and greater number of gas vesicles in P-replete cells compared to the P-limited cells [51, 52].

The motility of lipid-producing green algae is also subject to the nutrient availability. Hansen *et al*. [32] discovered the swimming speed variation of green algae *Chlamydomonas reinhardtii* cells under different nutrient conditions. In the growth cycle, the *Chlamydomonas* cells increase swimming speed when nitrogen is depleted; and then when nitrogen starvation continues, the cells greatly slow down their swimming speed. In short-term experiments, they demonstrated the increase of swimming speed of cells exposed to ~ 1 hr nitrogen removal. No significant changes in swimming speed of *Chlamydomonas* cells were reported in response to altered P levels in their study. In addition to nutrient availability, fluid flow conditions also affect the motility of lipid-producing green algae. Previous studies demonstrated differences in swimming behaviors of *Duanliella* cells in the shear flow compared to in the quiescent flow, as well as the changes of swimming velocities in the flows with different Reynolds number [53, 54].

In addition to the growth and motility, the metabolism of aquatic microorganisms is also influenced by the environmental factors. Lipid content in the microalgal cells is affected by the nutrient availability in the growth environment, and nutrient limitation is one of

the important environmental stressors [30]. Among all the nutrient stressors, nitrogen limitation is the most critical one influencing the lipid accumulation [33]. Increase in lipid accumulation in response to the nutrient/nitrogen limitation has been reported for many microalgal species, particularly *Dunaliella* species. The increased lipid content under stress conditions are primarily neutral lipids, mainly TAGs, for the TAG synthesis and deposition of TAG into cytosolic lipid bodies play active roles in stress response [33]. *Dunaliella salina* has been reported to accumulate more lipid under nutrient starvation [55], and its highest lipid content could be achieved by nitrogen and complete nutrient deprivation [31]. The enhancement of lipid accumulation under nutrient limitation can be related to the growth phase and physiological status. The lipid content varies during the growth cycle and often achieve the maximum during stationary phases [33]. For instance, the intracellular lipids content of *Dunaliella tertiolecta* reaches the highest value at the stationary phase in both the normal medium culture and the N-deficient medium culture [30]. It is also reported in this study that intracellular neutral lipid bodies, which were not present in exponential growing cells, were observed by the third day of nitrogen deprivation. However, there are also studies reporting higher intracellular lipid content of *Dunaliella primolecta* and *Dunaliella salina* in nutrient replete conditions than in N-deficient conditions [56]. The inconsistent response to nutrient/nitrogen availability may be due to the experimental design and the difference between nutrient deficiency and nutrient limitation. Algae in nutrient limitation conditions generally adapted to an environment with an insufficient supply of the limiting nutrient, while in nutrient deficiency conditions they need to use endogenous reserves because the exogenous supply is exhausted, and the growth will stop if the nutrient

deficiency is prolonged [57]. The shift from an increase in lipid content in N limited condition and to decrease of lipid content in N deficient condition of *Dunaliella primolecta* cells in the study of Thomas *et al*. [58] may be explained by the difference between N limitation and N deficiency.

The cyclic heptapeptide toxins, microcystins (MCs), are the secondary metabolites of some cyanobacteria, such as *Microcystis* and *Dolichospermum*. The relationship between environmental factors and MC production have been investigated in many studies, but the results are not very consistent, and the relationship remains unclear in certain level due to the complex interactions and combinations of the triggers. Nutrient level including N and P is one of the investigated triggers for MC production. Batch culture experiments in Sivonen [23] suggested the correlation between high nutrient levels and high MC production, but Vezie *et al*. [59] showed that the correlation varies under different interactive levels of nitrogen and phosphorus. The enhancement of MC production by high nitrogen and phosphorus may be due to the impact of nutrients on the specific growth rate of cells, or on the control of MC biosynthesis [60]. It has been suggested that fast- growing Microcystis aeruginosa cells under nitrogen-limited conditions tend to be smaller and to produce more intracellular toxins [61]. MC producing strains of cyanobacteria possess a set of MC synthesis genes, *mcyA- mcyJ* [25]. Transcription of *mcy* genes in *Microcystis aeruginosa* occur via a central promoter between *mcyA* and *mcyD*, and the global nitrogen regulator (NtcA) binding sites were observed in the promoter region, which implies the role of nitrogen in microcystin biosynthesis control [62, 63]. In contrast, the investigation by Sevilla *et al*. [64] suggested that there is no direct correlation between excessive nitrate level and the *mcy* transcription and MC

production. Graham *et al*. [65] reported the increasing trend of MC presence and concentration along the gradient of trophic status in the investigated lakes in the midwestern United States. Iron starvation has also been suggested as a trigger of MC production. Lukac and Aegerter [66] has reported the increased toxin production correlated to low iron concentration. The iron starvation was found to increase *mcy* transcripts and MC levels [67]. High light intensity has also been suggested to increase the *mcy* gene transcription and toxin production rates, but it was the MC isoforms instead MC that changed in response to the light intensity change [68].

Temperature is also suggested as an environmental trigger for MC production. The elevated temperature was reported as a stressor that increases the expression of the *mcyB* gene [70]. The study of Davis *et al*. [25] showed the increased growth rates of the toxic *Microcystis* strains at the elevated temperature and indicated that warmer temperatures favor the growth of toxic strains more than non-toxic strains. It was also suggested that the temperature elevation combined with P enrichment greatly increase the growth rate of toxic strains. MC concentration in lakes varies with locations and is associated with temperature, wind and cyanobacterial biomass. The study of MPCA in 2006 found that 94% of near-shore water samples contained detectable MC concentrations. MC levels at the sites with a distinct surface cyanobacterial scum are more likely to fall in the moderate to the very high-risk group defined by WHO [24].

Moreover, lysis of Microcystis cells can sensed by the rest cells and induce the *mcyB* gene accumulation and thereby enhancing the MC production [70]. This is potentially a reason for the different timing of cyanobacterial biomass peaks and MC peaks occurring

in lakes. Cellular MC content is strain dependent and the maximum production within each strain also vary with environmental conditions, which increases the difficulty in studies of MC production and environmental triggers.

Research Objectives and Significance

Despite the previous research achievements on the effects of environmental factors on the growth, motility and metabolism of aquatic microorganisms, there are still large gaps to be filled in the research of cyanobacteria and lipid-producing microalgae in different environmental conditions. For instance, limited previous studies reported growth rates of primary bloom-forming cyanobacteria (e.g., *Microcystis*) at consecutive temperatures to investigate the temperature effects on their growth over a full span of their tolerable growth temperatures. Most current temperature-growth models are unable to predict the cyanobacteria growth rate with an inflection point at the optimal temperatures. Limited research has studied the buoyancy of cyanobacteria at different temperature settings in laboratory experiments. The motility and neutral lipid content of lipid-producing microalgae at various growth phases and their correlations with the nutrient availability has never been explored over an entire growth cycle of the microalgae. Swimming behaviors of these algae have not been visualized and classified into types of motions in previous studies. The optimal timing of algal harvesting for optimal biofuel yield and its relationship with algal cell motility has never been established. Moreover, field studies are essential for prediction and mitigation of cyanobacteria HABs. Most previous studies focused on large shallow lakes, such as Lake Taihu and Lake Erie, while limited studies

have been conducted on the relatively small and deep lakes distributed worldwide as important drinking and recreational waters. Systematic explorations of cyanobacteria biomass, cyanotoxin concentrations and the corresponding meteorological and water conditions in a lake throughout a bloom season are urged for, in order to minimize the detrimental impacts of HABs.

This dissertation aims to fill in some of the above-stated knowledge gaps and improve the understanding of growth, motility (swimming or buoyancy regulations) and metabolism of cyanobacteria and lipid-producing microalgae in different fluid environments, by a set of laboratory experiments and field studies. Chapter 2 presents the growth rate of *Microcystis aeruginosa* cultivated at seven different temperatures and the newly established temperature-growth model validated from 5˚C to 35˚C. It also demonstrated the vertical migration trajectories and the differences in buoyant velocities of *Microcystis aeruginosa* colonies at different temperatures. Chapter 3 discusses the differences in swimming signatures (speed and motions) and neutral lipid content of the green algae, *Dunaliella primolecta*, through a series of laboratory experiments. Correlations between motility and neutral lipid content discovered in the experiments and the potential application of microalgal signatures as indicators of growth conditions and harvest timings for the microalgal biodiesel production are also discussed in this chapter. Chapter 4 extends the discussion of environmental impacts on cyanobacteria to a field study in a small, eutrophic and stratified freshwater lake. This chapter discusses the vertical and temporal heterogeneities of cyanobacteria biovolume and MC concentration, and how the heterogeneities are affected by multiple abiotic environmental variables, including air and water temperature, wind speed, water column stability and nutrient

availability. Finally, Chapter 5 outlines the conclusions of this dissertation and recommendations for monitoring and prediction strategies developed from the results present here in the cyanobacteria HABs management and the microalgal biofuel production.

Chapter 2

Temperature Effects on the Growth and Buoyancy of *Microcystis aeruginosa*

Introduction

Microcystis is a cosmopolitan genus of toxic cyanobacteria often present in eutrophic lakes which frequently dominates HABs and toxin production within them [3, 20]. Their ability to competitively proliferate at high temperatures, compared to other species of algae, is one of the characteristics making cyanobacteria prevalent in summer blooms [22]. Previous studies reported selective promotion of cyanobacteria blooms at increased water temperatures due to climate change [3, 20, 71]. For instance, extremely dense blooms of *Microcystis* occurred in the Swan River estuary, Australia, in 2000, which had an above average water temperature [46, 47, 48]. Previous studies also suggested greater

growth rates of *Microcystis* at higher temperatures [3, 5, 72, 73,74], and reported the temperature optima for cyanobacterial growth [72, 75, 76, 77].

Microcystis strains containing gas vesicles can change their cell density and corresponding buoyancy to form blooms at different vertical locations in the water column [10]. Like other buoyant cyanobacteria, *Microcystis* prefers calm water columns, in which they can adjust their buoyancy and regulate their vertical position [11, 13, 78]. Increasing temperature reduces vertical mixing, intensifies and prolongs vertical stratification, and provides *Microcystis* with more stable environments [48, 49]. These conditions tend to favor *Microcystis* bloom formation [3, 13, 71].

The mechanisms of buoyancy regulation have been investigated and used in studies concerning the vertical distribution and oscillation of *Microcystis* colonies [14, 15, 79, 80, 81, 82, 83, 84, 85]. Most of these studies used simulations to obtain the depths of *Microcystis* colonies in the water column and their relationship with environmental variables such as light intensity and nutrient concentration. However, the temperature effects on buoyancy have been reported in a limited number of studies. Rabouille *et al*. [15] simulated the dynamic vertical distribution of *Microcystis* colonies at different temperatures, and Thomas and Walsby [86] tested the buoyancy recovery (the process by which non-buoyant colonies regain their buoyancy) under two different temperatures. In addition, despite the measurement in Nakmura *et al*. [80] and Rowe *et al*. [87] using microscopic videography, buoyant velocities of *Microcystis* colonies were not measured. This study, therefore, is motivated to visualize the movement of *Microcystis aeruginosa* (*M. aeruginosa*) using a digital inline holographic microscope which allows us to track 3-

dimensional (3D) motion of microorganisms without adjusting the camera focus [88], and examine the possible differences in their buoyant/settling velocities under different temperatures.

Most of the current models predicting the growth of *Microcystis* use the Arrhenius equation [47], which was originally developed to describe the effects of temperature on chemical reactions [89, 90]. However, the Arrhenius models are unable to predict the observed phenomenon in which temperatures higher than a threshold value can strongly reduce the algal growth [89]. Thus, additional research is needed to predict the growth rate of *Microcystis* over the whole temperature range that can occur in aquatic ecosystems. A cardinal temperature model with inflection (CTMI) was proposed [91, 92] to extend the prediction of microbial growth to those at temperatures higher than the optimal temperature. Bernard and Rémond [93] validated the CTMI model in predictions of growth of various microalgae including diatoms, green algae, dinoflagellates and filamentous cyanobacteria, which did not include colony forming genus *Microcystis*. This study aims to investigate the growth of *M. aeruginosa* in laboratory batch cultures at different temperatures and develop a CTMI model specific for *M. aeruginosa*. The model with the derived parameters is expected to aid predictions of the specific growth rate of *M. aeruginosa* at any temperature within the temperature range common to aquatic ecosystems.

Materials and Methods

Growth rate measurements at different temperatures

The *M. aeruginosa* strain (B3-R-7) was obtained from the Department of Fisheries and Allied Aquacultures, Auburn University, Alabama and isolated in 2010 [94]. This strain was subjected to laboratory cultivation in tanks at room temperature (which varied from 20-25˚C) and natural light (average photosynthetically active radiation (PAR) of 169 µmol/m^2s). The cultures were inoculated into fresh growth media periodically and examined under a microscope periodically to ensure no contamination. The inoculations and transfers were performed under a laminar flow hood and sterilized conditions. Before each experiment, samples taken from these cultures were diluted in 500 mL 1:50 diluted BG-11 50X media (Sigma *C3061*, Sigma-Aldrich, St Louis, MO, USA) with Milli-Q water (Millipore, Billerica, MA, USA) and allowed to grow on a sterilized bench with natural light (average PAR of 169 µmol/m^2s, average natural daylight durations of 12-15 hours) at room temperature (20-25˚C) for 4 days as a stock culture. The method for stock culture development and inoculation was similar to that used in Missaghi *et al*. [94] and Wilkinson *et al*. [95]. The volume of the stock culture to be inoculated into experimental culture flasks was calculated based on the cell counts on the fourth day to ensure the initial cell concentration of ~ 10^5 cells/mL. The stock culture was inoculated by a pipette into three 250 mL conical flasks, each containing 4.5 mL BG-11 (*C3061 SIGMA*, 50X liquid), and diluted to 225 mL experimental cultures with Milli-Q water. The triplicate cultures of *M. aeruginosa* were incubated in the incubator (*PERCIVAL SCIENTIFIC*) under PAR of 142 µmol/m^2s, shaken at 20 rpm and under 14/10 hour light/dark cycles.

The growth experiments were conducted under temperatures of 5˚C, 10˚C, 15˚C, 20˚C, 25˚C, 30˚C, and 35˚C.

The cells were counted daily in a 0.1 mm deep haemocytometer under an optical microscope (Nikon Eclipse E400) with a 40X objective and 10X ocular lenses. For each flask, four of 10 µL samples were counted and the cell concentrations recorded. The averaged value was designated as the final cell concentration if the four counts differed by <10%. Otherwise, additional counting was conducted. Each experiment was conducted for 10 days, except for the one at 5˚C (17 days) and 10˚C (17 days) because the cells enter exponential phase and stationary phase much slower than cells under higher temperatures, necessitating additional days to acquire measurements at these states.

Temperature-growth model

The model developed in this study is based on the model proposed by Bernard and Rémond [93], which predicts the specific growth rate (k) at different temperature as follows:

$$k = \begin{cases} 0 \text{ for } T \le T_{\min} \\ k(T) \text{ for } T_{\min} < T < T_{\max} \\ 0 \text{ for } T \ge T_{\max} \end{cases}$$

and

$$k(T) = k_{\text{opt}} \frac{(T - T_{\max})(T - T_{\min})^2}{(T_{\text{opt}} - T_{\min})\left[(T_{\text{opt}} - T_{\min})(T - T_{\text{opt}}) - (T_{\text{opt}} - T_{\max})(T_{\text{opt}} + T_{\min} - 2T)\right]} \quad (2.1)$$

where k_{opt} (1/day) is the specific growth rate at the optimal growth temperature, T_{opt} (°C). T_{max} (°C) and T_{min} (°C) represent the upper and lower temperature limits, respectively, between which cells can survive.

The specific growth rate at each temperature was calculated based on the cell concentration data during exponential growth, using the growth rate equation similar to Guillard [96]:

$$k(T) = \frac{\ln (N_C / N_{C0})}{t - t_0} \tag{2.2}$$

where N_C is the cell concentration (#cells/mL) at incubation time t (day), N_{C0} is the initial cell concentration at $t = t_0 = 0$, and T (˚C) is the temperature at which the cells were incubated. Eq. 2.2 was rearranged as

$$\ln N_C = \ln N_{C0} + k(T)t \tag{2.3}$$

where $k(T)$ was estimated by plotting the natural logarithm of cell concentration, ln N, versus incubation time, t, and fitting Eq. 2.3 to have the best fit to the series of observed data points.

The optimal values of the parameters (k_{opt}, T_{opt}, T_{max}, and T_{min}) were determined by minimizing the differences between the proposed model (Eq. 2.1) and the observed data of $k(T)$ using the non-linear curve fit analyzer in Origin 9.1 (OriginLab Corporation).

Holographic measurement

Holographic measurements were conducted at two different temperatures, 17.5±1.0˚C and 28.0±1.0˚C. The only experimental variable was the ambient temperature and all other environmental variables including cell culture, light, and nutrient conditions were held constant. For the holographic measurements, water samples were collected in July 2016 from Powderhorn lake, an urban lake in Minneapolis, Minnesota, United States (44˚56′29.6″N, 93˚15′29.4″W). For each experiment, a culture sample of *M. aeruginosa* was isolated manually from other organisms in the water and acclimated in an incubator at the experimental temperature for 24 hours prior to the experiment. The digital inline holographic microscope (DIHM) (see Figure 2.1) consists of a Thorlabs CPS532 laser (4.5 mW with 3.5 mm beam diameter), an Azzota 1 mm Pathlength Optical Glass Cuvette with 0.35 mL volume, an Edmund Optics 5X M plan objective with 34 mm working distance and 0.14 NA, and a Mitutoyo 1X MT-4 tube lens connected to a Flare 2M360-CL camera with maximum image size of 2048 x 1088 pixels, 5.5 µm pixel size, 13 µs shutter, and a frame rate up to 337 frames/s (fps) at full sensor size. The laser wavelength (532nm, green) was selected because the major pigments found in *Microcystis* have a low absorption at this wavelength, reducing the influence of the laser on the behavior of the sample [97, 98]. A T5 growth light system with two 24W bulbs (Milliard #MIL-GLS24W2, 36 µmol/m^2s) was placed over the sample cuvette to simulate the 14/10 hour light/dark cycle. The culture sample was gently shaken for 30 seconds before a 0.3 mL sample was transferred to the cuvette. Images were recorded by a 1TB Digital Video Recorder (DVR) Express Core (IO Industries Inc.) at the rate of 5 Hz continuously for 10 minutes every hour, with each experiment lasting for 28 hours. In

order to minimize the risk of temperature fluctuations over the course of the experiment, the room temperature in which the experiment was conducted was adjusted in advance to match the experiment temperature of 17.5˚C and 28.0˚C. Monitoring of the room temperature during the experiment indicated that the temperature fluctuation was limited to ±1.0˚C. Similar holographic systems have been utilized by Hong *et al*. [98] and Kumar *et al*. [99] to examine the behaviors of copepods and fruit flies, respectively.

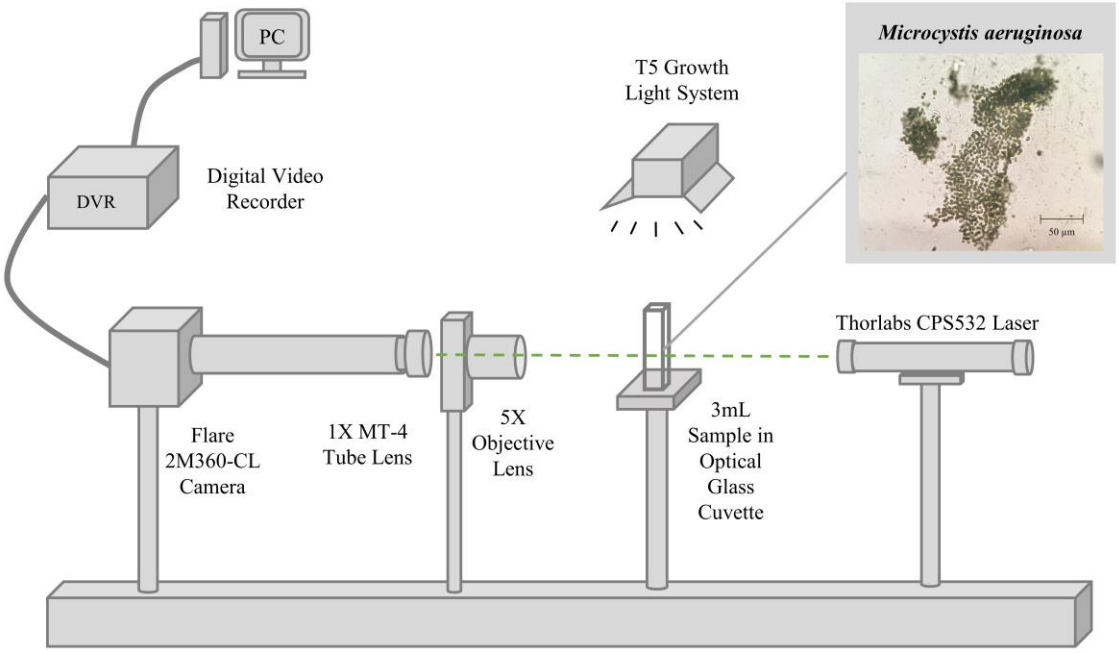

Figure 2.1. Digital inline holographic microscope set up.

The recorded holograms were enhanced by dividing by the time-averaged background of each recording and normalizing such that the image contained 99.7% of the intensity information. The enhanced holograms were digitally reconstructed by convolving them

with the Kirchoff-Fresnel diffraction kernel which is represented in the Fourier domain as follows [88]

$$H_z(m,n) = \exp\left(-j\pi\lambda z\left[\left(\frac{m}{MR}\right)^2 + \left(\frac{n}{NR}\right)^2\right]\right) \tag{2.4}$$

where λ is the laser wavelength (μm), z is the reconstruction distance (μm), R is the spatial resolution of the recording (μm/pixel), m and n are matrix indices, and M and N are the width and height of the recorded image, respectively. The remainder of the processing consisted of elementary image processing operations. For 2D segmentation of the colonies, the 3D reconstructed volume was projected onto a 2D (xy) plane using a minimum intensity projection. The projected images were binarized using a constant global threshold calculated by first finding a threshold using Otsu's method for each image in a random subset of 100 images. The global threshold was 60% of the mean Otsu threshold. After binarization, the images were filtered using the morphological opening and closing operations with circular structuring elements with radii of 2 pixels and 5 pixels respectively. These sizes were selected based on the observed sizes of the projected *M. aeruginosa* colonies. The area and centroid of each connected component (with 8-connectivity) were extracted. The binarization, morphological filtering, and connected component processing steps were all performed using MATLAB built in functions (Mathworks, Inc., R2014a). The colony tracking was performed using the method of Crocker and Grier [100] to build trajectories from the centroids and find the average velocity for each colony. To further remove noise particles, only trajectories lasting for 20 seconds (i.e. 100 frames) or longer were included in the analysis.

Buoyant velocity and velocity-density model

The temperature effects on the buoyancy of *M. aeruginosa* colonies were analyzed by comparing their moving trajectories and buoyant velocities at the two different temperatures. The differences in buoyancy of *M. aeruginosa* colonies were due to their density change. A model was developed to correlate the density of each colony with its the buoyant velocity in order to estimate the density change of *M. aeruginosa* colonies at different temperatures. This model was similar to that for the settling velocity of particles (i.e. Stokes drag) but with the positive velocity direction defined opposite to the direction of gravity.

Modelling an *M. aeruginosa* colony as a sphere, the equation of momentum for a colony in quiescent fluid includes the buoyant force, drag force, gravity, and an added mass term, which can be expressed as

$$\rho_{\mathrm{col}} V_{\mathrm{col}} \frac{\mathrm{d}W_{\mathrm{b}}}{\mathrm{d}t} = \rho_{\mathrm{col}} V_{\mathrm{col}} g - \rho_{\mathrm{w}} V_{\mathrm{col}} g + \frac{1}{2} \rho_{\mathrm{w}} C_{\mathrm{D}} A_{\mathrm{P}} W_{\mathrm{b}}^2 - \rho_{\mathrm{w}} C_{\mathrm{m}} V_{\mathrm{col}} \frac{\mathrm{d}W_{\mathrm{b}}}{\mathrm{d}t} \qquad (2.5)$$

where ρ_{col} is the colony density, ρ_w is the water density, V_{col} is the volume of colony, W_{b} is the buoyant velocity of the colony (upward vertical velocity), A_{P} is the projected area of colony, C_{D} is the drag coefficient, g is the gravitational acceleration, and C_{m} is the added mass coefficient. In a moving fluid, relative colony velocity is given by $W_{\mathrm{r}} = W_b - W_{\mathrm{f}}$ where W_{f} is the fluid downward velocity. Our DIHM set up was designed to minimize W_{f} in the cuvette which implies that $W_{\mathrm{r}} \approx W_b$. The inspection of W_{b} over time revealed minimal change, therefore, $\frac{\mathrm{d}W_{\mathrm{b}}}{\mathrm{d}t} \approx 0$. Thus, Eq. 2.5 simplifies as

$$(\rho_w - \rho_{col})V_{col}\,g = \frac{1}{2}\rho_w C_D A_p W_b^2 \quad (2.6)$$

The drag coefficient depends on the particle Reynolds number ($Re_p = \frac{W_b D}{\nu}$, where D is the diameter of the *M. aeruginosa* colony and ν is the kinematic viscosity of water) and is further discussed in the results section.

Statistical Analyses

A one-way ANOVA was conducted to determine the significance of differences in specific growth rates at different temperatures (df = 6, α = 0.05). A pair-sample t-test was conducted to determine the significance of differences between buoyant velocities at 28˚C and those at 17.5˚C (df = 27, α = 0.05). The ANOVA and t-test were carried out with Origin 9.1 (OriginLab Corporation).

Results

Temperature effects on growth

Growth at different temperatures

Cell concentration of *M. aeruginosa* in each sample at each temperature was recorded daily (Figure 2.2). Based on the cell concentration data, the specific growth rate of cells at each temperature was estimated. Only the data points of pre-stationary phases were used to calculate the specific growth rates. Before reaching the stationary phase, the cell concentration of *M. aeruginosa* followed the exponential growth pattern. Figure 2.3

shows the natural logarithm of the pre-stationary data of mean cell concentration at each temperature. The specific growth rate at each temperature is depicted by the slope of the solid line (Eq. 2.3). Culture 1 at 5˚C did not show detectable growth so only Culture 2 and 3 were used in the calculation of growth rates and model development. Rather than calculating the mean cell concentration and the standard deviation based on two samples at 5˚C, the cell concentration of each culture time series was presented individually in Figure 2.2 (a) and (b), and the corresponding specific growth rate was calculated and shown in Figure 2.3 (a) and (b).

Our experiments indicated that the specific growth rate of *M. aeruginosa* cells increased with temperature from 5˚C to 30˚C, while it decreased from 30˚C to 35˚C. The cells incubated at 30˚C achieved the highest specific growth rates among all the incubation experiments in this study (Figure 2.3). This indicated the optimal temperature for the growth of *M. aeruginosa* cells should be close to 30˚C. The duration of growth phases at each temperature changed with the specific growth rate. It took less time for cells to reach the exponential phase as temperature increased (Figure 2.2). For example, the cells entered the exponential phase after 7 days of incubation at 10˚C, while it took only 3 days for the cells to reach the exponential phase at 30˚C. However, when the temperature was as high as 35˚C, the growth slowed down and the growth cycle became longer so it took 5 days for the cells to reach the exponential phase. Moreover, due to the low temperature, the two cultures at 5˚C grew successfully but very slowly without a clear change between the lag and exponential phase.

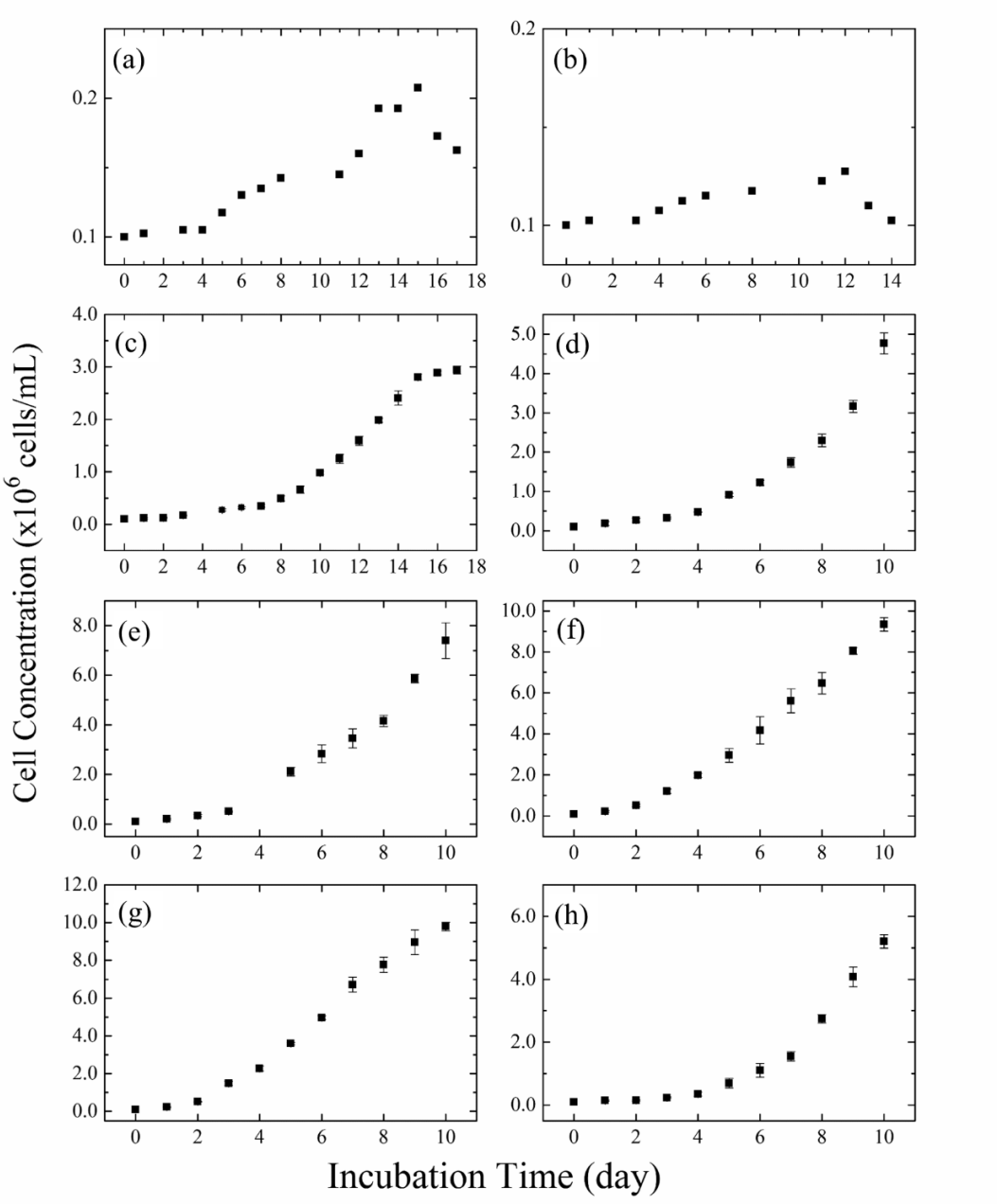

Figure 2.2. Growth of Microcystis aeruginosa at (**a**) 5˚C (Culture 2), (**b**) 5˚C (Culture 3), (**c**) 10˚C, (**d**) 15˚C, (**e**) 20˚C, (**f**) 25˚C, (**g**) 30˚C and (**h**) 35˚C. The mean cell concentrations of the triplicate samples in (**c**) – (**h**) were plotted with +/- 1 S.D. error bars. Note differences in x-axes and y-axes scales.

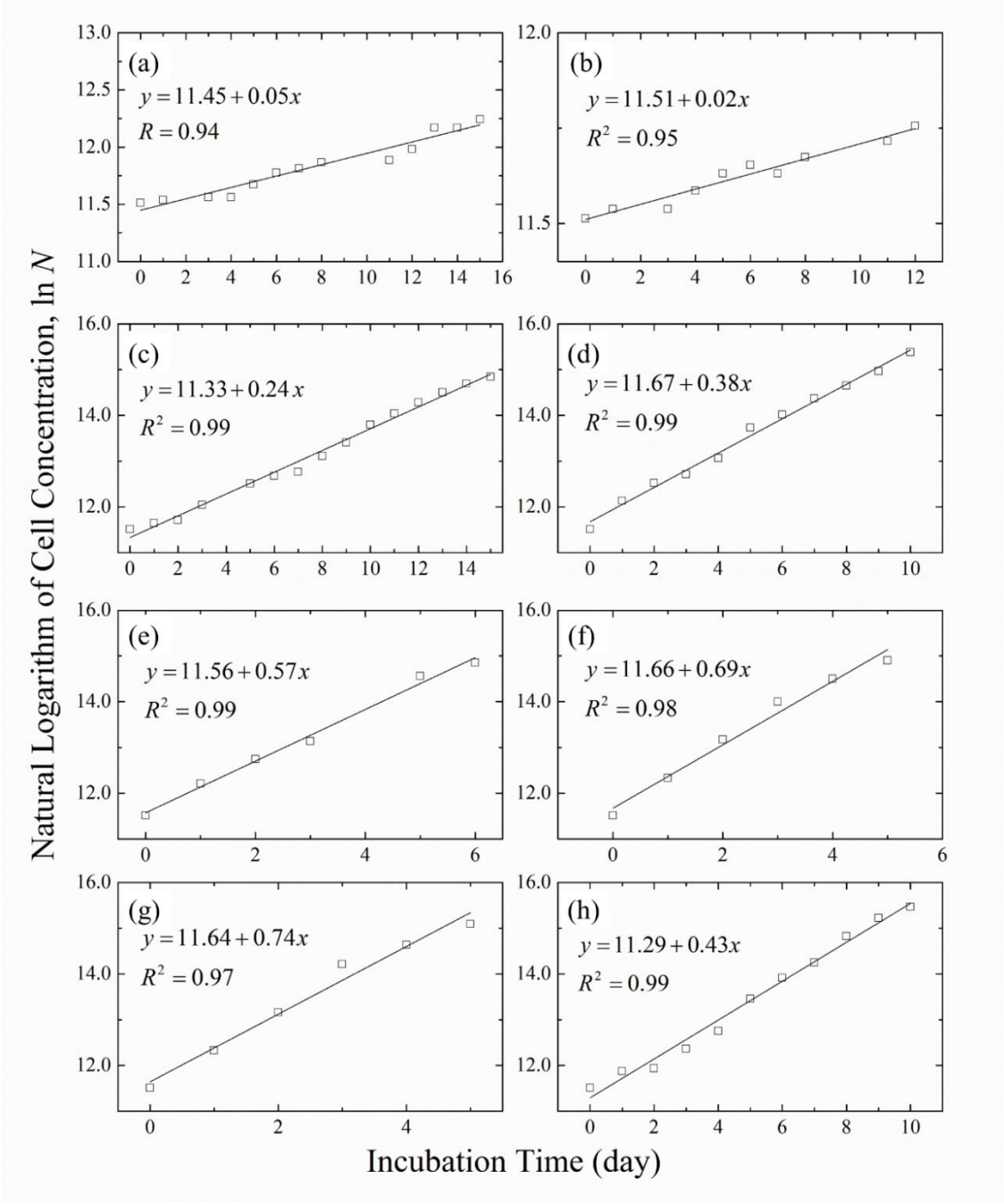

Figure 2.3. Natural logarithm of the mean cell concentration of the triplicate *Microcystis aeruginosa* cultures versus incubation time during exponential growth phase at (**a**) 5˚C (Culture 2), (**b**) 5˚C (Culture 3), (**c**) 10˚C, (**d**) 15˚C, (**e**) 20˚C, (**f**) 25˚C, (**g**) 30˚C and (**h**) 35˚C. The linear fitting lines are shown with equations. The slope of the fitting line is the

specific growth rate, $k(T)$, and the intercept is the natural logarithm of the initial concentration, ln N_0. Note differences in x-axes and y-axes scales.

Temperature-growth model

The values of specific growth rate at seven temperatures were plotted (Figure 2.4) and substituted into Eq. 2.1 for iterative analysis (Origin 9.1) to generate the best fit curve with values of the parameters (k_{opt}, T_{opt}, T_{max}, and T_{min}). The analysis of the data revealed k_{opt} = 0.74/day, T_{opt} =27.5˚C, T_{max} = 38.4˚C, and T_{min} = 0˚C. The estimated parameters (T_{max} and T_{min}) provided the temperature limits for *M. aeruginosa* growth. The cells would achieve the greatest growth rate of 0.74/day at the temperature of 27.5˚C. The R-square of this analysis is 0.98, which implies the proposed model describes 98% variability of growth rates.

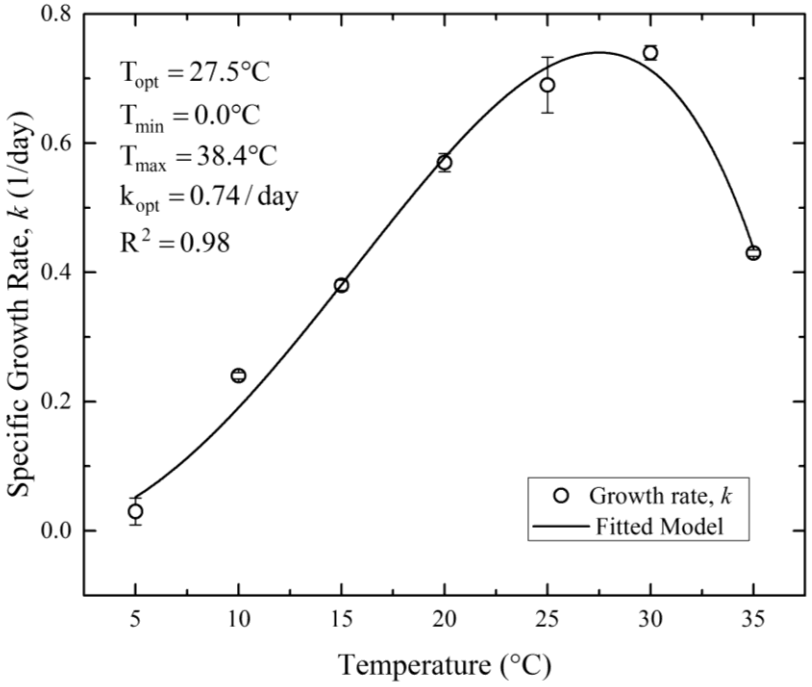

Figure 2.4. CTMI model for Microcystis aeruginosa. The specific growth rate (with +/- 1 S.D.) at each temperature was plotted and fitted into the model (Eq. 2.1). The parameters for the model were derived and shown in the graph.

Temperature effects on buoyancy

Trajectories and velocities

The spatial position data of each colony was obtained from the holograms and the movement trajectories were tracked as the displacement from frame to frame. Figure 2.5 shows the first 20 seconds of trajectories for experiments at 28.0±1.0˚C and 17.5±1.0˚C, respectively. In total, 6579 particles for the 28˚C experiment and 3453 particles for the 17.5˚C experiment were selected, and their trajectories plotted. Since each of these trajectories is of the same duration, the length is surrogate for the velocity. It is evident

that the *M. aeruginosa* colonies at 28˚C exhibit longer displacement in 20 seconds than those at 17.5˚C (Figure 2.5). Mean vertical velocities were calculated for all the particles in each recording, with a recording period of one hour (Figure 2.6). The mean vertical velocity of *M. aeruginosa* colonies at 28˚C is significantly greater than colonies at the 17.5˚C at all times during the 28 hr measurement period (*t*-test, $p < 0.01$), while the spread of velocities at 28˚C is also greater than that at 17.5˚C.

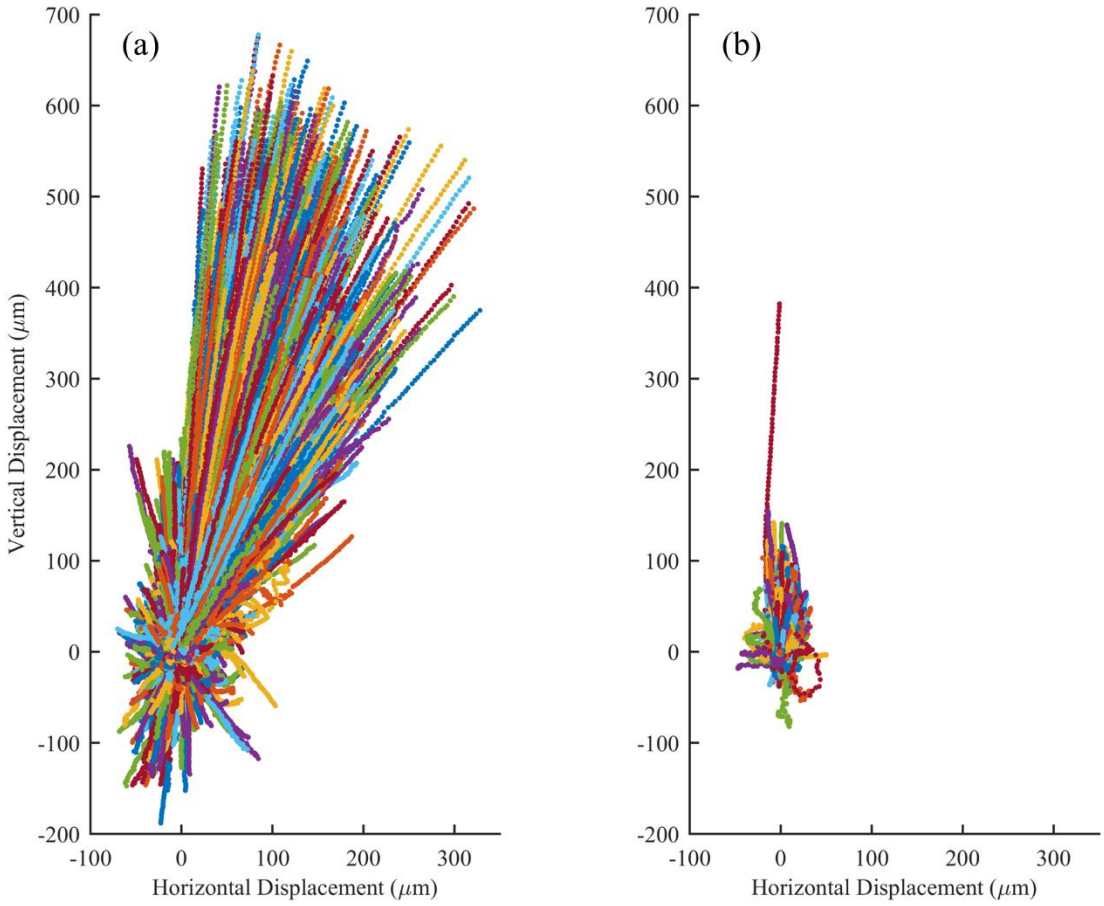

Figure 2.5. First 20 seconds of trajectories of Microcystis aeruginosa colonies at (**a**) 28˚C and (**b**) 17.5˚C. Only the particles with trajectories lasting for 20 seconds or longer were

selected. The trajectories were normalized to the origin, and each trajectory represents a particle tracked in the holographic measurement.

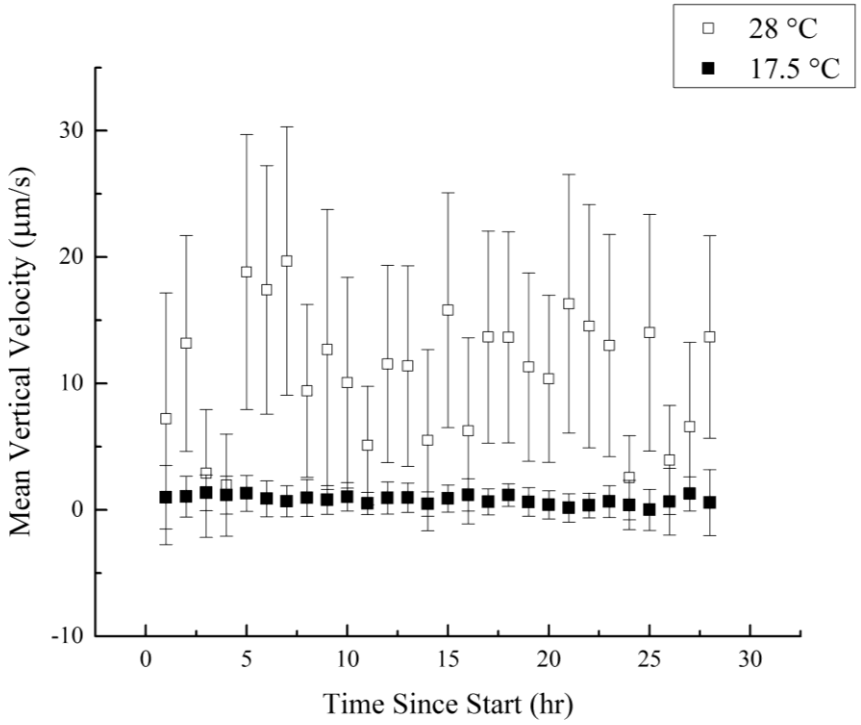

Figure 2.6. Mean vertical velocity of Microcystis aeruginosa colonies in each hour from the start of holographic measurement at temperature of 28˚C and 17.5˚C.

Velocity-density model

The vertical velocities of *M. aeruginosa* colonies were averaged over all the data points in each experiment, which provides an averaged velocity for the 17.5˚C experiment and one for the 28˚C experiment. Projected areas for colonies estimated from the holographic measurement were converted to equivalent spherical diameters and averaged over all data

points in each experiment. Using the averaged velocities and averaged areas, a typical Reynolds number of colonies was calculated to be

$Re_{\mathrm{p}} = \frac{W_{\mathrm{b}} D}{\nu} \approx \frac{10 \cdot 10^{-6}\, m/s \cdot 20 \cdot 10^{-6}\, m}{10^{-6}\, m^2/s} = 2 \cdot 10^{-4} \ll 1$, indicating that Stokes' law is applicable and the drag coefficient in Eq. 2.6 can be substituted by $C_{\mathrm{D}} = \frac{24}{Re_{\mathrm{p}}}$. Eq. 2.6 then becomes

$$\rho_{\mathrm{col}} = \rho_{\mathrm{w}} - \frac{18 W_{\mathrm{b}} \rho_{\mathrm{w}} \nu}{g D^2} \tag{2.7}$$

Averaged densities of each colony for the 28˚C and 17.5˚C experiments were calculated by substituting the averaged velocities and diameter into Eq. 2.7. The parameters and calculation results are shown in Table 2.1. The density of colonies at the high temperature is significantly smaller than that at the low temperature, thereby leading to greater density difference between colonies and water. The colonies exhibit greater buoyancy change due to density change in the 28˚C environment than in the 17.5˚C environment.

Table 2.2. Results from holographic measurement and velocity-density model of *Microcystis aeruginosa.*

Temperature (˚C)	**W_b, (μm/s)**	**Area of colony (μm^2)**	***D*, diameter of colony (μm)**	**ρ_w, density of water (kg/m^3)**	***v*, kinematic viscosity of water (10^{-6} m^2/s)**	**ρ_{col}, density of colony (kg/m^3)**
28.0	11.9	312.3	19.9	996.2	0.8	950.8
17.5	2.3	398.1	22.5	998.5	1.1	990.0

Discussion

The objectives of this study were to investigate the growth and buoyancy of *M. aeruginosa* under laboratory conditions at different ambient temperatures. The growth data enabled the formulation of functional relationship, the CTMI model, between the specific growth rate and the temperature. The digital holographic *in situ* data of the buoyant velocities of *M. aeruginosa* colonies revealed that the ambient temperature influences the colony density that regulates their buoyancy. In this section, we discuss the validation of the CTMI model and temperature effects on buoyancy including colony movement trajectories, sizes, and densities.

Validation of the CTMI model for M. aeruginosa

The specific growth rate changes significantly with temperature (ANOVA, $p < 0.01$). The relationship between the specific growth rate and the temperature established from our experimental results agrees with the results of Chu *et al*. [73] and Imai *et al*. [101]. These reported laboratory studies both indicated significant differences of specific growth rate of *M. aeruginosa* at 20˚C and 30˚C.

The cardinal temperature model with inflection originally proposed by Rosso *et al*. [92] has been validated for description of a large range of bacteria [92, 102], and a variety of microalgal species [93]. However, this study is the first to validate and parameterize the CTMI model for *Microcystis*. Validation of the model identifies the four parameters for Eq.1.1: k_{opt} = 0.74 /day, T_{opt} = 27.5˚C, T_{min} = 0˚C, and T_{max} = 38.4˚C (Figure 2.4). The estimated model parameters are in close agreement with reported experimental values

[72, 75, 103]. The proposed CTMI model of growth agrees with the conceptual model of *Microcystis* growth shown in Jöhnk *et al*. [3], whose data points were obtained from Reynolds [72], with slight differences in values. The parameters were derived from the best fit of the model curve which generated the highest adjusted R-square (0.98). However, since our experimental results ranged only from 5˚C to 35˚C and the growth at 5˚C was very small, the CTMI model was only validated for growth of *M. aeruginosa* at temperatures from 5˚C to 35˚C, i.e., $k = k(T)$ for $5^{\circ}C < T < 35^{\circ}C$.

Temperature effects on buoyancy

Movement trajectories and buoyant velocities

The major vertical direction of the trajectories shown in Figure 2.5 displays a deviation from the gravitational vertical direction, particularly in the measurements of the 28˚C experiment. The deviation is due to circulation inside the cuvette, proven with additional measurements with larger field of view using preserved *M. aeruginosa* cells (approximately neutrally buoyant) as tracking particles. These additional measurements also showed a very small speed (<1 μm/s) of the tracking particles, indicating that the circulation has a minimal impact on the magnitude of colony velocities. The fan-like divergence of the trajectories is due to the geometry of *M. aeruginosa* colonies. The colonies are assumed as spherical particles while they are, in fact, irregular shapes ranging from flakes to ellipsoids. Each colony may have a trajectory departing from the reference axis (major direction), due to the theory of Stokes flow over particles in arbitrary shape [104].

The trajectories show that most colonies were moving upwards, indicating a buoyancy gaining or colony density decreasing process. Based on previous studies [15, 105], the buoyancy of *Microcystis* can be regulated in three ways: 1) turgor collapse when exposed to pressure or light over a critical value; 2) regulating the rate of gas vacuoles synthesis and relative gas vacuoles content compared to rate of cell growth and division; 3) regulating the relative content of the intracellular dense carbohydrates ("ballast") produced by photosynthesis. Both experiments in this study were conducted under the same conditions except for temperature so turgor collapse is not the mechanism of buoyancy regulation in these experiments. The experiments only lasted for 28 hours which is too short for the regulation to be dominated by cell growth and division. Thus, the variation of the intracellular dense carbohydrates content is likely to the reason for the density change of *Microcystis* colonies. The synthesis of cell materials (e.g., proteins and lipids) from dense carbohydrates and nutrients, and the respiration of cells, which generates energy from carbohydrates degradation, are two of the major activities causing the variation of intracellular carbohydrates. The higher buoyancy in the 28˚C environment compared to the 17.5˚C environment indicates an enhancement of cell material syntheses and/or cell respiration of *Microcystis* at the high temperature, and thereby leading to the greater buoyancy change (i.e., lower colony density). The comparison between mean velocities of 28˚C and 17.5˚C experiments also agrees with the temperature impact on buoyancy regulation. The buoyant velocity in the 28˚C environment is approximately 5 times as great as that in the 17.5˚C environment.

In the 28˚C experiment, 90% colonies showed a positive buoyant velocity (i.e. the colonies were floating), while in the 17.5˚C experiment, only 80% colonies showed a

positive buoyant velocity. This result agrees with the relation between buoyancy recovery and temperature reported in Thomas and Walsby [86], which showed 84% recovery of non-buoyant colonies at 30˚C and only 10% recovery at 7˚C. The percentage difference is smaller in this study due to the smaller temperature difference. This also illustrates that the observed sudden increases in sedimentation of *Microcystis* colonies after bloom disappearance in autumn could be partly due to worse buoyancy at low temperatures [15, 85].

Diurnal changes in depths, velocities or colonial densities over several consecutive days have been reported in other studies [15, 81, 82]. The mean buoyant velocities in Figure 2.6 show no periodic patterns but fluctuations in velocities at the temperature of 28˚C. One possible explanation is that the colonies were affected by more than one mechanism of buoyancy regulation and thus were experiencing longer regulation cycle. Since the experiments in this study lasted only for 28 hours, the colonies remained at the buoyant phase for the entire duration of the investigation.

Colony sizes

The averaged sizes in this study (shown in Table 2.1) are relatively small compared to *Micocystis* colonies in some other studies. For instance, Nakamura *et al*. [80] reported colony diameters from 10^1 to 10^3 μm and Rowe *et al*. [87] reported 117 μm as the median of colony diameters. Meanwhile, the averaged buoyant velocity in the present study is also relatively small. We produced 3D histograms showing the frequency of buoyant velocity (4 μm/s bin width) and colony diameter (21 μm bin width) for both the 28˚C and the 17.5˚C environment in Figure 2.7. It shows that the buoyant velocity ranges from 0 to

40 µm/s and the colony diameter ranges from 0 to 210 µm. These ranges agree with the results of a subrange (colony diameter < 100 µm) of Sample #900803 in Nakamura *et al*. [80]. However, our colony diameters are dominated by relatively small values (Figure 2.7), and therefore no clear relationship between buoyant velocity and colony diameter can be established from our results as in the above studies. The buoyant velocity distributions in the present study show smaller magnitudes but similar shapes as that in Rowe *et al*. [87] (Figure 4c in their paper). It reveals that our samples contain relatively smaller colonies that slowly migrate upwards instead of oscillating over depths diurnally. This agrees with the statement in Okada and Aiba [106] that the amplitude of oscillation will be increased by increasing the colony radius.

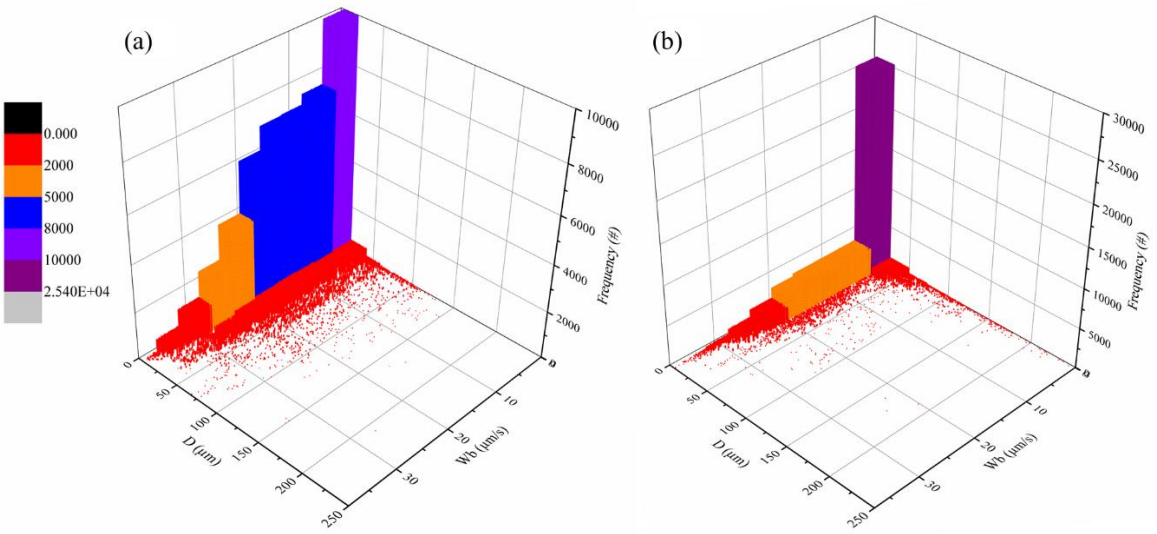

Figure 2.7. Three-dimensional histogram showing the frequency of buoyant velocity (W_b) and diameter (D) of Microcystis aeruginosa colonies in (**a**) 28˚C experiment and (**b**) 17.5˚C experiment. Bin width is 4 µm/s in W_b x 21 µm in D for both graphs.

Colony densities

The velocity-density model in the present study is based on Stokes' law which has been applied in simulations for several strains of buoyant cyanobacteria in previous studies [15, 81, 82, 83, 84]. Although the density of a *Microcystis* colony changes periodically even at the same temperature due to photosynthesis and biosynthesis, our results show that the averaged density of the colonies in higher temperature environments appeared to be lower than that in lower temperature environments.

Based on Eq. 2.6, buoyant velocity is related to water density, colony density and kinematic viscosity of water as $W_b \sim \frac{(\rho_w - \rho_{col})gD^2}{18\rho_w \nu}$. Assuming colony density is not affected by temperature, i.e. buoyant velocity only depends on two variables (ρ_w and ν shown in Table 2.1), the ratio of buoyancy velocity at 28˚C and 17.5˚C $\frac{W_{b,28}}{W_{b,17.5}} \approx 1.3$. However, the ratio in our result is 5.1, which indicates there is a significant difference in colony densities at the two temperatures.

Limitations, applications and future studies

The *M. aeruginosa* strain B3-R-7 used in the growth experiments was subjected to long-term laboratory cultivation. The cells mostly existed as individual cells instead of colonies and no vesicle structures were observed inside the cells under the optical microscope. In addition, no movements of the cells could be captured by the DIHM system, although the cells did not sink to the bottom because they were close to neutral

buoyancy. The observations implied that there were deficiencies in the synthesis of gas vesicles (GV) in these cells and they did not have the buoyancy regulation-based migration ability. The GV-deficient mutations have been reported for *M. aeruginosa* in laboratory cultures, where GV synthesis is no longer needed due to sufficient nutrient and light supplies in laboratory environments [17]. The difference in growth between GV-deficient *M. aeruginosa* and wild-type *M. aeruginosa* (e.g. samples from Powderhorn Lake) needs to be studied further.

The CTMI model for *M. aeruginosa* provides a prediction tool to estimate growth rates at a variety of temperatures. The model will be instrumental in water quality models which can successfully predict 3D water temperature variability in response to meteorological forcing (e.g., Chung *et al*. [107]) to predict spatial and temporal heterogeneities of *Microcystis* in aquatic ecosystems. For the first time, we demonstrate that ambient temperature has strong effects on the buoyant velocities of *Microcystis*. This inspires the incorporation of temperature factors into the model development of *Microcystis* migration in the future. The findings also provide motivations for further investigations into the biochemical and physiological changes of *Microcystis* that arise as a result of different ambient temperatures and provide fundamental mechanisms for the behaviors described in this study. The observations of microalgal movements were made possible by the implementation of the digital inline holographic microscope. The DIHM system is low cost, highly compact and a promising laboratory and field technology. It can be readily integrated with existing autonomous/robotic devices used in the field for long-term and large-scale *in situ* quantification of plankton distribution and behavior.

Conclusions

Laboratory measurements were conducted to investigate the effects of ambient temperatures on *M. aeruginosa* specific growth and vertical migration. We demonstrate that the specific growth rate of *M. aeruginosa* increases with temperature up to the optimal growth temperature of 27.5˚C. At higher temperatures, the specific growth rate is inversely affected. The CTMI model with the inflection point located at 27.5˚C describes 98% variability of the growth of *M. aeruginosa* at experimental temperatures from 5˚C to 35˚C. The ambient temperature is also shown to have an impact on vertical migration of *M. aeruginosa*. The buoyant velocities of *M. aeruginosa* colonies at 28˚C are approximately five times as great as those at 17.5˚C. The temperature is shown to influence the colony density of *M. aeruginosa*, which regulates their buoyancy. We propose a functional dependence of the *M. aeruginosa* colony density on the buoyant velocity and colony size. The results will facilitate the prediction of *M. aeruginosa* growth and buoyant velocities at a variety of ambient temperatures in aquatic ecosystems.

Chapter 3

Microalgal Swimming Signatures and Neutral Lipids Production Across Growth Phases

Introduction

Microalgae have been advocated as a promising source of food, energy and pharmaceutical products. Owing to their high growth rate, competitive lipid production, low environmental impact, and tolerance of harsh environments including wastewater streams, microalgae have been cultivated in large outdoor ponds and closed photo-bioreactors for biofuel production [27, 56, 57, 108, 109, 110]. Microalgae capture solar energy and store it as neutral lipids, primarily comprising of triacylglycerols (TAGs), which can be trans-esterified into biofuel [30, 111, 112]. Challenges remain in

commercializing biofuel production from microalgal lipids due to the high costs and low energy efficiency of large-scale algal cultivation and harvest [113, 114, 115, 116]. One key remaining question is when during the cultivation process the biomass yield and intracellular lipid accumulation are maximized. Preferably, the high-lipid timing should be used to initiate harvesting.

As the impacts of environmental stressors on the growth and vertical migration of cyanobacteria demonstrated in Chapter 2, environmental stressors may also play roles in the swimming and metabolism of other aquatic microorganism, such as lipid-producing microalgae. Researchers have investigated the microalgal lipid accumulation in response to environmental stress induced by nutrient limitation. Nitrogen starvation has been reported to facilitate lipid accumulation in green algae cells [30, 31, 55, 117, 118]. The reported impact of nitrogen starvation on algal lipid production differs among species [56] and is also affected by experimental design and the extent of nitrogen starvation. Environmental stresses also influence the motility of microalgal cells. Swimming behaviors of green alga *Dunaliella* are influenced by fluid flow conditions [53, 54], and increased swimming velocities of freshwater green alga *Chlamydomonas* have been observed under nitrogen limitation [32]. Limited research has been done to directly relate swimming behaviors of algal cells to their metabolism (e.g., lipid accumulation) and physiological stages.

Due to their high lipid content, halotolerance and lack of rigid cell wall, the motile green algae, *Dunaliella*, was chosen as the model organism to investigate swimming signatures and intracellular lipid accumulation under different environmental conditions. Our

primary hypothesis is that swimming velocities and trajectory patterns of *Dunaliella primolecta* (*D. primolecta*) are correlated with the intracellular neutral lipid accumulation. Micro-particle tracking velocimetry (micro-PTV) and digital inline holographic particle tracking velocimetry (DIH-PTV) were employed to analyze the swimming signatures (velocities and trajectories) of *D. primolecta* cells with different intracellular neutral lipid content. The results demonstrate statistically different swimming signatures of *D. primolecta* during the lag, exponential, and stationary growth phases, which correspond to different neutral lipid content in the cells. Since microalgal signatures can be obtained *in situ* and in real-time, the findings will be instrumental for cultivating and harvesting microalgal cells with maximum lipid content.

Materials and Methods

Strain selection and cultivation

D. primolecta is a species of unicellular, motile, bi-flagellated green algae which lives in brackish water, making it preferable organism for monoculture cultivation under field conditions. The lipid content in *Dunaliella* ranges from 15% - 40%, and most of the TAGs are accumulated in cytoplasmic lipid droplets [34, 35, 36]. Batch cultures of *D. primolecta* UTEX LB1000 were incubated in the three groups of modified Erdschreiber's medium with 30%, 70% and 100% initial nitrogen concentrations and labeled as 30%N, 70%N and 100%N, respectively (details of growth medium in Appendix B). All the cultures were started at approximately 2×10^4 cells/mL in 250 mL Erlenmeyer flasks, and incubated in an incubator at 20˚C under PAR of 51 $\mu E/m^2s$ with 14/10-hour light/dark

cycles, maintained mixed by a shaker table (New Brunswick Scientific Co., USA) at 30 rpm and manually shaken twice daily. Trial cultivation experiments with above conditions had been conducted twice to have a clear understanding of the cultivation duration before the cultivation of *D. primolecta* for lipid and swimming analyses. The cultivation lasted for 51 days, including the entire growth cycle until the beginning of the decline phase.

Nitrate analysis, dry weight measurement, and microscopic observation

Samples were collected from replicate *D. primolecta* cultures with 30%N, 70%N and 100%N growth medium, respectively, at each growth phase for the measurement of dry cell weight (detailed method in Appendix B) and nitrate concentration. Nitrate analysis was performed with the Trilogy laboratory fluorometer (Turner Designs Inc., USA) and the nitrate test kit (LaMotte Nitrate Nitrogen Kit, 0.25 -10 ppm, LaMotte company, USA). *D. primolecta* cells from samples of lag, exponential, early stationary and late stationary phases were observed under a Nikon Eclipse 90i microscope with a 100X oil immersion DIC objective and images were captured using a Nikon DS-Fi2 color CCD camera in the field of 1260 x 960 pixels at 0.07 µm/pixel (cell fixation details in Appendix B).

Determination of intracellular neutral lipid content

The relative quantity of intracellular neutral lipid of *D. primolecta* cells was determined by the Nile red fluorescence according to Chen *et al*. [119] throughout the growth cycle. Samples were taken from replicate cultures of each growth medium group (i.e., 30%N, 70%N and 100%N) on each measurement day. *D. primolecta* samples were incubated in

96-microwell plates in the dark at 25˚C for 30 min to get the algal cells stained. The fluorescence emissions were then recorded by a BioTek Synergy Neo2 Hybrid multi-mode reader (BioTek Instruments, Inc., USA), with an excitation wavelength of 530 nm and an emission wavelength of 575 nm. The fluorescence signals were normalized by the cell concentration to the fluorescence intensity per 10^7 cells. The neutral lipid content of algal samples from eight different cultures at various growth phases were determined by the gravimetric method modified from Bligh and Dyer [120] and Alonzo and Mayzaud [121] to calibrate the Nile red fluorescence intensity with the neutral lipid content (more details in Appendix C).

Measurement of swimming velocities

Swimming velocities of *D. primolecta* were measured at lag, exponential, early stationary and late stationary phases. A micro-PTV system developed by TSI Inc. (USA) was employed to quantify the swimming velocities. The micro-PTV system set up was similar to the one described in Chengala *et al.* [53] with modifications (Figure 3.1). At least four samples were collected from each culture group (30%N, 70%N and 100%N) and two image sequences were recorded at a frame rate of 5 Hz (ΔT=200000 μs) to provide at least 100 pairs of frames for each sample. The processing of images was based on PTV (particle tracking velocimetry) analysis, which measured the horizontal velocities (x-direction and y-direction) of each particle (algal cell) in pairs of images by tracking the displacement of particles between each pair of frames and generating velocity vectors (more details in Appendix D).

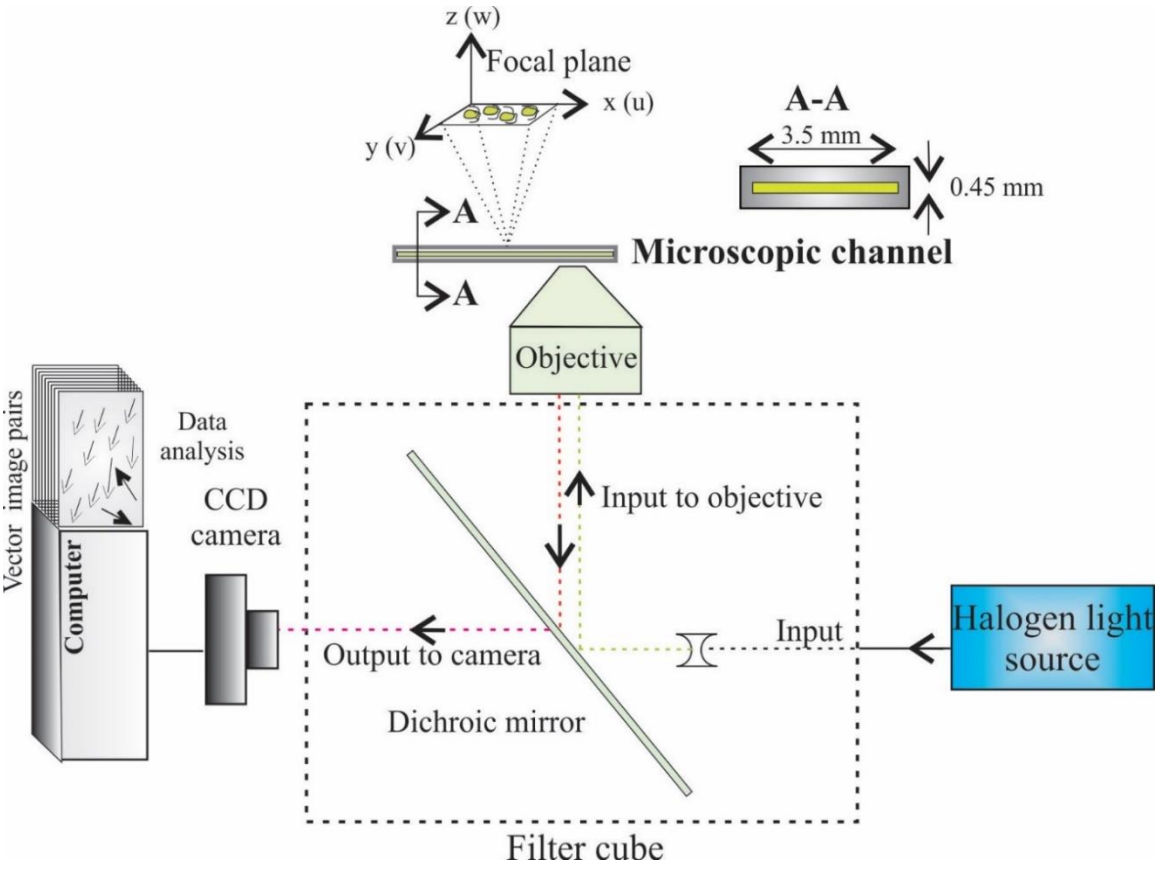

Figure 3.1. The micro-PTV set up for analysis of *D. primolecta* swimming velocities.

Tracking of swimming trajectories

The swimming trajectories of *D. primolecta* were recorded using a DIH-PTV system similar to but partly modified from the one used in Chapter 2. It consisted of a 532 nm diode laser (Thorlabs CPS532), an optical spatial filter and collimating lens assembly, 5X microscopic objective (Mitutoyo 10X/0.14 NA), and a CCD camera (Flare 2M360-CL) (Figure 3.2). Compared to conventional microscopy methods, DIH-PTV has a much larger depth of focus and is capable of tracking objects in 3D [122]. The holograms were

recorded at a framerate of 100 Hz with an exposure time of 50 μs and cropped to a 1024 pixels × 1024 pixels window for processing. Measurements of replicate 30%N cultures were performed at the lag, exponential, and early stationary phases. Recordings of five samples were made for each culture with recording volume of 1 μL. Each sample was recorded for 20 seconds (2000 frames) with the exception of the lag stage samples which were recorded for 60 seconds in order to increase the total number of cells recorded at the lowest concentration. Positions of each cell in the recorded hologram were extracted using the Regularized Inverse Holographic Volume Reconstruction (RIHVR) method presented by Mallery *et al*. [123]. The cell positions were tracked in time using the method of Crocker and Grier [100] to produce trajectories illustrating the swimming mode of each cell.

The swimming trajectories were classified into five behavior modes: 1) circular which rotate about a fixed point with minimal net motion; 2) helical which rotate about a moving point, forming a helix; 3) random walk which do not rotate and have minimal directionality; 4) linear which have no rotation and minimal deviation from a principle direction of motion; 5) meandering which is similar to linear but with greater deviation from the principle direction. The trajectories were automatically labeled using a binary decision tree based on a set of measured trajectory features.

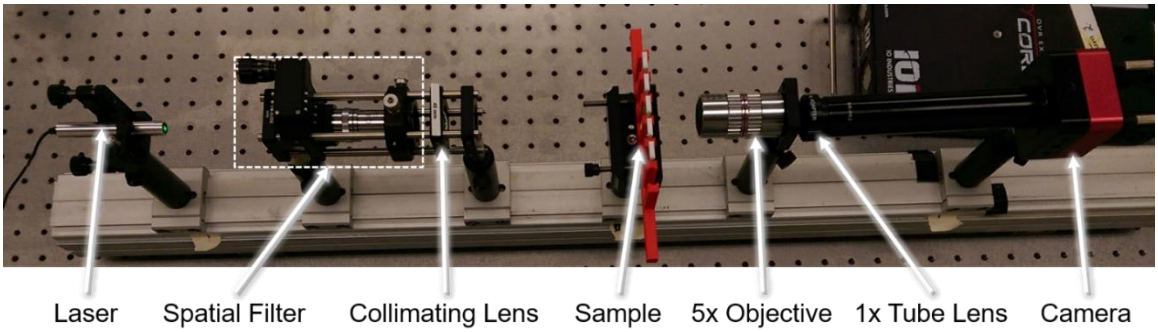

Figure 3.2. The DIH-PTV system for analysis of *D. primolecta* swimming signatures.

Statistical analyses

One-way ANOVA tests were conducted for each culture group to determine the significance of differences in the neutral lipid content and swimming speed of *D. primolecta* cells at different growth phases ($df = 3$, $\alpha = 0.05$). One-way ANOVA tests were also conducted at each growth phase to determine the significance of differences in the neutral lipid content and swimming speed of *D. primolecta* cells in cultures with different initial nitrogen availability ($df = 2$, $\alpha = 0.05$). To determine the significance of differences in the swimming behavior among growth phases (the lag, exponential and early stationary phases), the one-way ANOVA tests were conducted for the swimming speed and fine motion frequency from the DIH-PTV results ($df = 2$, $\alpha = 0.05$).

Results and Discussion

Intracellular neutral lipid content accumulation

During the growth cycles, all the cultures maintained at the lag phase for the first few days adapting to the new environment, and then grew exponentially, after which the cells entered the stationary phase with constant populations until the cell population started to decline (Figure 3.3a). The growth cycle can be divided into four growth phases: 1) lag phase - day 1, i.e. 24 hours after the beginning of cultivation; 2) exponential phase - day 16; 3) early stationary phase – 2 or 3 days after the beginning of the stationary phase (day 25 for 30%N cultures and day 35 for 70%N and 100%N cultures); and 4) late stationary phase - the stage right before the decline phase (day 45).

The intracellular neutral lipid content of *D. primolecta* changed correspondingly to the growth phases (Figure 3.3b). The neutral lipid content slightly increased but remained relatively low for all cultures from lag to exponential growth phases. Starting from the late exponential phase, the neutral lipid content of the 30%N cultures increased drastically, reaching the peak at the early stationary phase (day 25) and decreasing at the late stationary phase. The increase of intracellular neutral lipid content in the 70%N and 100%N cultures were not drastic until the late stationary phase. The peaks of neutral lipid level occurred on day 45 for 70%N and 100%N cultures, and the peaks were lower than the peak for the 30%N cultures. Converting the Nile red fluorescence intensity to neutral lipid content (standard curve in Figure 3.4), the intracellular neutral lipid content for all the cultures was under 5% of cell dry weight during lag and exponential phases. The neutral lipid content of cells in the 30%N cultures reached its peak of 35.9% of dry

weight at the early stationary phase and decreased to 7.7% of dry weight at the late stationary phase. In contrast, the intracellular neutral lipid content in 70%N and 100%N cultures remained under 10% of dry weight and increased to the peak of 20.5% and 16% of dry weight, respectively, at late stationary phase. Both the timing and the extent of the peak of the intracellular neutral lipid content were negatively influenced by the initial nitrogen availability in the cultures.

Relating the neutral lipid content with the nitrate concentration, we observed that the sharp rise of the neutral lipid content did not occur until the nitrate concentration in the culture became less than 1 mg/L (Figure 3.5). The nitrate concentration in the 30%N cultures decreased below this threshold during the late exponential phase, around day 17, soon after which the neutral lipid level reached the peak. The nitrate concentration of the 70%N and 100%N cultures decreased from slightly above the threshold to below the threshold during the stationary phase, day 35 to day 37, and therefore showed the peaks of neutral lipid at late stationary phase. For all the three groups of cultures, the neutral lipid content was approximately 0.1 mg per 10^7 cells when the nitrate concentration was near the 1 mg/L. Our experimental results agree with the previous research by Gao *et al*. [31], Mai *et al*. [55] and Wang *et al*. [118] indicating that *Dunaliella* cells respond to the nitrogen starvation by rapidly transferring previously stored carbon to neutral lipids and enhancing lipid accumulation. The timing of peak values is also consistent with that reported in Chen *et al.* [30] which stated that the lipid content of *Dunaliella* cells reaches the highest value at the stationary phase in both the normal medium culture and the N-deficient medium culture.

Under the light microscope, changes in the intracellular structure and contents of *D. primolecta* cells were observed at the four growth phases (Figure 3.6). The cup-shaped chloroplast with pyrenoid was observed in cells at lag and exponential phases (Figure 3.6a-c, d-f). During the stationary phase, the cytoplasm of cells was no longer as clear, and refractive starch granules appeared in the chloroplast. Most of the cells at the late stationary phase were observed to be spherical or near-spherical due to the unfavorable growth conditions and exhibited a yellow-brownish color associated with the age of cells and the increase of intracellular neutral lipid (Figure 3.6j-l). The microscopic observations were consistent with the study by Eyden [124] of the *D. primolecta* cells under light and electron microscope, and the study by Davidi *et al*. [33], which reported observation of a fragmented chloroplast with multiple cytoplasmic lipid droplets in the N-deficient cells. It also agrees with the report by Chen *et al.* [30] that intracellular neutral lipid bodies started to be observed by the third day of nitrogen deprivation, and the statement in Hu *et al*. [33] that the deposition of TAGs into cytosolic lipid bodies play active roles in stress response.

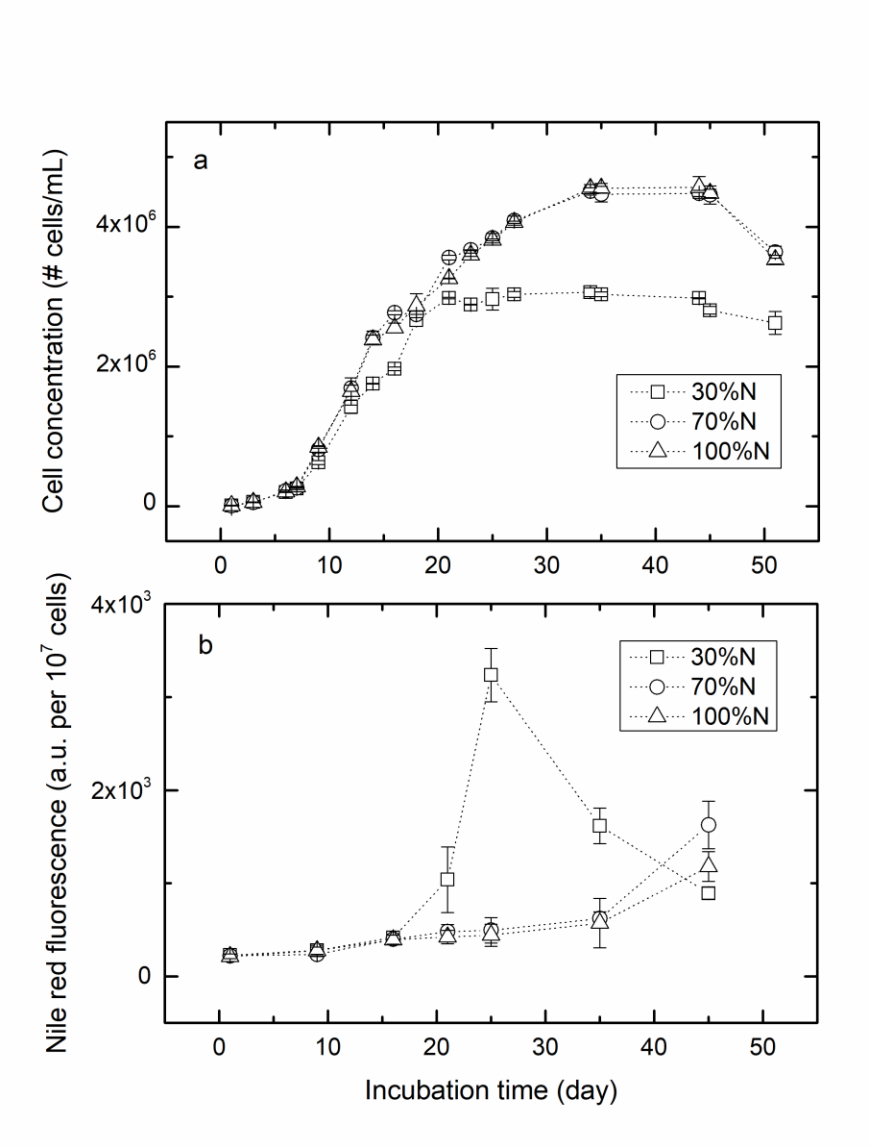

Figure 3.3. Growth curves and intracellular neutral lipid content of *D. primolecta* cultures. (**a**) Cell concentrations of an entire growth cycle of the three groups of *D. primolecta* cultures. Error bars correspond to the s.d. (n=8). (**b**) Intracellular neutral lipid content reflected by the intensity of Nile red fluorescence detected at 530/575 nm excitation/emission wavelength for 30%N cultures (□), 70%N cultures (○) and 100%N cultures (Δ). Error bars correspond to the s.d. (n=4).

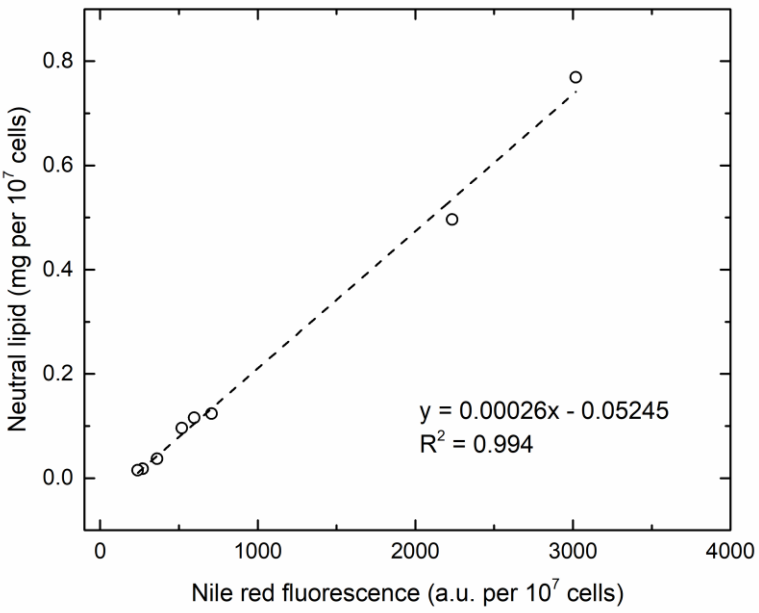

Figure 3.4. Neutral lipid content versus Nile red fluorescence intensity. The trend line was used as the standard curve in conversion of Nile red fluorescence to neutral lipid in the text of the article.

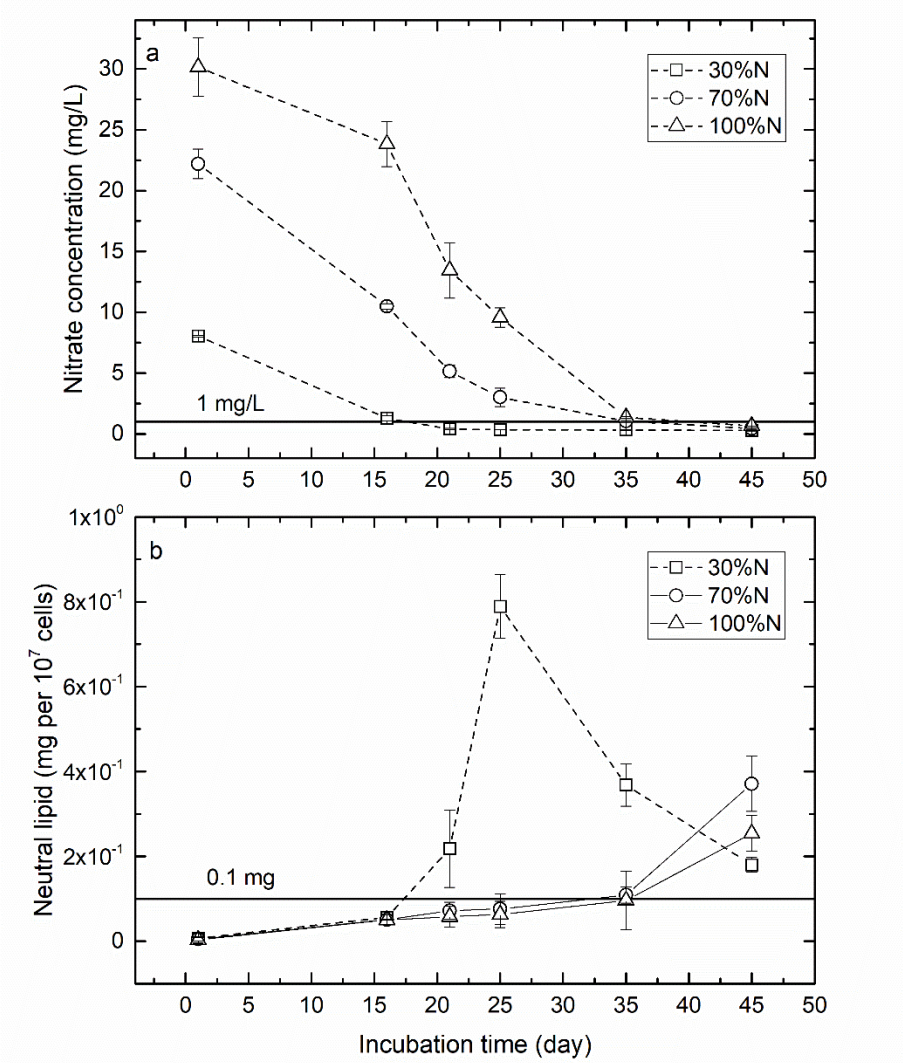

Figure 3.5. Nitrate concentration and intracellular neutral lipid content of *D. primolecta* cultures. (**a**) Nitrate concentration of the three groups of *D. primolecta* cultures at six time points throughout the growth cycle. The "30%N", "70%N" and "100%N" represents the cultures incubated in 30%, 70% and 100% initial nitrogen (NO_3^-) concentration of original Erdscheiber's medium, respectively. Error bars correspond to the s.d. (n=3). The solid line (-) corresponds to nitrogen concentration of 1 mg/L. (**b**) Intracellular neutral lipid content of 30%N cultures, 70%N cultures and 100%N cultures. Error bars correspond to the s.d. (n=4). The solid line (-) corresponds to neutral lipid content of 0.1 mg per 10^7 cells.

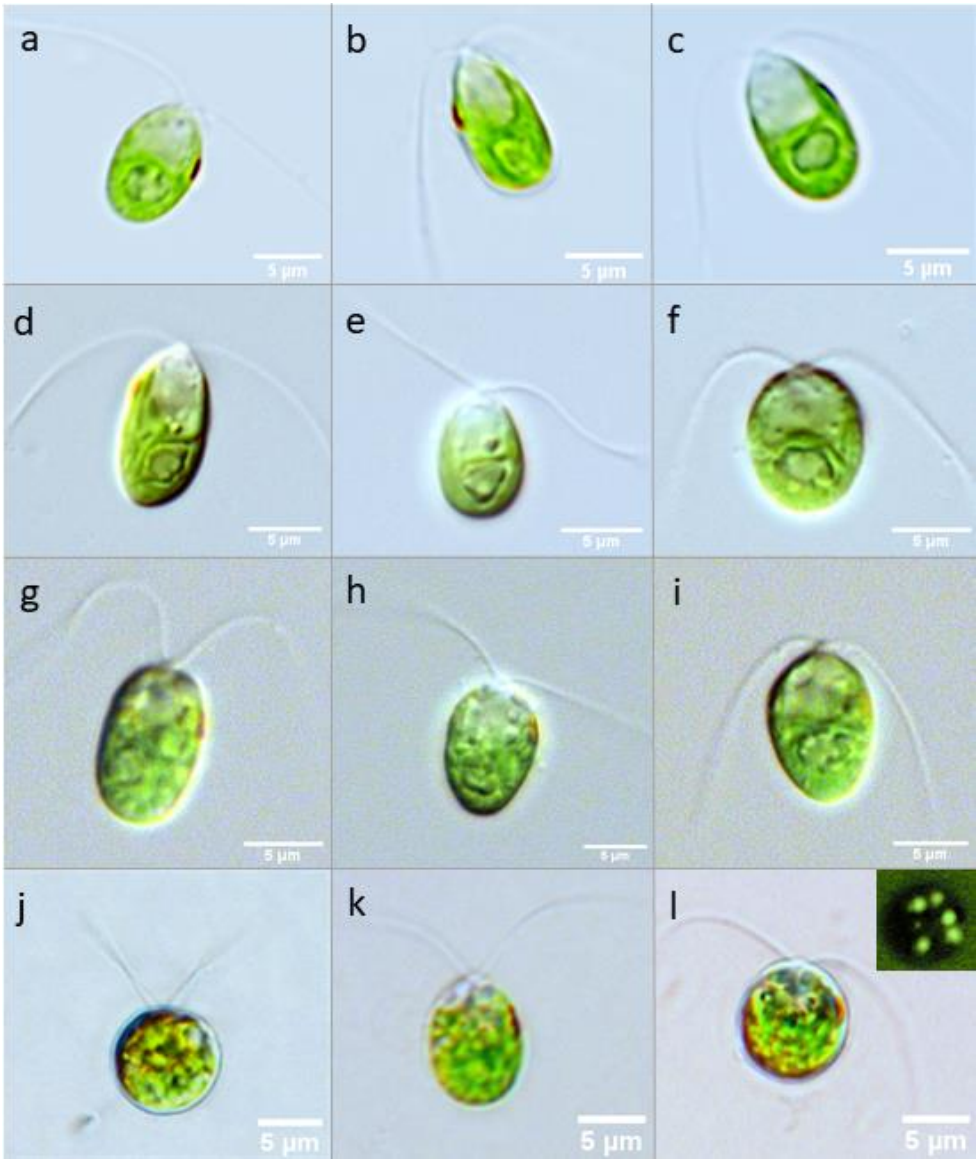

Figure 3.6. *D. primolecta* cells at various growth phases under a light microscope. (**a**)-(**c**) Cells at the lag phase of 30%N, 70%N and 100%N cultures, respectively. (**d**)-(**f**) Cells at the exponential phase of 30%N, 70%N and 100%N cultures, respectively. (**g**)-(**i**), Cells at the early stationary phase of 30%N, 70%N and 100%N cultures, respectively. (**j**)-(**l**) Cells at the late stationary phase of 30%N, 70%N and 100%N cultures, respectively. The insert in (**l**) is a BODIPY stained live cell of D. primolecta, where the green fluorescent dots represent the lipid droplets in the cell.

Microalgal swimming speed and trajectories

The motility of *D. primolecta* changed corresponding to growth phases and the initial nitrogen availability in the growth media. The scatter plots of horizontal velocities in *x*- and *y*- directions were all in circular/near-circular modes, centered around the origin (0,0) and expanding or shrinking showing the velocity changes with growth phases (Figure 3.7). All the velocities from the experimental results were within the range of -120 to 120 μm/s. The velocities were relatively low at lag phase and increased from lag to early stationary phase for all culture groups. The velocities of the cells in the 30%N cultures at the early stationary phase concentrated at higher values with a decrease when reaching the late stationary phase, while the velocities of the cells in the 70%N and 100%N cultures kept increasing till the late stationary phase.

The swimming speed, *v*, of *D. primolecta* cells in the horizontal *x*-*y* plane were all within 5 to 120 μm/s. The distribution of the swimming speed also varied with growth phases and initial nitrogen availabilities (Figure 3.8). The probability density function (PDF) of swimming speed for each culture group at each growth phase was approximated by a Kernel distribution, and the approximations were confirmed by the Chi-square goodness-of-fit tests at $\alpha = 0.05$. The variation of swimming speed distribution indicated that the swimming speed of *D. primolecta* cells increased from the beginning of a growth cycle until reaching a peak during the stationary (early stationary or late stationary) phase, when the nutrient deprivation occurred and the cell population stopped increasing. The 30%N cultures showed left-skewed speed distribution earlier than the 70%N and 100%N cultures, and the mean of the distribution for the early stationary 30%N cultures (81

μm/s) was higher than that for the late stationary 70%N and 100%N cultures (67 μm/s and 62 μm/s, respectively), which implied an impact of the initial nitrogen availability on the variation of swimming speed.

Measurements of the *D. primolecta* swimming velocities using DIH-PTV showed similar trends to the micro-PTV measurements. The lag phase showed the lowest mean swimming speed, with increasing speeds seen in both the exponential and early stationary stages. There was no significant difference in speed among the three nitrogen levels for the lag or exponential phase. Swimming trajectory measurements using DIH-PTV indicate a change in the complex behavior modes of the swimming cells (Figure 3.9a-c). We observed five swimming modes including circular, helical, random walk, meandering, and linear. These can be further grouped into fine motions (circular and helical) and gross motions (linear and meandering) with random walk serving as an intermediate that is neither fine nor gross. We trained a binary decision tree to autonomously classify the measured trajectories into one of these classes. We applied this classification to $n = 421$ trajectories from the lag phase, $n = 6306$ from the exponential phase, and $n = 7874$ from the early stationary phase. The most significant trend is the decrease in the frequency of fine motions from exponential to early stationary phase (Figure 3.9d-f). The helical and circular behaviors are hardly seen in the early stationary stage. The fine motions account for 48% of tracks in the lag phase, 16% in the exponential phase, and only 2% in the early stationary phase.

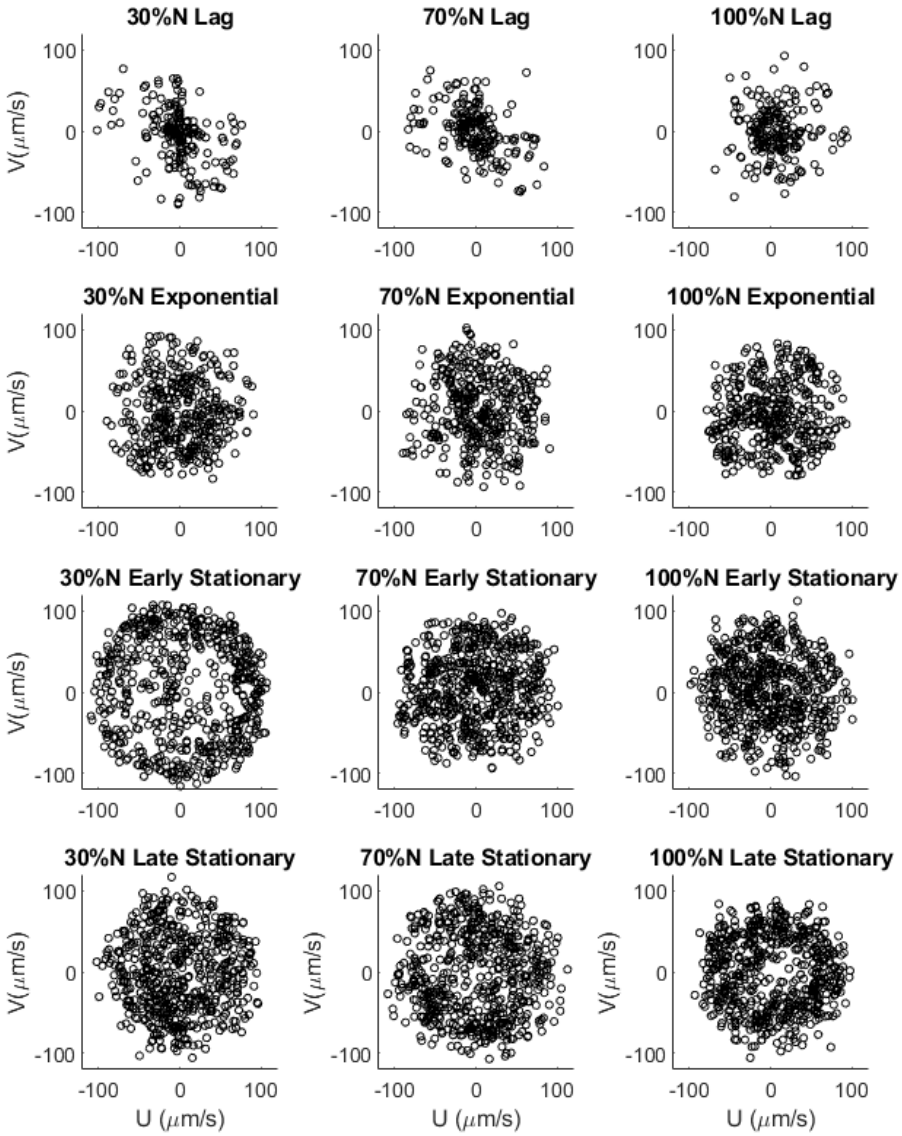

Figure 3.7. Swimming velocities of *D. primolecta* cells in x- and y- directions. U (µm/s) is the velocity in the x-direction and V (µm/s) is the velocity in the y-direction. Each column of subplots corresponds to a group of culture and each row of subplot corresponds to a growth phase. The number of data point for each growth phase was n=200 lag phase, n=400 exponential, n=600 early and late stationary phases.

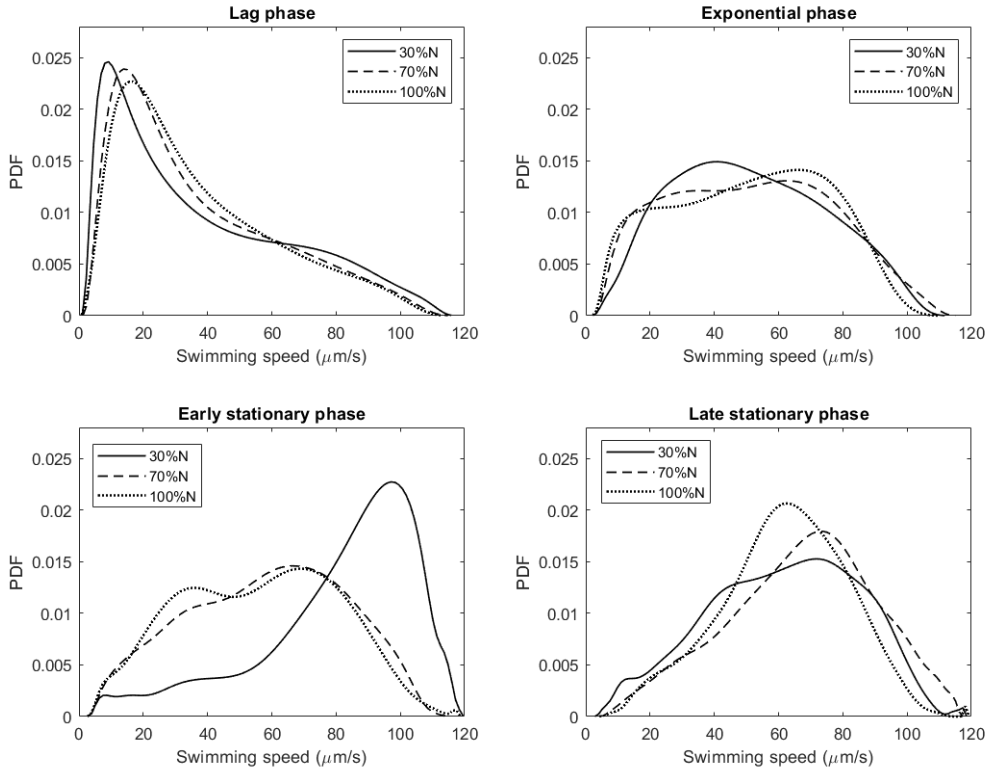

Figure 3.8. Fitted probability density functions for *D. primolecta* swimming speeds at four growth phases. The probability density functions were produced by fitting the data into Kernel distributions (goodness-of-fit confirmed by Chi-square tests at α=0.05).

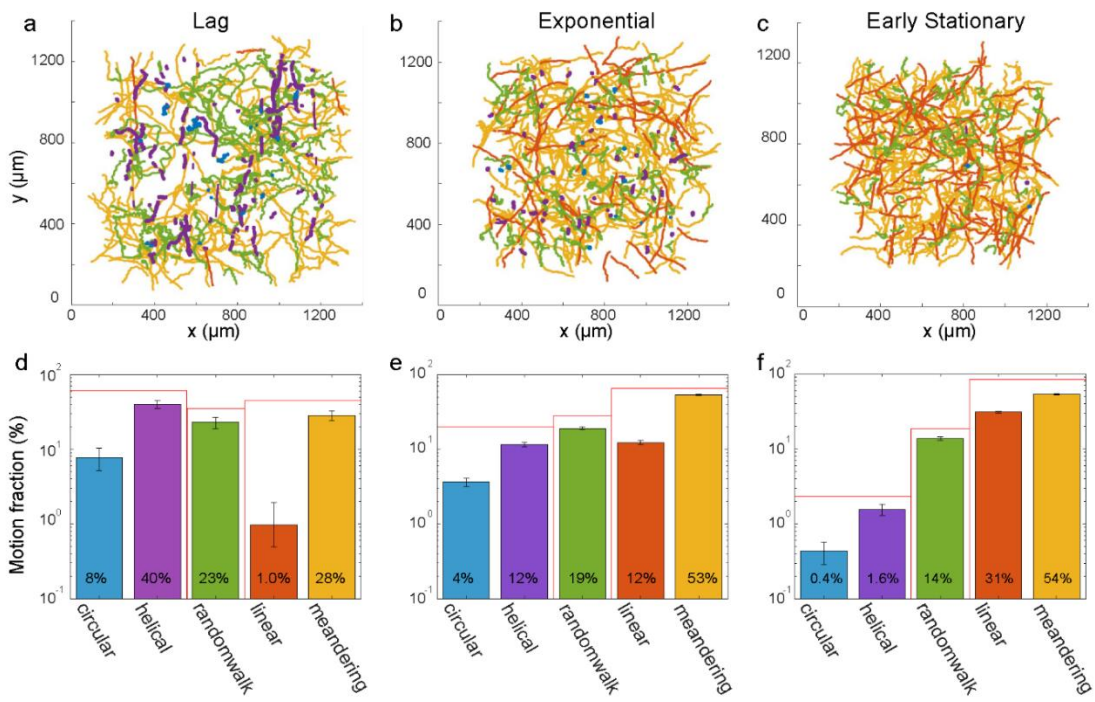

Figure 3.9. Classified swimming trajectories of *D. primolecta* cells in 30%N cultures. (**a**)-(**c**) Selection of n=400 random trajectories from each of the three stages measured with DIH-PTV. Trajectories are colored according to their assigned behavior mode. (**d**)-(**f**) The frequency of each behavior mode for each of the growth stages.

Correlation between neutral lipid accumulation and swimming signatures

The experimental results revealed that both the intracellular neutral lipid accumulation and the swimming signatures of *D. primolecta* cells changed under the stress of nutrient limitation. Noticeable similarities in the trend of the changes and timing of the peak values were discovered between the lipid accumulation and swimming speed (Figure 3.10). The neutral lipid content and swimming speed of cells in all the three culture groups increased from the lag phase to the early stationary phase. Cells in the 30%N

cultures achieved their maximum neutral lipid content and swimming speed at the early stationary phase, while the maxima for the 70%N and 100%N cultures were achieved at the late stationary phase. On the other hand, the initial nitrogen availability was observed to have a negative impact on the extent of changes in both neutral lipid and swimming speed. The lower the initial nitrogen concentration in the growth medium, the higher the maximum neutral lipid and swimming speed were. The cells in the 30%N cultures could accumulate neutral lipid content as high as 35.9% of dry weight when their average swimming speed reached the highest value of 81 μm/s, while the peak values of neutral lipid content for the 70%N and 100%N cultures were 20.5% and 16% of dry weight, coinciding with their peak swimming speeds of 67 μm/s and 62 μm/s, respectively.

The statistical results from the one-way analysis of variance (ANOVA) showed the consistency between neutral lipid accumulation and swimming speed variation of *D. primolecta* cells (Table 3.1). Both the neutral lipid and swimming speed of cells changed significantly ($\alpha = 0.05$, $P < 0.01$) across the four growth phases. No significant differences in the neutral lipid content or the swimming speed were determined among the three cultures with various initial nitrogen availabilities in the lag and exponential phases, while the differences in both the neutral lipid content and the swimming speed were significant among the three culture groups at the early and late stationary phases ($\alpha = 0.05$, $P < 0.01$).

The swimming speed of *D. primolecta* cells and the nitrogen transport to the cells by molecular diffusion were quantified by the Peclet number,

$$Pe = \frac{t_{diff}}{t_{swim}} \tag{3.1}$$

where t_{diff} is the diffusion time taken for nitrate to diffuse over an average cell diameter, and t_{swim} is the swimming time taken for *D. primolecta* cells to swim over a distance equivalent to an average cell diameter. The diffusion time and swimming time can be expressed as

$$t_{diff} = \frac{L_c^2}{D_{NO_3^-}} \tag{3.2}$$

$$t_{swim} = \frac{L_c}{v} \tag{3.3}$$

where v is the average swimming speed of the cells (μm/s), L_c is the average diameter of the cells (μm) obtained from the micro-PTV measurements (data shown in Table 3.2), and $D_{NO_3^-}$ is the molecular diffusion coefficient of nitrate (1700 $\mu m^2/s$). Substituting Eq. 3.2 and Eq. 3.3 into Eq. 3.1, the Peclet number can be expressed as

$$Pe = \frac{v L_c}{D_{NO_3^-}} \tag{3.4}$$

The highest Peclet number, Pe = 0.5, in this experiment was achieved by the 30%N cultures at the early stationary phase, accompanied by the highest intracellular neutral lipid content. Two trends were observed between the neutral lipid content and the Peclet number (Figure 3.11). A linear trend from lag to exponential phase (R^2 = 0.97, 0.2 < Pe < 0.31) and another linear trend with a much steeper slope for exponential, early stationary and late stationary phases (R^2 = 0.94, 0.31 < Pe < 0.5) were observed. The coefficient of determination, R^2, indicates that at least 94% of the variations of the neutral lipid content

in the cells are explained by the linear models of neutral lipid content versus normalized swimming speed (Peclet number). Therefore, the analysis supports our hypothesis that the swimming speed of the unicellular green alga *D. primolecta* is correlated with the intracellular neutral lipid accumulation. The results indicate a transition point occurring around the late exponential phase. In the lag and exponential phases, the nitrogen availability was sufficient for the cells to grow, so the change in swimming speed was not triggered by the nutrient deficiency, and therefore the neutral lipid content only increased slightly with the increase of Peclet number. In contrast, once the cells entered the late exponential phase (i.e., after the time point of the maximum growth rate), the nitrogen availability in the environment shifted from sufficient to limited, which triggered the increase of the swimming speed of cells (greater Peclet number) to actively seek the nutrient while at the same time increasing the neutral lipid accumulation in the cells. This linear correlation corresponding to the late exponential – stationary phases provides a way to reflect the neutral lipid accumulation by measuring the swimming speed of cells under the conditions of nutrient limitation and nutrient deprivation.

The changes of swimming modes identified from the *D. primolecta* swimming trajectories also correspond to the intracellular neutral lipid content changes across growth phases. The statistical one-way ANOVA results indicate that the percentage of cells exhibiting fine motions are statistically different at each growth phase ($\alpha = 0.05$, $P < 0.01$) (Table 3.3). The variation of swimming behaviors across growth phases could be associated with the nutrient availability and chemotaxis of microalgal cells. The nutrient distribution in the growth environment is hardly homogeneous – nutrient patchiness forms for many reasons. Chemotactic response of *Dunaliella* cells to the ammonium and

several amino acids have been reported [125]. Akin to the run-tumble transitions of bacterial chemotaxis [126], the cells move towards a nutrient patch through the gross (linear and meandering) motions while remaining in the patch to utilize the nutrients through the fine (helical and circular) motions. At early growth phases, the nutrients are sufficient, so the frequency of fine motions is high since the shorter net displacement of helical and circular motions allow the cells to maintain in a nutrient-rich region for longer time and maximize the nutrient uptake. When the photosynthesis is limited by the low nutrient, the algal cells tend to become positively chemotactic which makes them travel faster in linear/meandering motions towards certain attractants [127]. At the stationary growth phase, the fine motions are significantly reduced due to nutrient scarcity and most of the cells exhibit larger net displacement with the gross motions to explore potential nutrient sources.

The reduction of the fine motions corresponds to the accumulation of intracellular neutral lipid content as both are induced by the nutrient limitation. When the intracellular neutral lipid content reached the maximum at the early stationary phase, the fine motions were hardly seen. There were approximately 8-fold differences in both the fine motions and neutral lipid content between the exponential and early stationary phases for the 30%N cultures. The strength of transition suggests that the relative frequency of behavior modes could be a potential indicator for the growth phase, and by association the neutral lipid content.

Hansen *et al.* [32] conducted experiments to investigate the impact of nitrogen starvation on the total fatty acids and swimming velocities of freshwater alga, *Chlamydomonas*

reinhardtii. The study demonstrated the increase of swimming velocities of cells exposed to short-term (~1 hr) nitrogen removal and the variation of swimming velocities of cells incubated in media with different initial nitrogen levels for 3 days. Also, the results demonstrated no significant change in swimming speed of *Chlamydomonas reinhardtii* cells when phosphate level was altered. Our study, in contrast to their relatively short-term experiments, conducted time-course experiments over the entire growth cycle (lag-exponential-stationary growth phases) to investigate the changes in the swimming speed, swimming modes, and the total neutral lipid content in the cells of the marine green alga, *D. primolecta*. Both studies demonstrated similar results of the change in swimming speed of cells in the nitrogen-reduced medium. We also revealed the timing of the maximum swimming speed and maximum neutral lipid content across growth phases. In addition, we elaborated the statistically different swimming modes of cells during the lag-exponential-stationary growth phases.

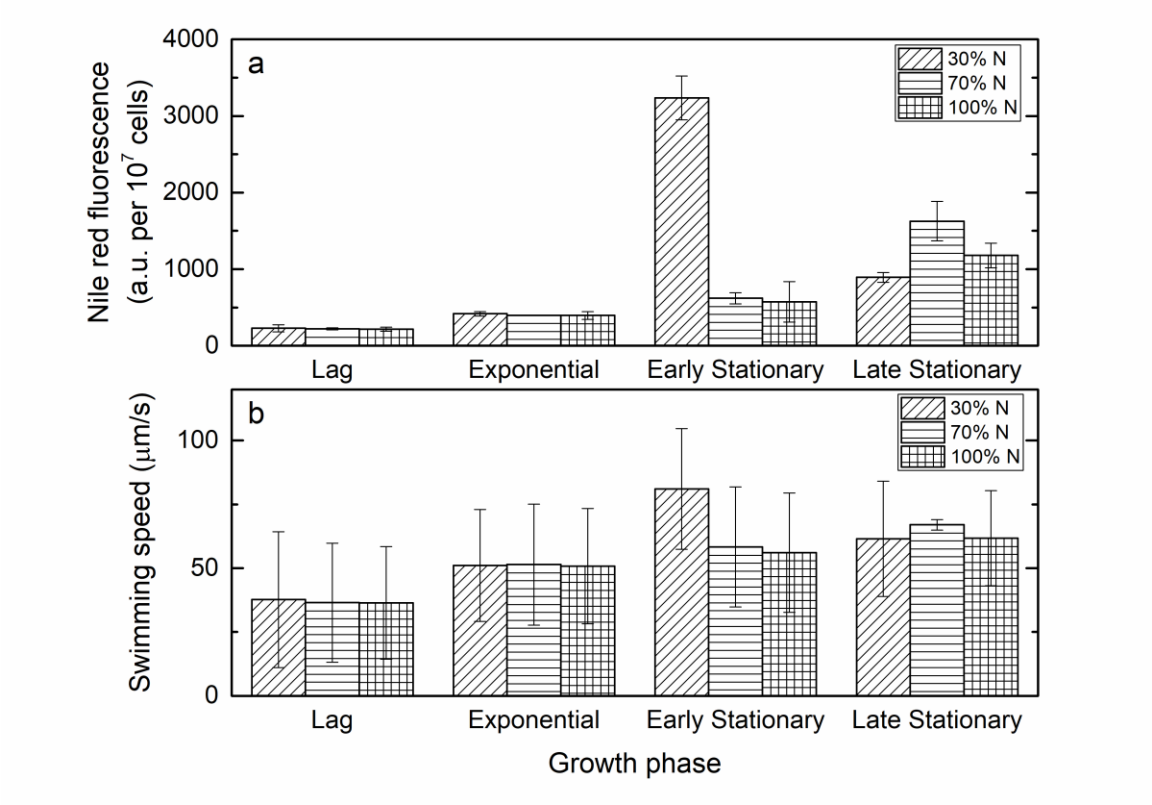

Figure 3.10. Intracellular neutral lipid content and swimming speed of *D. primolecta* at four growth phases. (**a**) Intracellular neutral lipid content reflected by the intensity of Nile red fluorescence for 30%N, 70%N and 100%N cultures at four growth phases. Error bars correspond to the s.d. (n=4). (**b**) The average swimming speed of 30%N, 70%N and 100%N cultures at four growth phases. Error bars correspond to the s.d. (n=200 for lag phase, n=400 for exponential phase and n=600 for early stationary and late stationary phase).

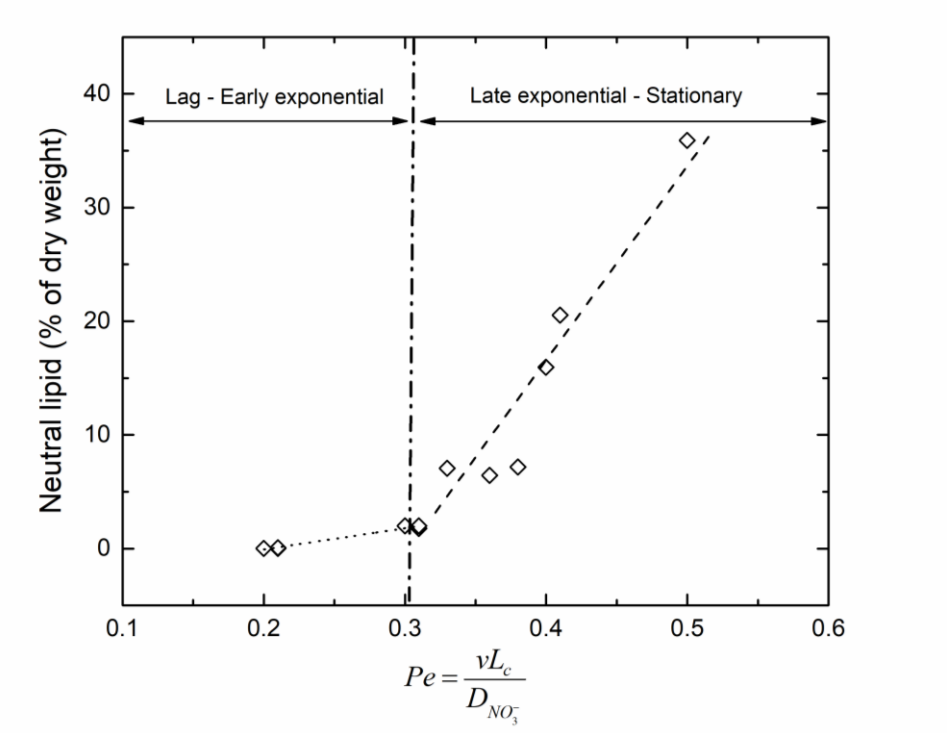

Figure 3.11. Neutral lipid content versus the Peclect number of *D. primolecta* cells. Data points (*n*=12) are from 30%N, 70%N and 100%N cultures at four growth phases. The vertical dash dot line (−·−) separates the graph into two areas based on growth phases: from lag to early exponential phase on the left, and from late exponential to stationary phase on the right. The dot line (··) corresponds to the linear trend line fitted to the data points from the lag and exponential phases (*n*=6, R^2=0.97). The dash line (−−) corresponds to the linear trendline fitted to the data points from exponential, early stationary and late stationary phases (*n*=9, R^2=0.94).

Table 3.2. Analysis of variance (one-way ANOVA) results of the micro-PTV measurements at the significance level $\alpha = 0.05$.

Factor	Source	df	SS	MS	*F* value	*P* value
Growth phase	30%N neutral lipid	3	1.7E7	6.0E6	215.2	2.2E-9
	70%N neutral lipid	3	4.0E6	1.3E6	44.7	9.9E-6
	100%N neutral lipid	3	2.1E6	7.1E5	20.1	9.1E-5
Initial nitrate concentration (N)	Lag phase neutral lipid	2	324.2	162.1	0.1	0.9
	Exponential phase neutral lipid	2	5.3E3	2.7E3	5.0	0.1
	Early stationary phase neutral lipid	2	1.5E7	7.6E6	110.7	1.5E-6
	Late stationary phase neutral lipid	2	1.0E6	5.1E5	12.4	2.6E-3
Growth phase	30%N swimming speed	3	3.8.5E5	1.3E5	233.9	0
	70%N swimming speed	3	1.6E5	5.2E4	98.6	0
	100%N swimming speed	3	1.0E5	3.5E4	74.2	0
Initial nitrate concentration (N)	Lag phase swimming speed	2	216.4	108.2	0.2	0.8
	Exponential swimming speed	2	77.7	38.9	0.1	0.9
	Early stationary phase swimming speed	2	2.3E5	1.1E5	206.6	0
	Late stationary phase swimming speed	2	1.2E4	5.8E3	12.9	2.7E-6

Table 3.2. Average diameter *(L_c)* and standard deviation (σ) of *D. primolecta* cells for each culture at each growth phase.

Initial nitrate concentration	Growth phase	Number of cells	L_c (µm)	σ (µm)
30%N	Lag	200	9.57	2.41
	Exponential	400	10.43	2.73
	Early stationary	600	10.52	2.47
	Late stationary	600	10.55	2.53
70%N	Lag	200	9.98	2.53
	Exponential	400	10.14	2.48
	Early stationary	600	9.59	2.62
	Late stationary	600	10.33	2.68
100%N	Lag	200	9.55	2.52
	Exponential	400	10.05	2.20
	Early stationary	600	10.88	2.52
	Late stationary	600	9.46	2.25

Table 3.3. Analysis of variance (one-way ANOVA) results of the DIH-PTV measurements at the significance level $\alpha = 0.05$.

Factor	Source	df	SS	MS	*F* value	*P* value
Growth phase	30%N swimming speed	2	1.4E3	711	66.7	3.5E-11
	30%N fine motion percent	2	1.4E4	6.8E3	52.4	5.0E-10
Growth phase (Exponential vs. Early Stationary)	30%N swimming speed	1	111.7	111.7	11.7	0.003
	30%N fine motion percent	1	1.0E3	1.0E3	88.3	2.3E-8

Application of swimming signatures to biofuel production

Our findings of the association between microalgal swimming signatures and intracellular neutral lipid content inspire a low-cost scalable sensor system utilizing DIH-PTV for high-throughput monitoring of the neutral lipid content in industrial-scale biofuel production. Such a system would improve control of cultivation conditions and harvest timing of microalgae, leading to a substantial biofuel yield and low-cost algae-based biofuels. Conventional methods for intracellular neutral lipid determination, such as lipid separation by column or thin-layer chromatography, fatty acid profiling by gas chromatography, and fluorometric determination of neutral lipids by Nile red / BODIPY

[119, 128, 129, 130, 131, 132], either require tedious extraction and/or transesterification work and expensive equipment, or test only small volume samples which are less representative for large-scale cultivations. In contrast to current lipid measurement methods, DIH-PTV has much higher throughput and better scalability. DIH sensors are low cost, small, and easily integrated with other instruments so that a network of DIH sensors could monitor multiple sites efficiently in open ponds or closed photo-bioreactors for industrial-scale biofuel production.

Exploiting microalgal swimming signatures as a possible indicator in microalgal growth and intracellular neutral lipid accumulation monitoring will potentially influence the pipeline of microalgal biodiesel production by enabling more optimal harvest timing and control of cultivation conditions (Figure 3.12). Our results showed a 3.6-fold increase in the intracellular neutral lipid content within only three days. The neutral lipid content at the early stationary phase is 20 folds higher than that at the exponential phase and 4.7 folds higher than that at the late stationary phase. Since lipid production is very sensitive to harvest timing, utilizing the drastic decrease of fine motions and increase in swimming speed to predict the timing of maximum neutral lipid accumulation can potentially enable more optimal harvest timing. This timing will also reduce the cost of consumables (including water, nutrient supplies, and electricity), some of the most substantial costs in biofuel production [133]. This can lower the net cost per unit biodiesel production, which is a major bottleneck inhibiting commercialization [133, 134].

These factors will together decrease the net energy ratio (NER, the energy input in cultivation and refinement divided by the energy output from the biomass), which is an

indicator of environmental sustainability and the overall energetic effectiveness of the biodiesel production [116]. Achieving a lower NER will make the microalgal biodiesel production more economically competitive. Besides reducing the net cost per unit biodiesel, the higher biomass and lipid yield can also result in increased beneficial by-products from the lipid extraction and transesterification processes. Appropriate use of the remaining biomass for animal feed, ethanol, or biogas, and glycerol for food industry, pharmaceutical applications, or personal care will contribute to the commercial viability of microalgal biofuel production [112, 135]. Overall, exploiting swimming signatures in a low-cost scalable sensor system for inline high-throughput monitoring of microalgal growth and neutral lipid accumulation will potentially lead the microalgae-based biofuel production to a more cost-effective and energy-effective future.

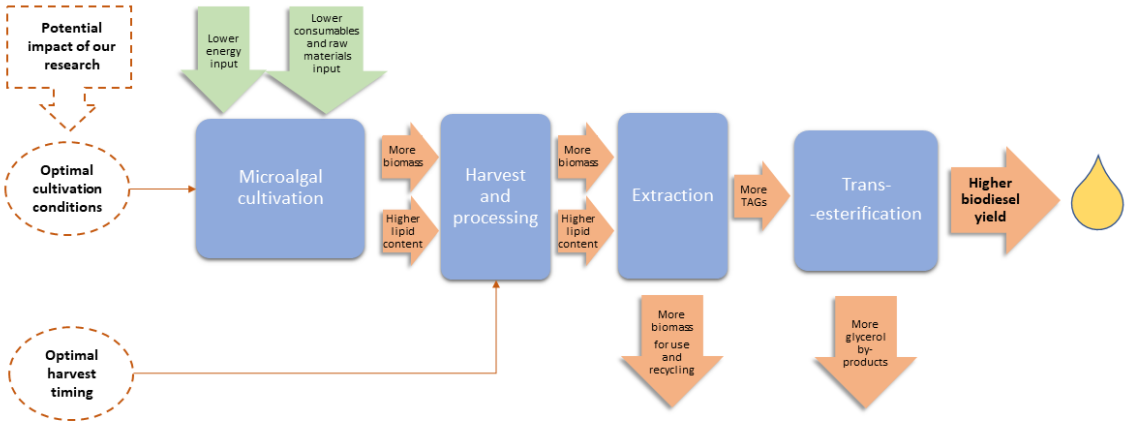

Figure 3.12. Potential impacts of exploiting swimming signatures in microalgal growth and lipid monitoring on the microalgal biodiesel production pipeline.

Conclusions

We quantified the neutral lipid accumulation and analyzed the swimming signatures (speed and trajectories) of the motile green alga, *D. primolecta*, during the lag-exponential-stationary growth cycle at different nutrient concentrations. We discovered significant changes in the neutral lipid content and swimming signatures of microalgae across growth phases. The swimming speed and neutral lipid content of *D. primolecta* cells increased from the beginning of a growth cycle until reaching a peak when the nutrient deprivation occurred and the cell population stopped increasing. The timing of the maximum swimming speed coincided with the maximum lipid content and both maxima occurred under nutrient stress at the stationary growth phase. Both the timing and the extent of the peaks were negatively influenced by the initial nitrogen availability in the cultures. Furthermore, the swimming trajectories suggested statistically significant changes in swimming modes at the stationary growth phase when the maximum intracellular neutral lipid content was observed. The frequency of fine motions of *D. primolecta* cells significantly decreased from the exponential to early stationary phase. Our results provide the potential exploitation of microalgal swimming signatures as possible indicators of the cultivation conditions and the timing of microalgal harvest to maximize the lipid yield for biofuel production. The findings can also be implemented to explore the production of food and antibiotics from other microalgal metabolites with low energy costs.

Chapter 4

Impacts of Abiotic Variables on Vertical and Temporal Heterogeneities of Cyanobacteria and Microcystin Concentrations in Stratified Lakes

Introduction

In Chapter 2 and 3, the impacts of environmental variables including temperature and nutrient availability on the growth, motility (buoyancy regulation) and metabolism (neutral lipid production) of cyanobacteria and lipid-producing microalgae are investigated through a set of experimental studies. In this chapter, the discussion is extended to a field study of freshwater lake systems to explore the vertical and temporal variations of cyanobacteria and microcystin (MC) concentrations and influence of

physical and chemical environmental variables on the cyanobacteria biovolume growth and metabolites (MCs) production.

Cyanobacteria blooms have been of global concern in recent decades due to its adverse impacts on water quality, ecological community and human health. Proliferations of cyanobacteria biomass can lead to deoxygenation of the water body, fish kills, unpleasant odors and taste, alterations of food webs, and the production of cyanotoxins posing a threat on animal and human health [1, 3, 41, 136]. One of the highly concerned cyanotoxins is the cyclic heptapeptide toxins, MCs, which are the secondary metabolites of some cyanobacteria, such as *Microcystis* and *Dolichospermum* (formerly named *Anabaena*). The structure of MCs made it chemically stable so they can persist in water for a long time. There are many variants of MCs and Microcystin-leucine arginine (MC-LR) has been reported to be the most common and potent one [137]. MCs can be accumulated and transferred to higher trophic levels through the food chain [137, 138]. In this way, MCs not only threaten the aquatic organisms, but also pose health risks on the terrestrial animals, including human beings, exposed to MC contaminated drinking water, MC accumulated aquatic products or agricultural products irrigated with MC contaminated water. [137, 139, 140]. Significant correlations between cyanotoxin and liver-disease deaths have been founded in the US [41]. Exposure to MCs has also been reported as adverse effects on the lakeside soil microbial community and soil health [140].

Abiotic environmental factors including water temperature, macronutrients such as nitrogen (N) and phosphorus (P), light intensity and turbulence potentially play roles in

the cyanobacterial blooms and their toxin production [40]. The ability of competitive growth at high temperatures makes cyanobacteria blooms prevalent in summers [21, 43]. Some genera of cyanobacteria are capable of fixing nitrogen for metabolism when N sources are limited [141, 142]. Some genera contain gas vesicles and are capable of buoyancy regulation and thereby adjusting their vertical positions in the water column to obtain optimal growth conditions [10, 50]. These cyanobacteria prefer stable water columns with lower mixings as well as relatively high temperature environment, which assist their buoyancy regulations [13, 79, 143, 144]. There are ongoing debates on the role of N and P in the eutrophication control associated with cyanobacteria bloom mitigation [40, 41, 145]. Increasing number of studies are showing that dual nutrients control of N and P is necessary, since the abundance of dual nutrients and the N:P ratio have greater impacts on the cyanobacteria abundance and toxin production [40, 41, 43, 146]. Moreover, toxic cyanobacteria strains tend to show stronger response to elevated temperature and nutrient availability [25]. The production of MCs and the toxicity are also affected by the nutrients and temperature [63, 147, 148, 149].

Under the global climate change scenario, water environments are expected to experience elevated temperatures, prolonged and intensified stratification periods, altered frequency and intensity of storm events, and modified nutrient dynamics, all of which are directly or indirectly related to the probability of increasing cyanobacteria blooms [44, 50, 150, 151]. Meanwhile, the over-enrichment of nutrients in the water environments due to increasing agricultural, urban and industrial expansion are promoting the frequency and intensity of cyanobacteria blooms and toxin production [146, 152]. It is essential to understand the characteristics of cyanobacteria blooms under the current climate change

and nutrient enrichment scenarios, and to explore the impact of relevant environmental factors on the bloom occurrence and toxicity. So far, a considerable number of such studies have been conducted for large lakes in the world, such as Lake Erie (USA-Canada), Lake Kasumagura (Japan), Lake Ocheechobee (USA), Lake Taihu (China), Lake Victoria (Kenya) and Lake Ijsselmeer (Netherland) [153, 154, 155, 156, 157], while limited studies have been reported for relatively small to medium lakes which stratify in summers, which are essential drinking, recreational and agricultural water resources broadly distributed worldwide. The dynamics of cyanobacteria blooms in such lakes frequently experience more rapid changes compared to large lakes, due to the broader range of stratification conditions throughout the blooming season [158, 159].

Therefore, the present study aims to investigate the temporal and vertical heterogeneities of cyanobacteria and MC concentration in a small eutrophic and stratified lake during summer. We investigated how the heterogeneities of cyanobacteria and MC concentrations are affected by the abiotic factors. We hypothesized that the variability of cyanobacteria and MC concentrations over the lake depth is significantly correlated with the thermal stratification dynamics. Furthermore, the composition of cyanobacteria community is associated with the vertical and temporal variabilities of nutrients availability.

Materials and Methods

Site description

Ramsey Lake (45˚12’27’’N, 93˚59’43’’W) is a residential and recreational lake located in Wright County in Minnesota (Figure 4.1a). It has a surface area of 1.28 km^2 and a maximum depth of 24.4 m with a mean depth of 6.5 m. The watershed land use is primarily agricultural. Minnesota Pollution Control Agency (MPCA) has set monitoring sites on Ramsey Lake and have reported data starting from 1980. Ramsey Lake is classified as a eutrophic lake, with the annual occurrence of excessive algae reported by MPCA and residents in the neighborhood. The lake becomes stratified during summers, as a result of the relatively small surface area and its water depth. Ramsey Lake was chosen as the research site because of its eutrophic status, thermal stratification, and water safety concerns related to excessive algae occurrence.

In situ research station

A floating research station designed and built at the St. Anthony Falls Laboratory (University of Minnesota, USA) was deployed onto the Ramsey Lake and anchored in the lake during the summer of 2018, from May to October (Figure 4.1b). The deployment location of the research station had a maximum water depth of 17.5 m, which enables profiling through the epilimnion, metalimnion and hypolimnion zones. The research station consisted of three major systems conducting synchronized monitoring, with similar configurations as described in Wilkinson *et al*. [160] and [161]: 1) a meteorological station 1.5-m above the water surface, collecting wind speed, wind direction, precipitation, air photosynthetically active radiation (PAR), air temperature and

relative humidity data; 2) an anchored thermistor chain, measuring the water temperature every 1m from surface to 8 m, and every 2 m from 8 to 14 m; and 3) a water quality profiler, Hydrolab DS5 Water Quality Multiprobe (Hach Environmental, CO, USA), collecting data of water temperature, dissolved oxygen, PAR, pH, specific conductivity and phycocyanin fluorescence (fluorometry produced by Turner Designs, CA, USA) every 0.5 m from 1 to 5 m and every 1 m from 5 to 14 m. The meteorological station and the thermistor chain both collected and updated data every 5 minutes, while the water quality profiler reported data every 2 hours. All the data was transferred to the main data logger (Campbell Scientific, UT, USA), from which the data was accessible by users via wireless data transfer to a server.

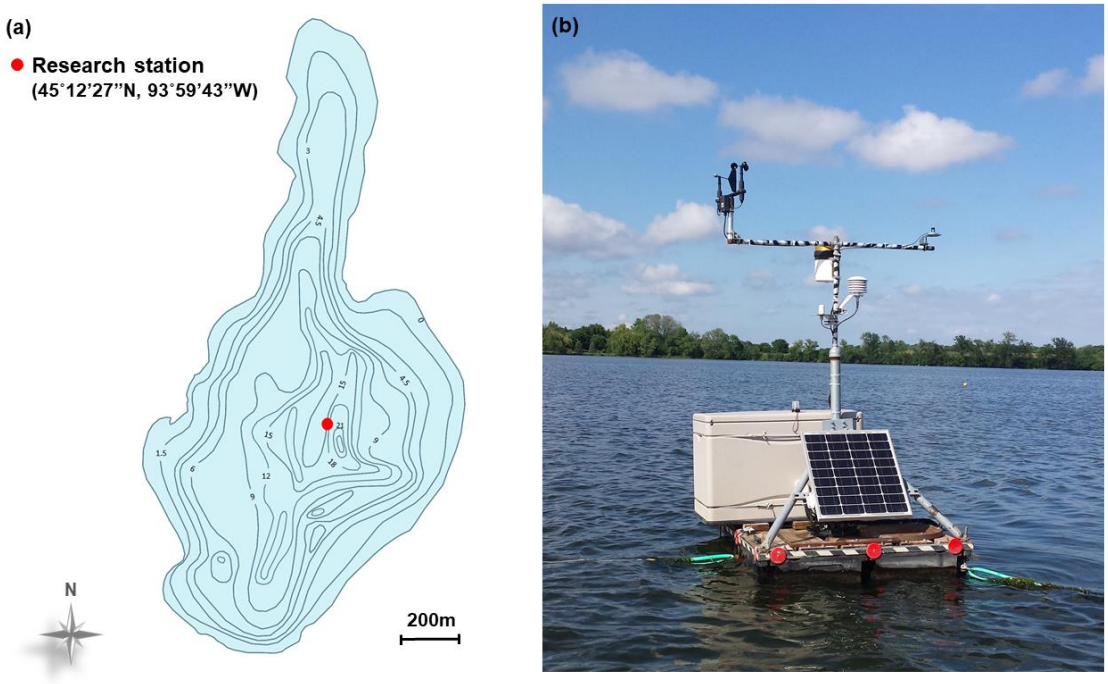

Figure 4.1. (**a**) Bathymetry of Ramsey Lake (contours labeled in the unit of meters) and location of the research station. (**b**) Configuration of the research station (photo credit: Jiaqi You).

Water Sample Analyses

Sample collection

Water samples (1 L each) were collected weekly or bi-weekly adjacent to the research station at ten selected depths from surface to 14 m. For each sample, 14 mL was preserved in Lugol's iodine solution at 2˚C for further microscopic observation, 45 mL was stored at -20˚C for total MC (free + cell bound) analyses, and the rest was filtered through GF/F filters (Whatman, GE Healthcare, UK). Filters and filtrates were stored at -20˚C for further chemical analyses.

Measurement of phycocyanin and nutrients

All the chemical measurements were conducted in duplicate from each water sample using Trilogy Laboratory Fluorometer (Turner Designs, CA, USA) (detailed method in Appendix A). Phycocyanin concentrations were measured with an orange module (PN 7200-044) using the similar methods as in Kasinak *et al.* [162]. The C-Phycocyanin from Spirulina (Sigma-Aldrich #P2172-10MG, Merck KGaA, Germany) was used in standard calibrations. The nitrate/nitrite concentrations were analyzed using the nitrate/nitrite module (PN 7200-074) with the LaMotte Nitrate/Nitrite Test Kit (LaMotte Company,

Maryland, USA). The phosphate concentrations were analyzed using the phosphate absorbance module (PN 7200-020).

Plankton identification and cyanobacteria biovolume

Preserved water samples were observed under an optical microscope (Nikon Eclipse E400) with a gridded Sedgewick-rafter counter (Wildlife Supply Co., FL, USA) at 100 X magnification. Four of 1mL replicates from each preserved water sample were observed to identify the dominant plankton genera. Microscopic images were recorded for the water samples at 0, 2 and 4 m depths in July and August, the period of thermal stratification and cyanobacteria dominance suggested by the data and samples, by randomly selecting 25 of 0.1 mm × 0.1 mm × 1 mm units from each replicate (i.e. 0.1 mL in total for each water sample). Plankton identification was aided by references including Canter-Lund and Lund [163], Bellinger and Sigee [164], Wehr *et al.* [7] and Nienaber and Steinitz-Kannan [165].

Microscopic images were analyzed using ImageJ 1.52i (National Institute of Health, USA). The unit biovolume (BV) of the three dominant cyanobacteria genera were estimated by: 1) multiplying colony area by the colony depth (estimated using microscope fine focus) for *Microcystis* spp. colonies, 2) summing up volumes of cells in a filament (assuming spherical cells and measuring diameters) for *Dolichospermum* spp., and 3) summing up volumes of filaments (assuming cylindrical cells and measuring diameters and lengths) for *Aphanizomenon* spp.. The shape assumptions of cyanobacteria and other plankton were supported by references including Hillerbrand *et al*. [166], Bellinger and Sigee [164] and Napiórkowska-Krzebietke and Kobos [167]. *Microcystis*

colony equivalent diameters (*D*) were estimated from the area of *Microcystis* colonies (*A*), assuming equivalent circular colony shape (i.e., $D = \sqrt{\frac{4A}{\pi}}$).

Toxin analyses

The concentrations of total MC (free + cell-bound) and the free MC (MC released in the water column, collected in the GF/F filtered water samples) in water samples were analyzed following the guides of EPA Methods 546 (USEPA, 2016) using the Microcystin-ADDA ELISA Microtiter Plate kits (PN520011, Abraxis Inc., PA, USA). The 96-well microplates were read by a BioTek EL800 96-well microplate reader with a wavelength of 450 nm (Winooski, VT, USA). Samples were from water samples at depths of 0, 2, 4, 6 and 8 m during July and August. The samples for total MC analyses were freeze-thaw cycled three times and filtered through GF/F filters (Whatman, GE Healthcare, UK) before analyses. All the samples were measured in duplicate. The cell-bound MC concentrations were estimated by subtracting the free MC from the total MC.

Physical Data Analyses

Physical data recorded by the research station was processes with Microsoft Excel (Microsoft Corporation), Origin 2016 (OriginLab Corporation) or Matlab R2018a (MathWorks Inc., Massachusetts, USA). The lake bathymetry data was obtained from the Minnesota Department of Natural Resources and processed with QGIS 3.4.12 (QGIS Geographic Information System, Open Source Geospatial Foundation Project). The bathymetry, water temperature and wind speed data was used as input for the Lake

Analyzer (codes developed by the Global Lake Ecological Observatory Network) operated in Matlab to generate the estimations of thermocline depths (Z_{TD}), top and bottom depths of metalimnion, shear velocity (u_*), Schmidt stability (St), Lake Number (LN) and mode-1 vertical seiche period [168]. All the meteorological and temperature reported from now on were averaged over the mode-1 vertical seiche period to capture the seiche variability.

Statistical Analyses

A principal component analysis (PCA) was conducted using Matlab with 18 observations (0, 2 and 4 m data of six sampling dates in July and August) and seven variables (Cyanobacteria BV, total MC, *Microcystis* colony equivalent *D*, BV ratio of *Microcystis*/(*Dolichospermum* + *Aphanizomenon*), water temperature, u_*, and N/P ratio). The data were scaled using the unit variance scaling method prior to analyses [169]. One-way ANOVAs ($\alpha = 0.05$) followed by Tukey's tests were conducted using Origin to determine the significance of the temporal ($df = 6$) and vertical ($df = 2$) variations of Microcystis colony equivalent *D*. Linear regressions ($\alpha = 0.05$, $df = 5$) were conducted using Matlab to investigate the correlation between phycocyanin concentration and cyanobacteria BV, between data of BV, MC and water column stability, and between nutrient ratio and cyanobacteria genera ratio.

Results and Discussion

Meteorological Conditions and Thermal Stratification

The wind speed, air PAR and air temperature data obtained showed relative consistency with slight decline throughout the season from late June to mid-September, while the differences between water surface temperature and air temperature (i.e., $T_{surface} - T_{air}$), as well as the water temperature profiles showed temporal variations (Figure 4.2). The water surface temperature was most of the time higher than the air temperature until late August, after which the temperature differences changed to negative values. The temperature difference facilitated a consistent cooling process and natural convection of the lake water surface until late summer. The contours of water temperature profiles over time indicated a persistent thermal stratification with high water surface temperature that occurred from the beginning of July to late August. The Schmidt Stability (St) is an ecologically relevant parameter, indicating the amount of work that would be required to mix the water temperature in the lake uniformly over the water column depth. Therefore, St indicates the strength of stratification, which has been shown to affect the proliferation of cyanobacteria biomass [107, 170, 171]. The St showed a similar pattern as the difference between surface water temperature and air temperature did, with several peaks from mid-July to mid-August.

Cyanobacteria BV were obtained for 0, 2, 4, 6, 8, 12 m for seven sampling dates: July 6th, July 13th, July 20th, July 27th, August 2nd, August 13th and August 30th. We demonstrated in Fig. 2f that the maximum thermocline depth-averaged cyanobacteria BV started on July 20th, following the St peak of the season. The second and third highest BV also

followed a small peak of St, respectively. The consistency of the time lag between BV and St peaks may imply the delay in the response of cyanobacteria proliferation to the onset of a calm and stable water column.

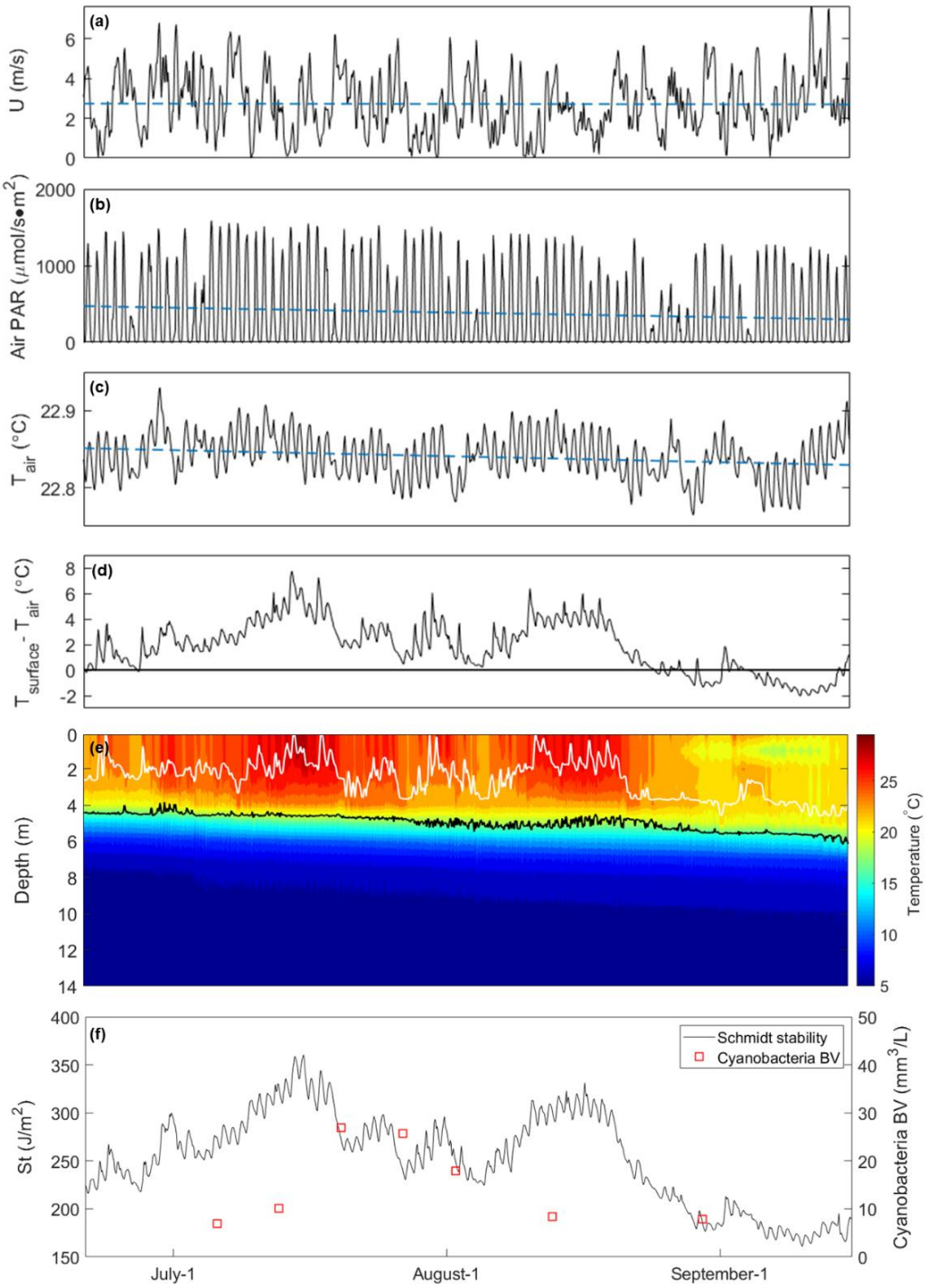

Figure 4.2. Meteorological and thermal stratification conditions from June 21st to September 15th. (**a**) Wind speed, U (**b**) Air PAR. (**c**) Air temperature, T_{air}. (**d**) Difference between water surface temperature and air temperature, $T_{surface}$ - T_{air}. (**e**) Water temperature profile contours with the mixed layer depths (white line) and the thermocline depths (black line). (**f**) Schmidt stability (St) and cyanobacteria biovolume (BV). Each BV data point was averaged with duplicate samples from 0, 2 and 4 m.

Dominant Cyanobacteria

Cyanobacteria were found to dominate the plankton community in Ramsey Lake during the thermal stratification period, with three major genera: *Microcystis* spp., *Dolichospermum* spp. and *Aphanizomenon* spp. (Figure 4.3). The detected phycocyanin level above the thermocline for the entire July and August was higher than 10 µg/L, which is an equivalent phycocyanin threshold for the WHO moderate risk alert of cyanobacteria blooms [172, 173]. The blooming season from July to August coincided with the duration of strong thermal stratification, which made it the period that our study focused on. The correlations between phycocyanin concentration and measured cyanobacteria BV were established by linear regression models (Figure 4.4) and the cyanobacteria BV values reported hereinafter were estimated from phycocyanin concentrations using the calibration equations. Figure 4.3b showed the composition of cyanobacteria community above the thermocline depth of seven sampling dates, which revealed an increase of cyanobacteria BV from July 6th to July 20th, including a drastic increase in *Microcystis* and a relatively small but notable increase in *Dolichospermum*

and *Aphanizomenon*. Not only the total cyanobacteria but also each of the three major genera reached their maximum BV on July 20th. *Microcystis* spp. dominated the cyanobacteria community during the blooming season, particularly from July 20th to August 2nd.

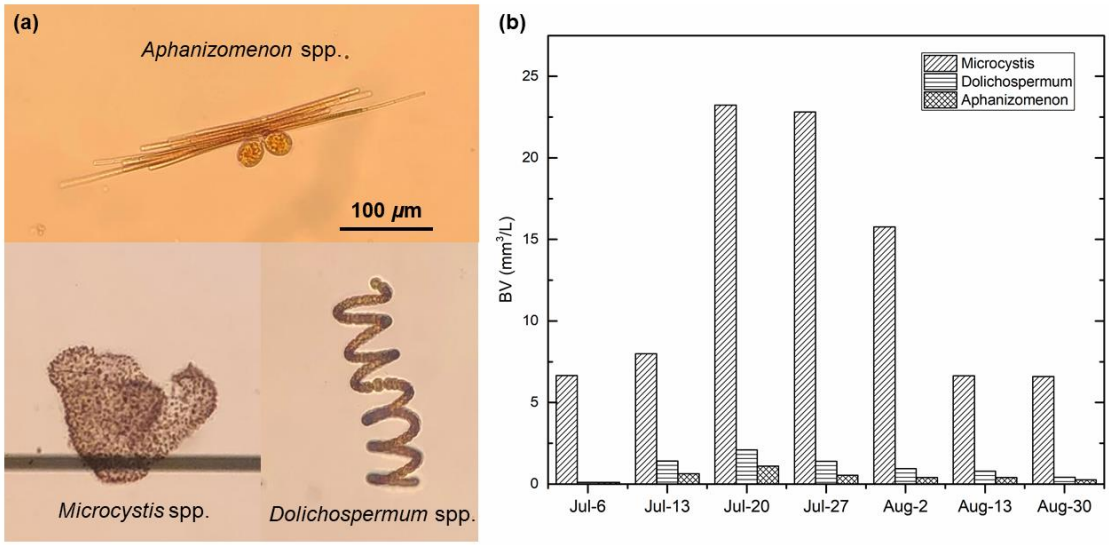

Figure 4.3. (**a**) Microscopic images of the three dominant cyanobacteria genera in Ramsey Lake in summer 2018. (**b**) Thermocline depth-averaged biovolume (BV) of the dominant cyanobacteria genera for seven sampling dates during July and August 2018. The BVs were averaged over data of 0, 2 and 4 m.

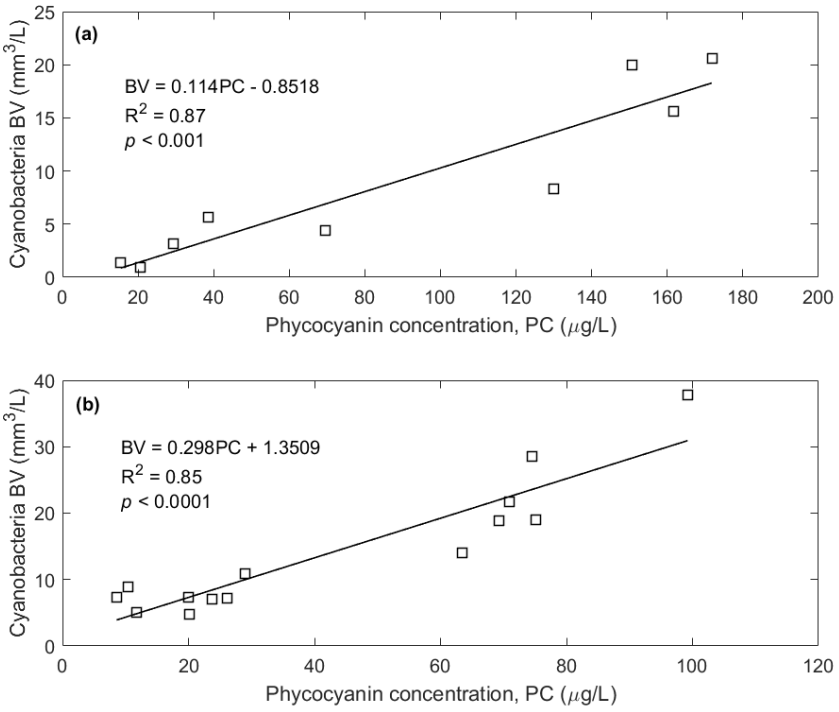

Figure 4.4. Linear calibration curves of cyanobacteria biovolume (BV) versus Phycocyanin concentration (PC) for (**a**) first period from July 6th to July 20th, and (**b**) second period from July 27th to August 30th. The solid lines represent the linear trendlines.

Principal Component Analysis

The PCA analyzed the physical and chemical factors that potentially affect the cyanobacteria BV, colony size and MC concentration. By displaying the systematic variation of the matrix analyzed, the PCA biplot illustrated the potential correlations between variables and the similarities among observations in the first two principal components (Figure 4.5). The grouping of the cyanobacteria BV, total MC and the

Microcystis colony equivalent *D* indicated close correlations between them. The ratio of *Microcystis* BV (BV_{Mic}) over *Dolichospermum* BV (BV_{Dol}) plus *Aphanizomenon* (BV_{Aph}), i.e., the ratio between non-N-fixing cyanobacteria and the N-fixing cyanobacteria, was closely related with the nutrient availability ratio of N and P, expressed as $(NO_3^- + NO_2^-)/PO_4^{3-}$. The water temperature (T) and shear velocity (u_*) were both positioned on the positive side of the first principal component whereas not grouped closely with the BV, MC and *Microcystis* colony *D*, which implies the potential indirect positive correlations between them. On the other hand, the distributions of the scores showed the similarities and differences of the data set on the first two principal components. For instance, July 20th data and July 27th data shared similarities in cyanobacteria BV, total MC and *Microcystis* colony *D*, while showed differences in the cyanobacteria genera ratios. Since the data was collected from three different depths of six sampling dates during the blooming season, the distribution of data scores suggested both vertical and temporal heterogeneities of the variables. Encouraged by the PCA results, these heterogeneities and their correlations were further analyzed in this study.

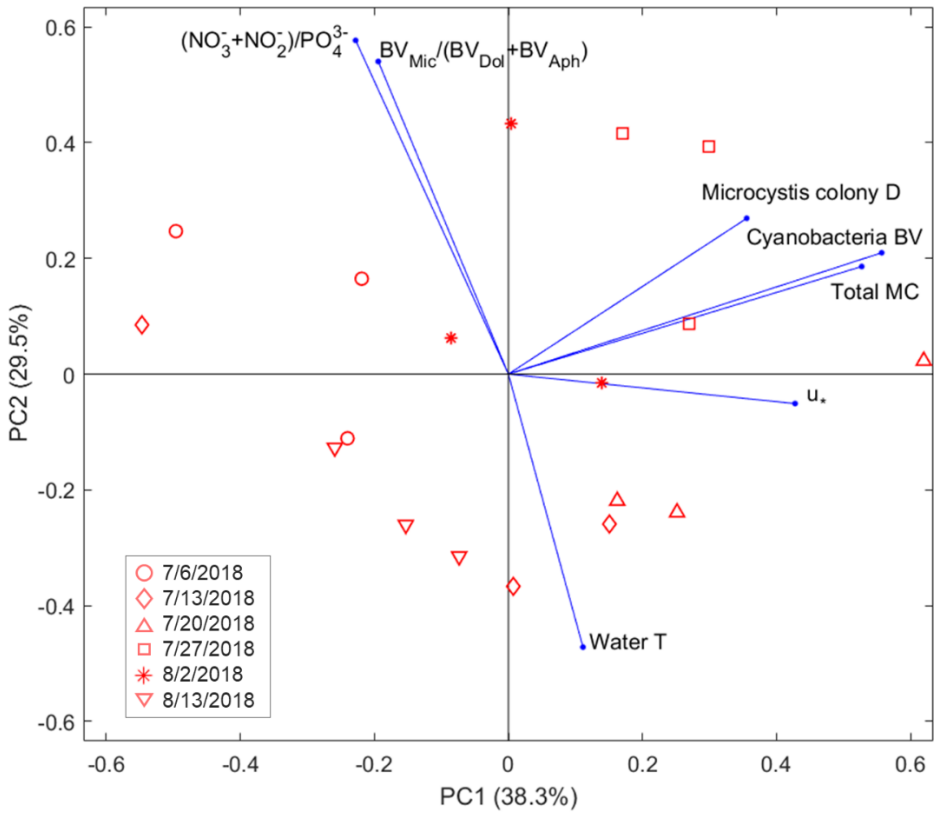

Figure 4.5. The PCA biplot of the first two principal components (PCs). The first PC explained 38.3% of variation and the second explained 29.5%. The scatter symbols represent the principal component scores and the lines with solid circles at the end represent the loading vectors of the seven variables. The data set covers the observations at 0, 2 and 4 m of six sampling dates.

Vertical Heterogeneities of Cyanobacteria and MC Concentrations

Cyanobacteria BV and total MC (free + cell-bound) profiles of six sampling dates showed their vertical heterogeneities in the stratified water column (Figure 4.6). The profiles revealed remarkable consistency between the cyanobacteria BV and total MC in

the vertical variations. The peaks of total MC occurred at the depth where the maximum cyanobacteria BVs were observed. Both BV and MC levels above the thermocline depth (0, 2 and 4 m data) were high and varied across sampling dates. In contrast, the levels below the thermocline depth remained low without significant variations. A surface bloom of cyanobacteria with relatively low BV occurred on July 13th. When the BV drastically increased from July 13th to July 20th, the surface bloom turned into a sub-surface bloom that persisted until mid-August. The findings agreed with the reports from the residents describing the deep green watercolor without a thick scum on the water surface. During the sub-surface blooms, the mixed layer depths were more in-depth than that during the surface blooms and the maximum BV occurred right above the mixed layer depths.

The total MC level in the first two meters of water from July 6th to August 2nd exceeded the World Health Organization (WHO) guideline value of 1 µg/L expressed as total MC-LR [143], and the United States Environmental Protection Agency (USEPA) guideline value of 0.3 µg/L MC for infants and pre-school age children and 1.6 µg/L MC for school-age children and adults in drinking water [174]. The total MC concentration ranged from 2 to 4 µg/L at the water surface. It reached > 4 µg/L at 2 m in sub-surface blooms, which also exceeded the guideline/lowest action levels for MCs in the recreational water use advised by WHO and many states in the US [175]. The MCs were primarily contained in the cells (cell-bound MCs) and the concentration of MCs released into the water remained relatively low throughout the blooming season (Figure 4.7). The cell-bound MC concentration showed similar vertical variations as the total MC concentration.

The average *Microcystis* colony equivalent *D* depicted different vertical variations from the cyanobacteria BV and MC concentrations (Figure 4.8). The one-way ANOVA results revealed that there were no significant vertical heterogeneities of *Microcystis* colony *D* above the thermocline depths on July 27th and August 2nd (p >0.05), i.e. the distribution of colony size was uniform. Among the rest sampling dates with significant vertical heterogeneity, the maximum *Microcystis* colony *D* (D_{max}) occurred mostly at the water surface, except for the July 6th when the D_{max} was observed at 2 m.

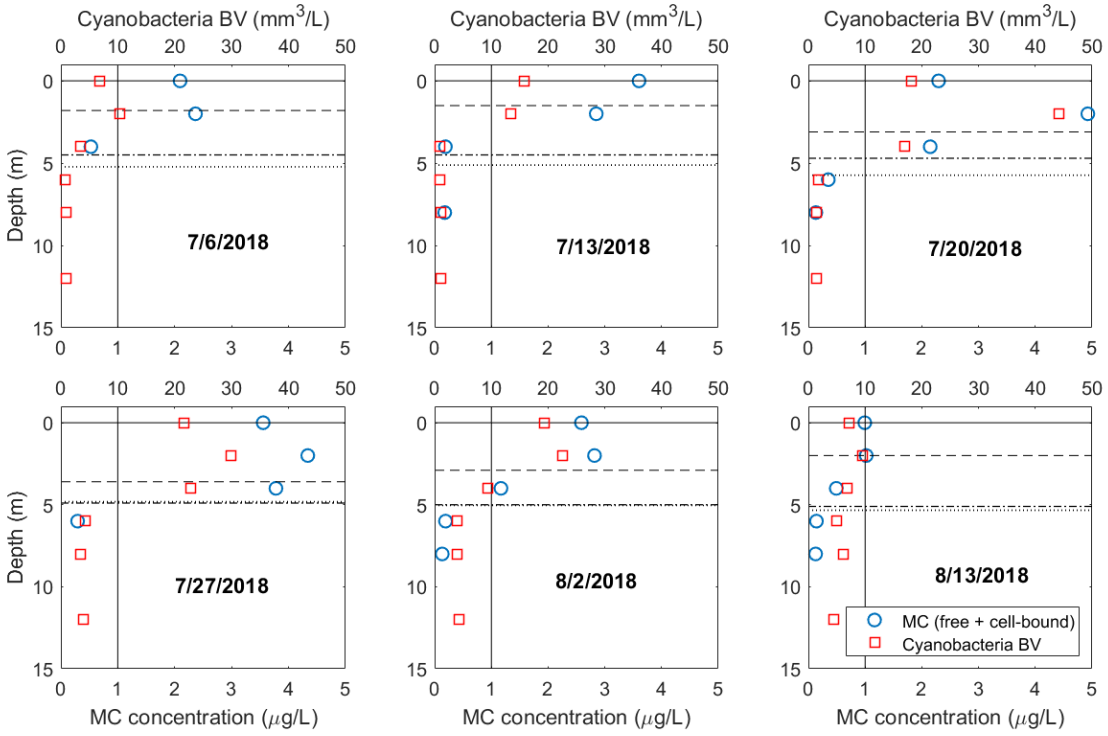

Figure 4.6. Profiles of cyanobacteria biovolume (BV) and total microcystin (MC) concentration (free + cell-bound). Each data point was averaged from duplicate samples. The dash lines represent the mixed layer depths, the dash-dot lines represent the thermocline depths, and the dotted lines represent the euphotic zone depths.

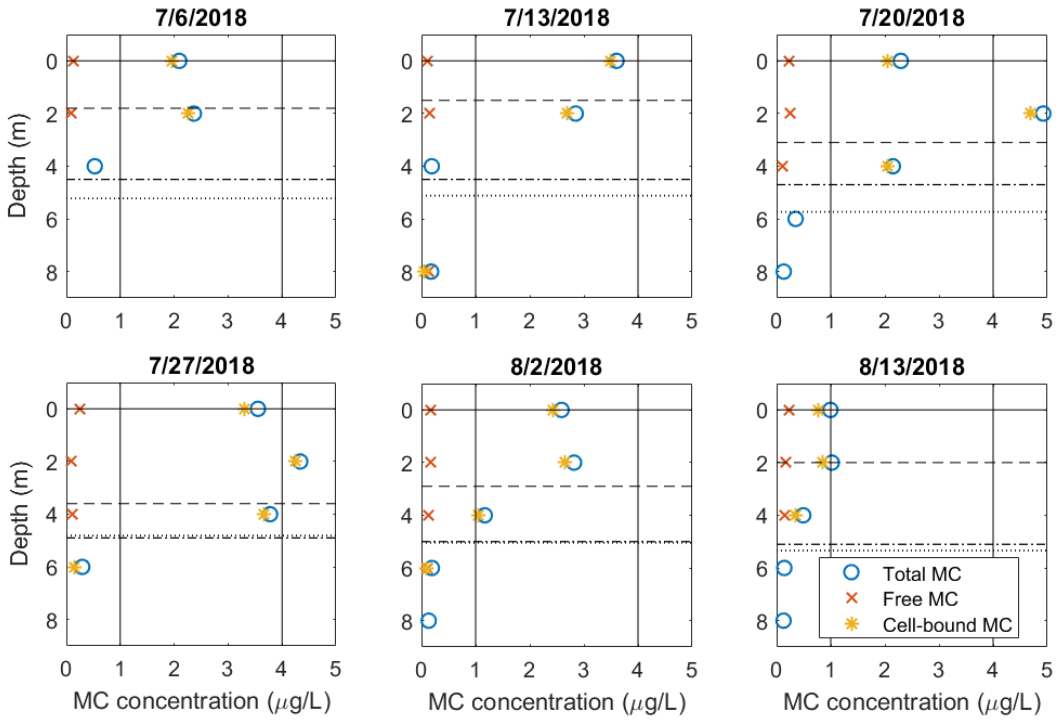

Figure 4.7. Profiles of total MC, cell-bound MC and free MC. Each data point was averaged from duplicate samples. The dash lines represent the mixed layer depths, the dash-dot lines represent the thermocline and the dotted lines represent the euphotic zone depths.

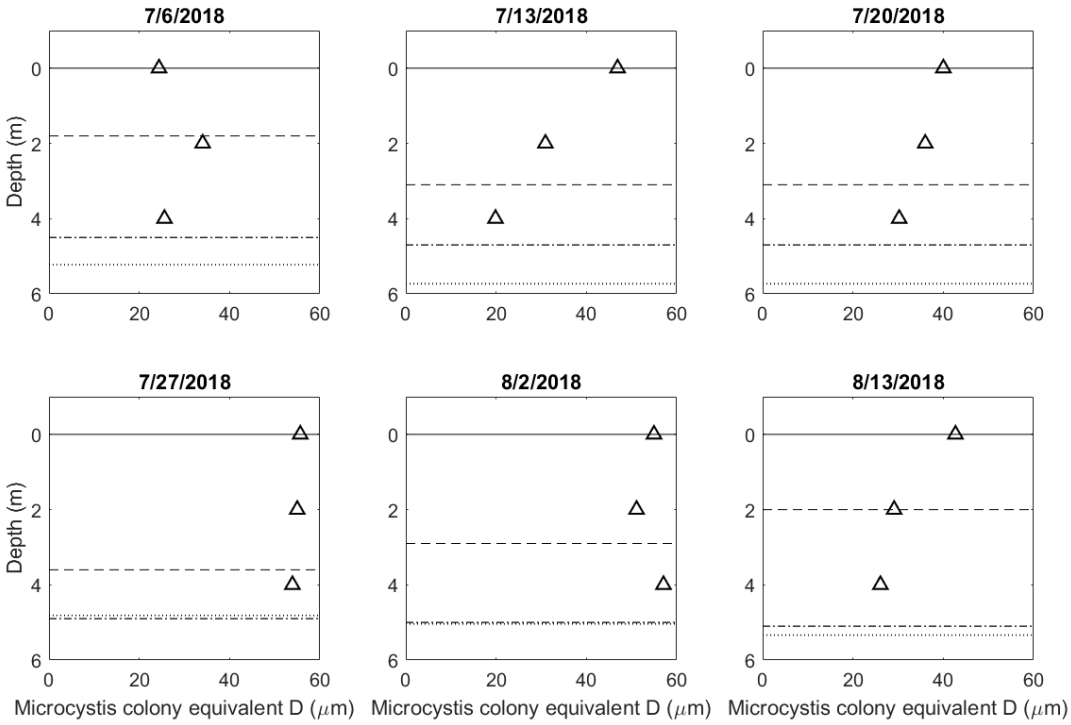

Figure 4.8. Profiles of *Microcystis* colony equivalent diameter (*D*) at depths above thermocline depths. Each data point was averaged from duplicate samples. The dash lines represent the mixed layer depths, the dash-dot lines represent the thermocline and the dotted lines represent the euphotic zone depths.

Temporal Heterogeneities of Cyanobacteria and MC Concentrations

The thermocline depth-averaged cyanobacteria BV, total MC concentrations and *Microcystis* colony equivalent *D* showed similar temporal variations through an increase towards a peak/plateau followed by a decrease during the blooming season. However, the peaks/plateaus occurred on different dates (Figure 4.9). The maximum cyanobacteria BV

occurred on July 20th, while the total MC concentration and *Microcystis* colony *D* reached their maxima one week later, on July 27th. Results of the ANOVA and Tukey's test indicated that the plateau of *Microcystis* colony *D* occurred from July 27th to August 2nd, as the data on these two days were significantly different from all other sampling dates ($p < 0.001$).

The delayed peak of the total MC compared to the cyanobacteria BV may be associated with the upregulation of MC biosynthesis in the *Microcystis* cells triggered by the increase of cell abundance [25]. The accumulation of MC synthetase (*mcy)* genes has been reported to be induced by the lysis of *Microcystis* cells sensed by the rest cells [70], and the peak of detected genes was reported to be before the MC concentration peak [176]. The one-week lag between the peak of free MC released in the water (July 20th) and the peak of cell-bound MC (July 27th) also agreed with the enhancement of MC biosynthesis by increased abundance of *Microcystis* or MC concentration in the water (Table 4.1). Previous studies also reported the temporal lag between the maximum MC concentration and the maximum cyanobacteria concentrations. Davis *et al*. [25] reported that the maximum MC occurred twelve days after the peak of *Microcystis* concentration (primarily comprised of toxic *Microcystis* strains) during the blooms dominated by *Microcystis* in the stratified Lake Ronkonkoma located on the Long Island, USA. Christensen *et al*. [176] also reported a delay of MC peak following the peaks of *Microcystis* and *Dolichospermum* concentrations in the Kabetogama Lake, a large lake in Minnesota. The data reported in Wilkinson *et al*. [161] showed that the maximum MC and maximum BV above the thermocline depth occurred on the same day in the South Center Lake, Minnesota, in 2017. The difference in temporal lags between our results and

Wilkinson *et al*. [161] may be related to the blooming types: the South Center Lake experienced uniform blooms above the thermocline depth during the period of maximum BV and MC, while the Ramsey Lake experienced blooms with a single peak above the thermocline depth.

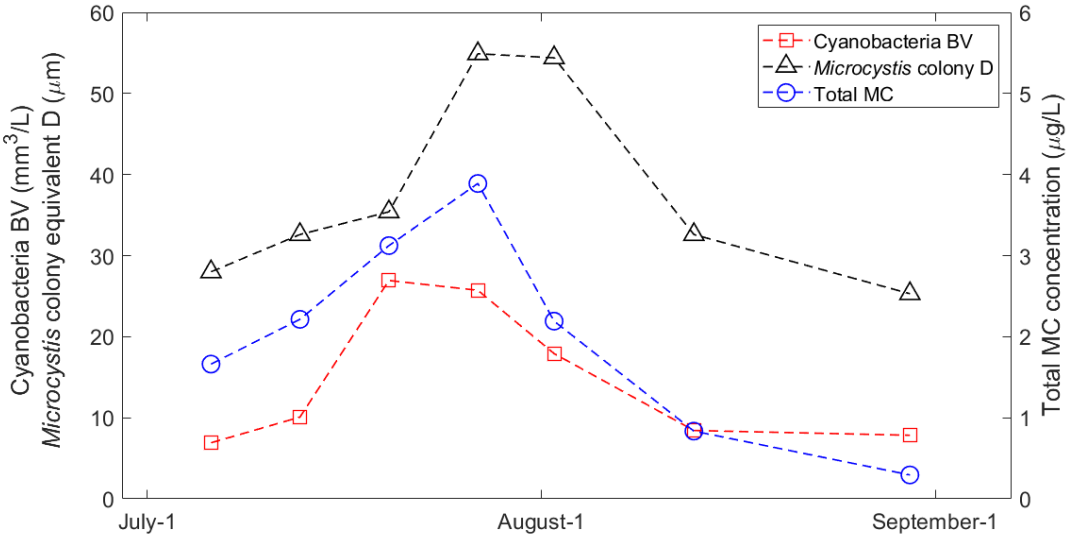

Figure 4.9. Temporal variations of cyanobacteria biovolume (BV), *Microcystis* colony equivalent diameter (*D*) and total microcystin (MC) concentration (free + cell-bound) averaged above thermocline depth with measurements at 0, 2, and 4 m. At each measured depth, BV and MC was estimated from duplicate samples, and the *Microcystis* colony *D* was estimated from at least 70 colonies.

Table 4.1. Average values of chemical and physical variables above the thermocline depth on sampling dates. The nutrient and MC concentrations are results of analyzed water samples. The values of physical variables are daily averaged results.

Sampling date	N (µg/L)	P (µg/L)	Cell-bound MC (µg/L)	Free MC (µg/L) [a]	u_* (m/s) [b]	St (J/m^2) [b]	LN [b]	Water T (˚C)
July 6	102.61	7.67	1.55	< 0.15	0.0032	275.24	22.49	24.49
July 13	134.24	16.37	2.08	< 0.15	0.0031	322.69	27.28	26.29
July 20	59.31	35.37	2.93	0.20	0.0054	268.14	8.12	24.58
July 27	77.08	1.87	3.74	0.15	0.0042	241.56	13.71	23.61
August 2	74.51	4.72	2.04	0.16	0.0035	248.34	18.44	23.76
August 13	53.95	6.03	0.65	0.18	0.0038	304.00	18.03	25.65
August 30	52.51	1.89	0.19	< 0.15	0.0035	182.29	16.01	21.32

[a] The MC concentrations that above the detection limit (0.10) but below the lowest standard concentration (0.15) are reported as < 0.15 µg/L.

[b] The u_*, St and LN did not change with water depths. The results are daily averages.

Impacts of Physical Variables

Water temperature is the primary driver of thermal stratification and thereby affecting the vertical distribution of cyanobacteria and MC concentrations. The water temperature profiles determined two important depths of the water column – the mixed layer depth and the thermocline depth. The mixed layer depth, which is the fraction of water depth that extends from the water surface to the bottom of epilimnion (also referred to as the

top of metalimnion), was calculated based on density gradients by the Lake Analyzer [168]. The thermocline depth represented the point with maximum density gradient in the water column and was also estimated by the Lake Analyzer. In the present study, both the cyanobacteria BV and the total MC concentrated in the zone above the thermocline depth. At the same time, the peaks of BV and MC occurred at or right above the mixed layer depth (Figure 4.6). *Microcystis* and *Dolichospermum*, the dominant genera of the blooms in the present study, were able to track the mixed layer efficiently and form blooms due to their fast vertical migration, especially in high temperature environments [50, 51, 144, 177].

Another essential physical factor affecting the cyanobacteria and MC concentrations were fluid motions and corresponding turbulence, expressed here as shear velocity (u_*) induced by the wind stress at the water surface. The key parameters, St and LN, evaluate the strength of the stratification and the stability of water column in resist to fluid motions. While St a quantitative index of the static stability of the water column which results from density stratification, LN is a quantitative index of the dynamic stability of the water column and explicitly integrates the destabilizing forces from wind at the lake surface in addition to the static stability. A LN = 1 indicates that the wind is sufficient to force the seasonal thermocline to be deflected to the surface at the windward end of the lake. For LN >> 1, stratification is stable and dominates the forces introduced by surface wind energy. The density stratification and wind energy reflected the indirect influence of lake thermal structure and fluid motion on the temporal heterogeneities of cyanobacteria BV, MC concentration and *Microcystis* colony size. The increasing trend of the maximum average *Microcystis* colony *D* normalized by the thermocline depth-averaged

D (D_{max}/D_{TD}) with increasing St shown in Figure 4.10a indicated that *Microcystis* colony size vertical distribution tended to shift from uniform to occurrence of a peak above the thermocline depth when St increased. Meanwhile, the cyanobacteria BV and total MC concentration at the water surface, normalized by the thermocline depth-averaged values ($BV_{surface}/BV_{TD}$ and $MC_{surface}/MC_{TD}$), increased with the LN (Figure 4.10b-c). In other words, cyanobacteria tend to form surface blooms with high MC at the water surface in the high LN regimes. These correlations were consistent with previous studies which revealed that stable thermal stratifications with relatively high water temperature and low turbulence assist the development of buoyant cyanobacteria surface blooms [107, 178]. In the present study, the surface bloom occurred on July 13th, the same day with the highest water T, the lowest u_*, and the highest St and LN above the thermocline depth among the seven sampling dates of the blooming season (Table 4.1).

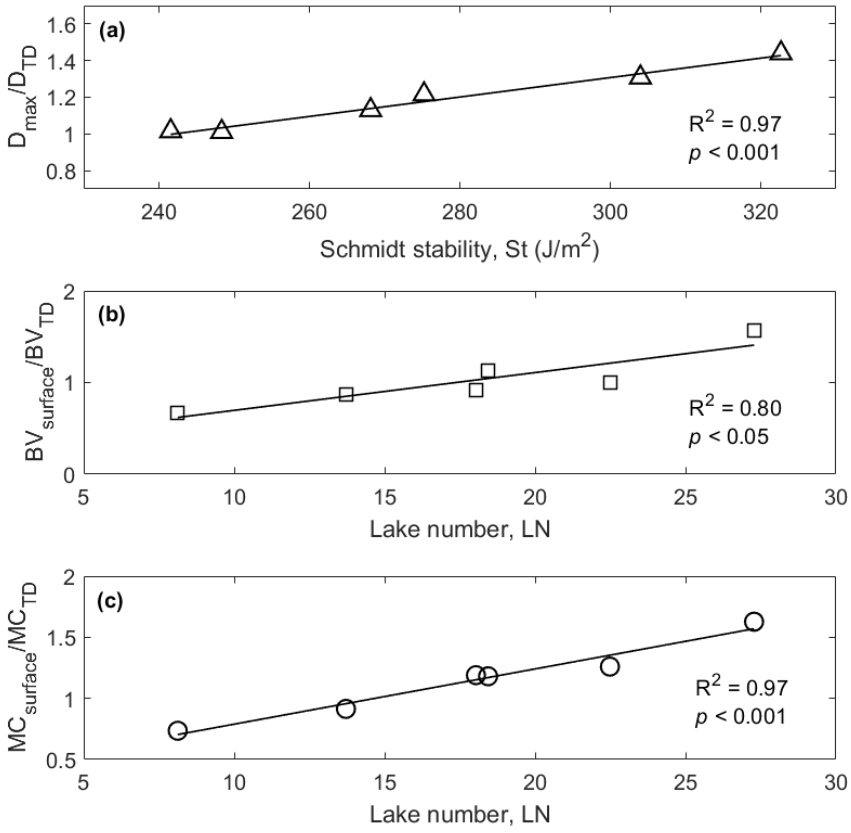

Figure 4.10. Linear regression models (α=0.05, n=6) of (**a**) maximum average *Microcystis* colony diameter normalized with thermocline depth-averaged *Microcystis* colony diameter (D_{max}/D_{TD}) versus the Schmidt stability (St); (**b**) average cyanobacteria biovolume (BV) at water surface normalized with thermocline depth-averaged cyanobacteria BV ($BV_{surface}/BV_{TD}$) versus the lake number (LN); and (**c**) average total microcystin (MC) concentration (free + cell-bound) at water surface normalized with thermocline depth-averaged total MC ($MC_{surface}/MC_{TD}$) versus the lake number (LN). The D_{max} represent the average value at the depth with the maximum average *Microcystis* colony diameter. The thermocline depth-averaged values (D_{TD}, BV_{TD} and MC_{TD}) were estimated from duplicate samples at 0, 2 and 4 m. The St and LN represent the average values of each sampling date.

Impacts of Chemical Variables

There have long been debates on the role of N and P in the eutrophication control relevant to cyanobacteria blooms mitigation [40]. Many studies in the past decade have reported the stimulation of both N-fixing and non-N-fixing cyanobacteria blooms by addition of both N and P, rather than the addition of a single nutrient [40, 43, 146]. The increased N loadings and N:P ratio have been reported to induce the non-N-fixing cyanobacteria blooms and suppress N-fixers in large lakes [40, 151]. We extended the investigation of the correlation between cyanobacteria composition variations and macronutrient availability into small stratified lakes. Nitrate and nitrite were assessed, since the major land use of Ramsey Lake watershed is cropland/agriculture, from which the N pollutions were reported to be primarily in the form of nitrate [40]. Phosphate was assessed as the primary dissolved inorganic P that can be directly assimilated by aquatic microbial organisms [179].

The profiles of the $(NO_3^- + NO_2^-)/PO_4^{3-}$ ratio (referred as N:P hereinafter) and the BV ratio of non-N-fixing cyanobacteria (*Microcystis* spp.) to N-fixing cyanobacteria (*Dolichospermum* spp. and *Aphanizomenon* spp.), i.e. $BV_{Mic}/(BV_{Dol} + BV_{Aph})$, depicted the similar vertical variations above the thermocline depth (Figure 4.11). As shown by previous studies, N:P = 14 (by mass) might be a critical threshold between N limiting and P limiting conditions for algal growth [41, 180, 181]. By plotting the N versus P and BV_{Mic} versus $BV_{Dol} + BV_{Aph}$ at three depths above thermocline depths of the six sampling dates, we found that every data point with N:P $\geq$ 14 corresponded to a data point with BV_{Mic}:$(BV_{Dol} + BV_{Aph}) \geq 14$ from the same samples (Figure 4.12a-b).

Nevertheless, when focusing on the high N:P regime (N:P $\geq$ 14), an inverse linear relationship was established between these two ratios (Figure 4.12c). The results demonstrated that higher proportions of *Microcystis* over N-fixing cyanobacteria occurred when N is substantial (i.e. P limiting conditions), while increase of P in these conditions will further enhance the dominance of *Microcystis*. The wider P selectivity, better nutrient storage and synthesis of high-affinity transporters make *Microcystis* dominant over other cyanobacteria under N-substantial and P-limited conditions, while better buoyancy by promoted gas vesicle production and thereby more efficient nutrient access with the addition of P may explain why *Microcystis* prefer relatively abundant P within the high N:P regime [52, 179, 182].

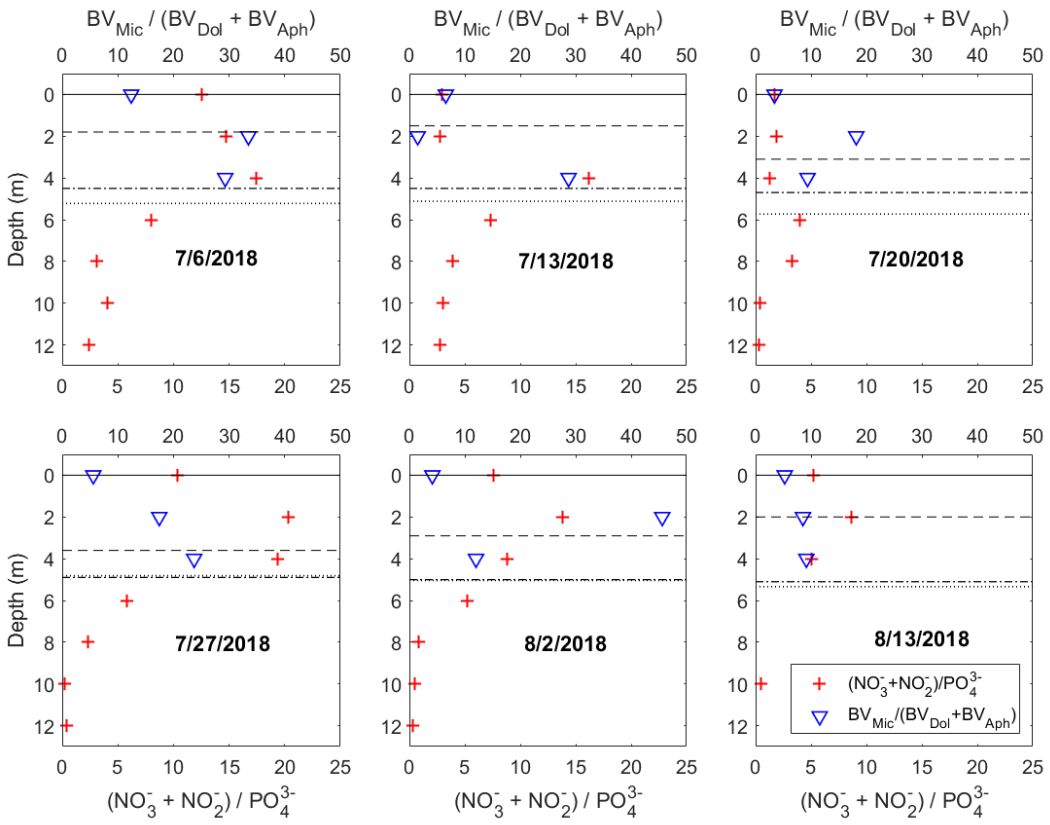

Figure 4.11. Profiles of the nutrient ratio of (nitrate + nitrite)/phosphate and the cyanobacteria genera biovolume ratio of *Microcystis*/(*Dolichospermum* + *Aphanizomenon*). Each data point was averaged from duplicate samples. The cyanobacteria genera ratios were only estimated for depths above the thermocline depths, for nearly no *Dolichospermum* and *Aphanizomenon* were observed under the thermocline depths. The dash lines represent the mixed layer depths, the dash-dot lines represent the thermocline depths, and the dotted lines represent the euphotic zone depths.

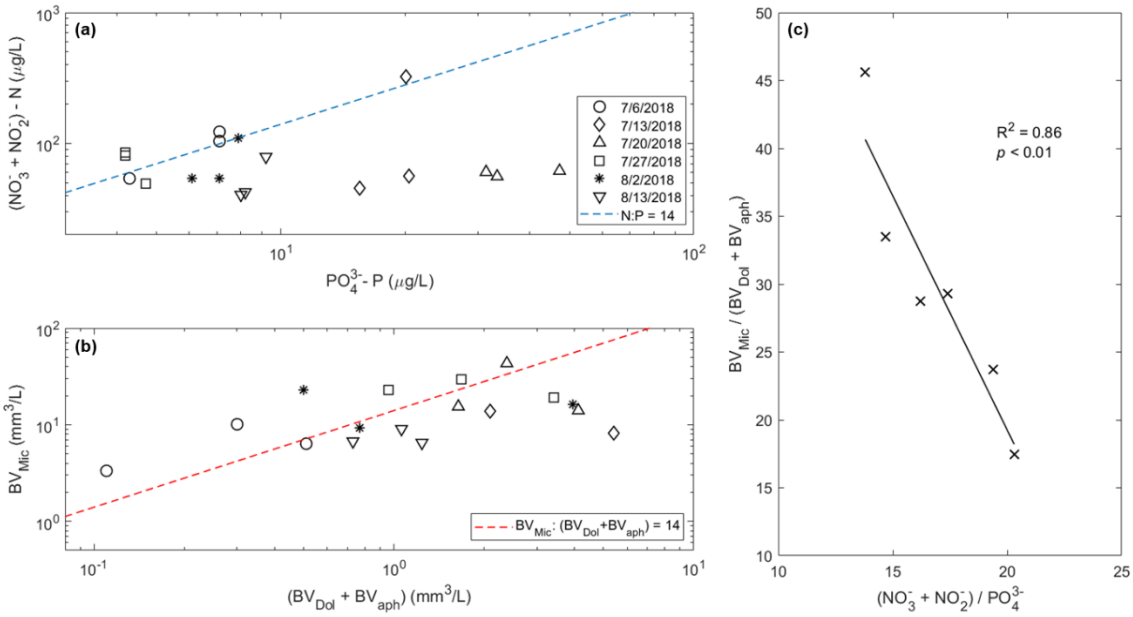

Figure 4.12. (**a**) Log-scale plot of nitrate + nitrite versus phosphate. The data points were averaged with duplicate samples from 0, 2 and 4 m. (**b**) Log-scale plot of *Microcystis* biovolume versus biovolume of *Dolichospermum* and *Aphanizomenon*. The data points were averaged with duplicate samples from 0, 2 and 4 m. (**c**) Biovolume ratio of *Microcystis*/(*Dolichospermum* + *Aphanizomenon*) versus nutrient ratio of (nitrate + nitrite)/phosphate. The data points were collected from the samples with nutrient ratio of (nitrate + nitrite)/phosphate greater or equal to 14.

Implications on Environmental Health

Under the progressive anthropogenic activities and climate change scenarios, cyanobacteria blooms are expected to occur with higher frequency and intensity, due to the prolonged and intensified thermal stratification and altered nutrient dynamics [146,

150, 183]. The complex combined influence of physical, chemical and biological affectors has made the prediction and management of cyanobacteria blooms and their toxicity difficult. The findings of the abiotic impacts on the heterogeneities of cyanobacteria bloom and toxicity in the current study provided implications on the environmental health that may be beneficial for relevant prediction and management work.

First, the increase of maximum *Microcystis* colony size, surface cyanobacteria BV and surface total MC levels with increasing St and LN indicated that more toxic surface blooms are anticipated to be observed with the global climate change. Genera capable of rapid buoyancy regulations and fast migrations, such as *Microcystis* and *Dolichospermum*, may thrive and dominate the cyanobacteria blooms. Thus, the findings of the present study, with *Microcystis* and *Dolichospermum* as two dominant genera, may be applied in a variety of future scenarios.

Second, the temporal lag between maximum cyanobacteria BV and maximum MC concentration need to be considered in the MC risk assessment and public health management. Although the linear relationship of MC versus BV using data above thermoclines was established, one must realize the similarity in vertical heterogeneities and differences in temporal heterogeneities reflected by the model when applying it in MC predictions (Figure 4.13). Also, the timing of maximum cyanobacteria BV and maximum cyanotoxin level may not coincide with the most robust water stability. Hence, it is critical for responsible authorities to evaluate the MC risk for the entire blooming

season before and after the BV peaks, in order to determine the appropriate actions to be taken.

Third, the highest cyanobacteria and cyanotoxin concentrations may occur as sub-surface blooms right above the mixed layer depth, which indicates that harmful bloom with notable cyanotoxin levels may impair the water health in the shallow layer, even if no visible scums appear on the surface. In contrast, a surface bloom could result in a high cyanotoxin level at the water surface, even if the cyanobacteria concentration is not at the peak of the season. For instance, the surface MC concentration reached two peaks in our study – one during the surface bloom with relatively low BV and the other one during the sub-surface bloom with high BV (Figure 4.14). As MC levels at the water surface or in the shallow mixed layer can pose health risks to humans not only via drinking water and recreational water uses, but also through consumptions of MC contaminated food (e.g., fish and mussels) and inhalation of toxin-containing aerosols. The bioaccumulation and biomagnification through food web may expose humans to MC levels exceeding the tolerable daily intake values, and the MC-containing aerosols may result greater health impacts on people with existing breathing disease [184, 185].

Fourth, nutrient control of both N and P should be implemented for cyanobacteria blooms prevention and mitigation. Each of N and P has certain impacts on the cyanobacteria concentration and toxicity, while excessive loadings of dual nutrients can result in amplified detrimental effects. In addition, the N:P ratio is closely related to the composition of the cyanobacteria community, which directly affects the blooming characteristics and toxic effects on the impaired water.

To sum up, the vertical and temporal heterogeneities of cyanobacteria and cyanotoxin concentrations were influenced by the physical and chemical drivers directly or indirectly. Most of the abiotic affectors play their roles interactively with other affectors. The prediction models and management actions for cyanobacteria blooms should take into account all the abiotic factors as well as biotic factors (not discussed in the present study), and their complex interactive impacts on cyanobacteria and cyanotoxin variations.

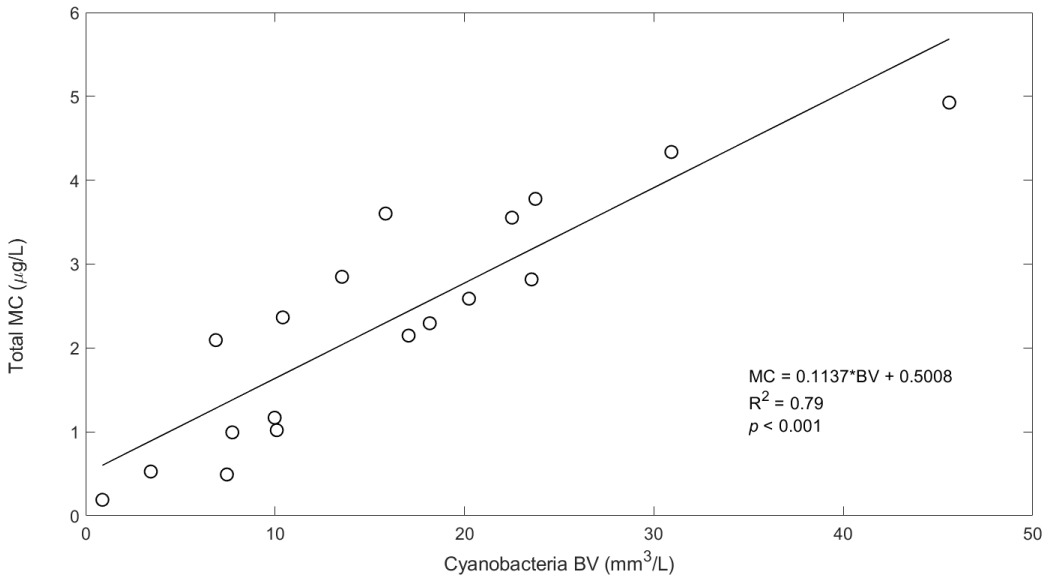

Figure 4.13. Linear regression model of total MC concentration versus the cyanobacteria BV (α=0.05, n=18). The circles represent data points from 0, 2 and 4 m of six sampling dates during blooming season. Each data point was averaged from duplicate samples. The solid line represents the linear trendline.

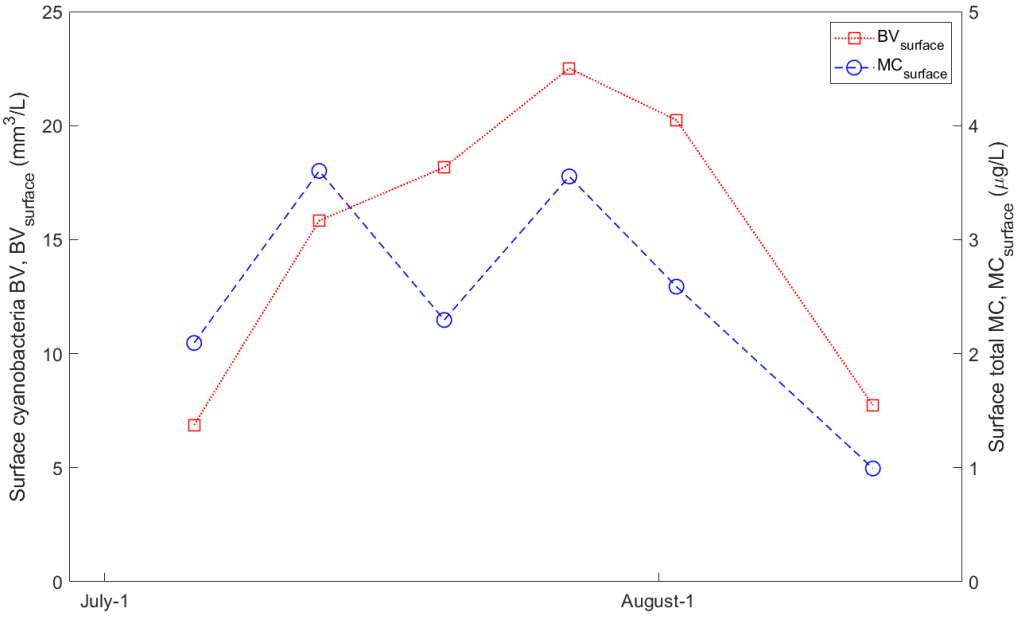

Figure 4.14. Temporal variations of surface cyanobacteria biovolume ($BV_{surface}$) and surface total MC ($MC_{surface}$). Each data point was estimated from duplicate samples at water surface.

Conclusions

Water temperatures and meteorological conditions above the lake surface were measured over the summer by the research station every five minutes and over the water depth in a small stratified lake. Chemical and microbiological analyses were conducted using the using the weekly or bi-weekly water samples collected over the lake depth adjacent to the research station. We documented the concentrations of cyanobacteria and MC and examined the impacts of the abiotic variables on the vertical and temporal

heterogeneities. Our findings demonstrated similarities in vertical heterogeneities of the cyanobacteria BV and the total MC concentration. Furthermore, the vertical heterogeneity of the nutrient ratio (N:P) depicted similar pattern as BV ratio of non-N-fixing cyanobacteria to N-fixing cyanobacteria BV_{Mic}:(BV_{Dol} + BV_{Aph}). Temporal lags on the order of one week were documented between the maximum cyanobacteria BV, the MC levels, and the *Microcystis* colony size. The stability of the water column in the lake, described by Schmidt stability and Lake Number, significantly mediated the maximum *Microcystis* colony size, the surface cyanobacteria BV and the surface total MC level. The temporal heterogeneities of cyanobacteria community composition were correlated with the nutrient dynamics of N and P concentrations in the lake. Our results could have significant implications on the management of cyanobacteria blooms and environmental health. Particularly, the temporal lag between the maximum cyanobacteria and MC concentrations as well as the high surface MC concentrations during both surface and sub-surface blooms should be considered in the bloom monitoring and MC risk evaluations. The influence of N:P variability over water depths on the cyanobacteria community heterogeneities should also be taken into account in the prediction of the cyanobacteria compositions during a bloom. The findings will facilitate the development of prediction models, management strategies and monitoring efforts to minimize the effects of cyanobacteria and cyanotoxins in small to medium size stratified lakes.

Chapter 5

Conclusions and Recommendations

Conclusions

This dissertation investigates the growth, motility and metabolism of cyanobacteria and lipid-producing microalgae in different fluid environments by both laboratory experiments and field studies. The findings of the dissertation will improve the understanding of the impacts of abiotic environmental variables, including temperature, nutrient availability, wind shear and water column stability, on the algal growth and migration as well as the metabolites production and accumulation. The relationships between environmental variables and microorganism behaviors established in this dissertation will facilitate the development of prediction models, monitoring strategies and decision makings in cyanobacteria HABs management and microalgal biofuel production industries.

Chapter 2 presents the results of the growth experiment of *Microcystis aeruginosa* (*M. aeruginosa*) at seven different temperatures and the buoyancy experiment of *M. aeruginosa* colonies at two different temperatures. The growth experiment demonstrates that the specific growth rate of *M. aeruginosa* increases with temperature up to the optimal growth temperature of 27.5˚C, while the specific growth rate is inversely affected at higher temperatures. A cardinal temperature model with the inflection point (optimal temperature) to predict the growth of *M. aeruginosa* from 5˚C to 35˚C has been proposed in this chapter. Meanwhile, the ambient temperature is also revealed to have an impact on the vertical migration of *M. aeruginosa* colonies, by the visualization and analysis of *M. aeruginosa* colonies using a digital inline holographic microscope (DIHM) system. The buoyant velocities of *M. aeruginosa* colonies at 28˚C are approximately five times as great as those at 17.5˚C. As temperature is shown to regulate the buoyancy by affecting the colony densities, a model is derived to calculate the density of a colony using the buoyant velocity and colony size. The results not only provide a better understanding of the temperature effects on the growth and buoyancy of *M. aeruginosa*, one of the most common bloom-forming cyanobacteria, but will also facilitate building prediction models and setting up monitoring systems for cyanobacteria blooms in aquatic ecosystems with various ambient temperatures.

Chapter 3 also uses laboratory experiments to demonstrate the motility and metabolism of aquatic microorganisms in different environments. The quantification of swimming signatures (speed and motions) and neutral lipid contents of lipid-producing motile green algae, *Dunaliella primolecta* (*D. primolecta*), during the lag-exponential-stationary growth cycle at different nutrient concentrations depicts significant variations in algal

motility and lipid accumulation across growth phases. The neutral lipid content and swimming speed of *D. primolecta* increases towards maxima at stationary growth phase when nutrient deprivation occurs, and the timing of maximum neutral lipid content coincides with the maximum swimming speed. The timing and the extent of the swimming speed and neutral lipid maxima are inversely affected by the initial nitrate availability of the growth environment. Inspired by the successful application of the DIHM system in the *M. aeruginosa* study present in Chapter 2, swimming trajectories have been recorded and analyzed using the similar and modified DIHM system for this study. The results demonstrate significant changes in swimming modes of *D. primolecta* at the stationary growth phase when the maximum neutral lipid content is observed. The frequency of fine motions decreases approximately 8 folds while the neutral lipid content increases approximately 8 folds from exponential to early stationary phase. The findings indicate the potential exploitation of microalgal swimming signatures in the monitoring the cultivation conditions and predicting the optimal algal harvest timing for microalgal biofuel production. This chapter may also provide some inspirations for the exploration of other production of food or antibiotics from microalgal metabolites with low energy costs.

The exploration of growth, motility (buoyancy regulations/vertical migration) and metabolism of cyanobacteria under different environmental conditions is extended to a field study in the freshwater lake ecosystem in Chapter 4. Ramsey Lake, the model lake studied in this chapter, is a relatively small eutrophic lake which stratified during summer and experiences faster changes in cyanobacteria bloom dynamics. The deployed research station measured water temperatures throughout the water column and meteorological

conditions above the lake surface every five minutes over the summer. Water samples were collected over the lake depth adjacent to the research station weekly or bi-weekly for chemical and microbiological analyses. This chapter documents the concentrations of cyanobacteria and microcystin (MC) and examines the impacts of the abiotic environmental variables on the vertical and temporal heterogeneities. The MC concentration depicts similar heterogeneities as cyanobacteria biovolume (BV). There are also similarities in the vertical variations of the nutrient ratio (N:P) and the BV ratio of non-N-fixing cyanobacteria to N-fixing cyanobacteria. The temporal lags on the order of one week are also documented between the maximum cyanobacteria BV, the MC levels, and the *Microcystis* colony size in this chapter. The surface cyanobacteria BV, the surface total MC level and the maximum *Microcystis* colony size are significantly mediated by the stability of the water column in the lake, described by the Schmidt stability and Lake Number. Relationships between temporal heterogeneities of cyanobacteria community composition and the nutrient dynamics of N and P concentrations in the lake is also established. The results could have significant implication on the environmental health associated with cyanobacteria blooms. In particular, the temporal lag between the maximum cyanobacteria and MC concentrations need to be taken into account when monitoring the bloom and evaluating the MC risks. The impacts of N:P dynamics over water depths on the cyanobacteria community heterogeneities should also be considered in the prediction of cyanobacteria compositions during a bloom. The findings will adds to systematic understanding of the cyanobacteria blooms in small to medium size stratified lakes, and will facilitate the development of

prediction models, management strategies and monitoring efforts to minimize the detrimental effects of toxic cyanobacteria blooms.

Recommendations

The competitive growth of cyanobacteria at relatively high temperatures makes cyanobacteria blooms prevailing under the climate change scenarios. It is essential to develop temperature-growth prediction models for primary bloom-forming cyanobacteria genera/species, which can be further involved into the complex bloom perdition models. One critical consideration for the temperature-growth model development is that the model should predict the real growth phenomenon of the certain cyanobacteria with an inflection point over which the growth is inversely affected, rather than using the previously established equations originally developed to describe the effects of temperature on chemical reactions. The CTMI model for *M. aeruginosa* provides a prediction tool to estimate growth rates at a variety of temperatures. Development of such models for other common bloom-forming cyanobacteria will aid not only the growth prediction of individual species but also the prediction of cyanobacteria composition in a bloom in a certain temperature regime. Water quality models are suggested to involve the instrumental temperature-growth models of cyanobacteria which can finally achieve the 3D prediction of spatial and temporal heterogeneities of cyanobacteria in response to the water temperature variability in aquatic ecosystems.

The temperature effects on the buoyancy of *Microcystis* suggest faster floatation of colonial cyanobacteria to form surface scums in high temperature regimes. Monitoring and prediction efforts for cyanobacteria blooms should consider the temperature impacts

on buoyancy regulations to properly evaluate the risks of surface scum formation and potential cyanotoxin exposure to the public. On the other hand, the DIHM system used in the study is a low cost, highly compact and promising technology, which can be integrated with existing autonomous/robotic devices used in the field for long-term and large-scale *in situ* quantification of plankton distribution and behaviors.

As one key remaining challenge for microalgal biofuel production is how to minimize the energy cost and maximize the yield, the findings in this dissertation regarding the swimming signatures and neutral lipid content across growth phases of *Dunaliella* provide indications and recommendations for potential monitoring and prediction strategies to harvest the cells with maximum lipid yields. It is suggested that the neutral lipid accumulation achieve it maximum at the stationary growth phase, while the timing and extent of the maximum is associated with the nutrient availability in the cultivation medium. Hence, cultivation protocols with optimal nutrient concentrations are recommended to be established for microalgal biofuel industries. Furthermore, since the lipid content varies drastically within a few days, the final lipid yield is sensitive to the harvest timing. An effective monitoring system for the neutral lipid content is urged. The findings of association between microalgal swimming signatures and neutral lipid content as well as the successful employment of DIHM-PTV system in recording of microalgal swimming motions inspire a low-cost scalable sensor system utilizing DIHM-PTV for high-throughput monitoring of neutral lipid content in industrial-scale biofuel production.

The field study of cyanobacteria and cyanotoxin concentrations and the impacts of abiotic variables on their heterogeneities have provided more implications on the environmental

health and HABs management. Firstly, the prolonged and intensified the stratification due to the climate change will increase the water column stability, which will lead to increase of maximum *Microcystis* colony size, surface cyanobacteria biovolume and the surface MC concentrations. Protocols are needed in response to anticipated intensified cyanobacteria blooms with elevated toxicity. Secondly, there may be temporal lags between the maximum cyanobacteria concentration and the maximum MC concentration during a bloom. Thus, the bloom monitoring and MC risk evaluation should be conducted for the entire blooming season before and after the biovolume/biomass peaks. Thirdly, the MC level at the water surface may achieve its maxima either in a surface bloom without high cyanobacteria concentrations, or in a sub-surface bloom with high cyanobacteria concentrations. In the other words, the surface MC level can be considerably high even if there is no surface scum occurrence throughout the season. Hence, it is critical for responsible authorities to monitor the MC levels throughout the blooming season, even if there are no notable scums, in order to take the appropriate actions in time to minimize the public health risks of MC exposure. Fourthly, nutrient control of both N and P should be implemented for cyanobacteria prevention and mitigation. It is also important to take into account the N:P ratio in the prediction of cyanobacteria community composition, which may affect the blooming characteristics and toxic effects on the impaired water. Lastly, the prediction models, management strategies and monitoring efforts for cyanobacteria blooms in the future should consider all the environmental variables and their complex interactive impacts on cyanobacteria and cyanotoxin variations.

Bibliography

[1] Paerl, H. W., Fulton, R. S., Moisander, P. H., & Dyble, J. (2001). Harmful freshwater algal blooms, with an emphasis on cyanobacteria. *TheScientificWorldJournal*, *1*.

[2] Hudnell, H. K. (Ed.). (2008). *Cyanobacterial harmful algal blooms: state of the science and research needs* (Vol. 619). Springer Science & Business Media.

[3] Jöhnk, K. D., Huisman, J. E. F., Sharples, J., Sommeijer, B. E. N., Visser, P. M., & Stroom, J. M. (2008). Summer heatwaves promote blooms of harmful cyanobacteria. *Global change biology*, *14*(3), 495-512.

[4] Heisler, J., Glibert, P. M., Burkholder, J. M., Anderson, D. M., Cochlan, W., Dennison, W. C., ... & Lewitus, A. (2008). Eutrophication and harmful algal blooms: a scientific consensus. *Harmful algae*, *8*(1), 3-13.

[5] O'neil, J. M., Davis, T. W., Burford, M. A., & Gobler, C. J. (2012). The rise of harmful cyanobacteria blooms: the potential roles of eutrophication and climate change. *Harmful algae*, *14*, 313-334.

[6] Hoagland, P., & Scatasta, S. (2006). The economic effects of harmful algal blooms. In *Ecology of harmful algae* (pp. 391-402). Springer, Berlin, Heidelberg.

[7] Wehr, J. D., Sheath, R. G., & Kociolek, J. P. (Eds.). (2015). *Freshwater algae of North America: ecology and classification*. Elsevier. USA.

[8] Pernthaler, J. (2005). Predation on prokaryotes in the water column and its ecological implications. *Nature Reviews Microbiology*, *3*(7), 537-546.

[9] Yang, Z., Kong, F., Shi, X., Zhang, M., Xing, P., & Cao, H. (2008). CHANGES IN THE MORPHOLOGY AND POLYSACCHARIDE CONTENT OF MICROCYSTIS AERUGINOSA (CYANOBACTERIA) DURING FLAGELLATE GRAZING. *Journal of Phycology*, *44*(3), 716-720.

[10] Reynolds, C. S. (2006). *The ecology of phytoplankton*. Cambridge University Press, New York.

[11] Reynolds, C. S., & Walsby, A. E. (1975). Water-blooms. *Biological reviews*, *50*(4), 437-481.

[12] Bartram, J., & Chorus, I. (Eds.). (1999). *Toxic cyanobacteria in water: a guide to their public health consequences, monitoring and management*. CRC Press.
[13] Huisman, J., Sharples, J., Stroom, J. M., Visser, P. M., Kardinaal, W. E. A., Verspagen, J. M., & Sommeijer, B. (2004). Changes in turbulent mixing shift competition for light between phytoplankton species. *Ecology*, *85*(11), 2960-2970.
[14] Rabouille, C. S., Oliver, R. L., & Walsby, A. E. (1987). Cyanobacterial dominance: the role of buoyancy regulation in dynamic lake environments. *New Zealand journal of marine and freshwater research*, *21*(3), 379-390.
[15] Rabouille, S., Salençon, M. J., & Thébault, J. M. (2005). Functional analysis of Microcystis vertical migration: A dynamic model as a prospecting tool: I—Processes analysis. *Ecological modelling*, *188*(2-4), 386-403.
[16] Visser, P. M., Ibelings, B. W., Bormans, M., & Huisman, J. (2016). Artificial mixing to control cyanobacterial blooms: a review. *Aquatic Ecology*, *50*(3), 423-441.
[17] Mlouka, A., Comte, K., Castets, A. M., Bouchier, C., & de Marsac, N. T. (2004). The gas vesicle gene cluster from Microcystis aeruginosa and DNA rearrangements that lead to loss of cell buoyancy. *Journal of Bacteriology*, *186*(8), 2355-2365.
[18] Sun, Q., Zhu, W., Li, M., & Tan, X. (2015). Morphological changes of Microcystis aeruginosa colonies in culture. *J Limnol. doi*, *10*.
[19] Paerl, H. W., & Huisman, J. (2009). Climate change: a catalyst for global expansion of harmful cyanobacterial blooms. *Environmental microbiology reports*, *1*(1), 27-37.
[20] Deng, J., Qin, B., Paerl, H. W., Zhang, Y., Ma, J., & Chen, Y. (2014). Earlier and warmer springs increase cyanobacterial (Microcystis spp.) blooms in subtropical Lake Taihu, China. *Freshwater Biology*, *59*(5), 1076-1085.
[21] Paerl, H. W., Joyner, J. J., Joyner, A. R., Arthur, K., Paul, V., O'Neil, J. M., & Heil, C. A. (2008). Co-occurrence of dinoflagellate and cyanobacterial harmful algal blooms in southwest Florida coastal waters: dual nutrient (N and P) input controls. *Marine Ecology Progress Series*, *371*, 143-153.
[22] Litchman, E., de Tezanos Pinto, P., Klausmeier, C. A., Thomas, M. K., & Yoshiyama, K. (2010). Linking traits to species diversity and community structure in phytoplankton. In *Fifty years after the ''Homage to Santa Rosalia'': Old and new paradigms on biodiversity in aquatic ecosystems* (pp. 15-28). Springer, Dordrecht.
[23] Sivonen, K. (1990). Effects of light, temperature, nitrate, orthophosphate, and bacteria on growth of and hepatotoxin production by Oscillatoria agardhii strains. *Applied and environmental microbiology*, *56*(9), 2658-2666.
[24] Lindon, M., & Heiskary, S. (2009). Blue-green algal toxin (microcystin) levels in Minnesota lakes. *Lake and Reservoir Management*, *25*(3), 240-252.
[25] Davis, T. W., Berry, D. L., Boyer, G. L., & Gobler, C. J. (2009). The effects of temperature and nutrients on the growth and dynamics of toxic and non-toxic strains of Microcystis during cyanobacteria blooms. *Harmful algae*, *8*(5), 715-725.
[26] Wood, S. A., Dietrich, D. R., Cary, S. C., & Hamilton, D. P. (2012). Increasing Microcystis cell density enhances microcystin synthesis: a mesocosm study. *Inland Waters*, *2*(1), 17-22.

[27] Chisti, Y. (2007). Biodiesel from microalgae. *Biotechnology Advances*, *25*(3), 294–306.
[28] Mutanda, T., Ramesh, D., Karthikeyan, S., Kumari, S., Anandraj, A., & Bux, F. (2011). Bioprospecting for hyper-lipid producing microalgal strains for sustainable biofuel production. *Bioresource technology*, *102*(1), 57-70.
[29] Phadwal, K., & Singh, P. . (2003). Effect of nutrient depletion on β-carotene and glycerol accumulation in two strains of Dunaliella sp. *Bioresource Technology*, *90*(1), 55–58.
[30] Chen, M., Tang, H., Ma, H., Holland, T. C., Ng, K. Y. S., & Salley, S. O. (2011). Effect of nutrients on growth and lipid accumulation in the green algae Dunaliella tertiolecta. *Bioresource Technology*, *102*(2), 1649–1655.
[31] Gao, Y., Yang, M., & Wang, C. (2013). Nutrient deprivation enhances lipid content in marine microalgae. *Bioresource Technology*, *147*, 484–491.
[32] Hansen, T. J., Hondzo, M., Mashek, M. T., Mashek, D. G., & Lefebvre, P. A. (2013). Algal swimming velocities signal fatty acid accumulation. *Biotechnology and Bioengineering*, *110*(1), 143–152.
[33] Hu, Q., Sommerfeld, M., Jarvis, E., Ghirardi, M., Posewitz, M., Seibert, M., & Darzins, A. (2008). Microalgal triacylglycerols as feedstocks for biofuel production: perspectives and advances. *The Plant Journal*, *54*(4), 621–639.
[34] Davidi, L., Katz, A., & Pick, U. (2012). Characterization of major lipid droplet proteins from Dunaliella. *Planta*, *236*(1), 19–33.
[35] Huesemann, M. H., & Benemann, J. R. (2009). Biofuels from Microalgae: Review of Products, Processes and Potential, with Special Focus on Dunaliella sp. In *The Alga Dunaliella: Biodiversity, Physiology, Genomics, and Biotechnology*. United States: A. Ben-Amotz, J.E.W. Polle, and D.V. Subba Rao; Science Publishers, New Hampshire, United States(US)
[36] Zweytick, D., Athenstaedt, K., & Daum, G. (2000). Intracellular lipid particles of eukaryotic cells. *Biochimica et Biophysica Acta (BBA) - Reviews on Biomembranes*, *1469*(2), 101–120.
[37] Ryther, J. H., & Dunstan, W. M. (1971). Nitrogen, phosphorus, and eutrophication in the coastal marine environment. *Science*, *171*(3975), 1008-1013.
[38] Xin, L., Hong-Ying, H., Ke, G., & Ying-Xue, S. (2010). Effects of different nitrogen and phosphorus concentrations on the growth, nutrient uptake, and lipid accumulation of a freshwater microalga Scenedesmus sp. *Bioresource technology*, *101*(14), 5494-5500.
[39] Ruangsomboon, S., Ganmanee, M., & Choochote, S. (2013). Effects of different nitrogen, phosphorus, and iron concentrations and salinity on lipid production in newly isolated strain of the tropical green microalga, Scenedesmus dimorphus KMITL. *Journal of applied phycology*, *25*(3), 867-874.
[40] Schindler, D. W. (2012). The dilemma of controlling cultural eutrophication of lakes. *Proceedings of the Royal Society B: Biological Sciences*, *279*(1746), 4322-4333.
[41] Wurtsbaugh, W. A., Paerl, H. W., & Dodds, W. K. (2019). Nutrients, eutrophication and harmful algal blooms along the freshwater to marine continuum. *Wiley Interdisciplinary Reviews: Water*, *6*(5), e1373.

[42] Paerl, H. W. (2018). Mitigating toxic planktonic cyanobacterial blooms in aquatic ecosystems facing increasing anthropogenic and climatic pressures. *Toxins*, *10*(2), 76.
[43] Xu, H., Paerl, H. W., Qin, B., Zhu, G., Hall, N. S., & Wu, Y. (2015). Determining critical nutrient thresholds needed to control harmful cyanobacterial blooms in eutrophic Lake Taihu, China. *Environmental science & technology*, *49*(2), 1051-1059.
[44] Paerl, H. W., Hall, N. S., & Calandrino, E. S. (2011). Controlling harmful cyanobacterial blooms in a world experiencing anthropogenic and climatic-induced change. *Science of the total environment*, *409*(10), 1739-1745.
[45] Michalak, A. M., Anderson, E. J., Beletsky, D., Boland, S., Bosch, N. S., Bridgeman, T. B., ... & DePinto, J. V. (2013). Record-setting algal bloom in Lake Erie caused by agricultural and meteorological trends consistent with expected future conditions. *Proceedings of the National Academy of Sciences*, *110*(16), 6448-6452.
[46] Atkins, R., Rose, T., Brown, R. S., & Robb, M. (2001). The microcystis cyanobacteria bloom in the Swan River-February 2000. *Water Science and Technology*, *43*(9), 107-114.
[47] Robson, B. J., & Hamilton, D. P. (2003). Summer flow event induces a cyanobacterial bloom in a seasonal Western Australian estuary. *Marine and Freshwater Research*, *54*(2), 139-151.
[48] Robson, B. J., & Hamilton, D. P. (2004). Three-dimensional modelling of a Microcystis bloom event in the Swan River estuary, Western Australia. *Ecological Modelling*, *174*(1-2), 203-222.
[49] Paerl, H. W., & Huisman, J. (2009). Climate change: a catalyst for global expansion of harmful cyanobacterial blooms. *Environmental microbiology reports*, *1*(1), 27-37.
[50] Carey, C. C., Ibelings, B. W., Hoffmann, E. P., Hamilton, D. P., & Brookes, J. D. (2012). Eco-physiological adaptations that favour freshwater cyanobacteria in a changing climate. *Water research*, *46*(5), 1394-1407.
[51] Brookes, J. D., Ganf, G. G., Green, D., & Whittington, J. (1999). The influence of light and nutrients on buoyancy, filament aggregation and flotation of Anabaena circinalis. *Journal of plankton research*, *21*(2).
[52] Brookes, J. D., Ganf, G. G., & Oliver, R. L. (2000). Heterogeneity of cyanobacterial gas-vesicle volume and metabolic activity. *Journal of Plankton Research*, *22*(8), 1579-1589.
[53] Chengala, A. A., Hondzo, M., Troolin, D., & Lefebvre, P. A. (2010). Kinetic responses of Dunaliella in moving fluids. *Biotechnology and Bioengineering*, *107*(1), 65–75.
[54] Chengala, A., Hondzo, M., & Mashek, D. G. (2013). Fluid motion mediates biochemical composition and physiological aspects in the green alga Dunaliella primolecta Butcher. *Limnology and Oceanography: Fluids and Environments*, *3*(1), 74–88.
[55] Mai, T., Nguyen, P., Vo, T., Huynh, H., Tran, S., Nim, T., … Bui, P. (2017). Accumulation of lipid in Dunaliella salina under Nutrient Starvation Condition. *American Journal of Food and Nutrition*, *5*(2), 58–61.

[56] Griffiths, M. J., & Harrison, S. T. L. (2009). Lipid productivity as a key characteristic for choosing algal species for biodiesel production. *Journal of Applied Phycology*, *21*(5), 493–507.
[57] Rodolfi, L., Chini Zittelli, G., Bassi, N., Padovani, G., Biondi, N., Bonini, G., & Tredici, M. R. (2009). Microalgae for oil: Strain selection, induction of lipid synthesis and outdoor mass cultivation in a low-cost photobioreactor. *Biotechnology and Bioengineering*, *102*(1), 100–112.
[58] Thomas, W. H., Seibert, D. L. R., Alden, M., Neori, A., & Eldridge, P. (1984). Yields, photosynthetic efficiencies and proximate composition of dense marine microalgal cultures. I. Introduction and Phaeodactylum tricornutum experiments. *Biomass*, *5*(3), 181-209.
[59] Vézie, C., Rapala, J., Vaitomaa, J., Seitsonen, J., & Sivonen, K. (2002). Effect of nitrogen and phosphorus on growth of toxic and nontoxic Microcystis strains and on intracellular microcystin concentrations. *Microbial ecology*, *43*(4), 443-454.
[60] Neilan, B. A., Pearson, L. A., Muenchhoff, J., Moffitt, M. C., & Dittmann, E. (2013). Environmental conditions that influence toxin biosynthesis in cyanobacteria. *Environmental microbiology*, *15*(5), 1239-1253.
[61] Long, B. M., Jones, G. J., & Orr, P. T. (2001). Cellular microcystin content in N-limited Microcystis aeruginosa can be predicted from growth rate. *Applied and Environmental Microbiology*, *67*(1), 278-283.
[62] Tillett, D., Dittmann, E., Erhard, M., Von Döhren, H., Börner, T., & Neilan, B. A. (2000). Structural organization of microcystin biosynthesis in Microcystis aeruginosa PCC7806: an integrated peptide–polyketide synthetase system. *Chemistry & biology*, *7*(10), 753-764.
[63] Ginn, H. P., Pearson, L. A., & Neilan, B. A. (2010). NtcA from Microcystis aeruginosa PCC 7806 is autoregulatory and binds to the microcystin promoter. *Applied and environmental microbiology*, *76*(13), 4362-4368.
[64] Sevilla, E., Martin-Luna, B., Vela, L., Bes, M. T., Peleato, M. L., & Fillat, M. F. (2010). Microcystin-LR synthesis as response to nitrogen: transcriptional analysis of the mcyD gene in Microcystis aeruginosa PCC7806. *Ecotoxicology*, *19*(7), 1167-1173.
[65] Graham, J. L., Jones, J. R., Jones, S. B., Downing, J. A., & Clevenger, T. E. (2004). Environmental factors influencing microcystin distribution and concentration in the Midwestern United States. *Water research*, *38*(20), 4395-4404.
[66] Lukač, M., & Aegerter, R. (1993). Influence of trace metals on growth and toxin production of Microcystis aeruginosa. *Toxicon*, *31*(3), 293-305.
[67] Sevilla, E., Martin-Luna, B., Vela, L., Bes, M. T., Fillat, M. F., & Peleato, M. L. (2008). Iron availability affects mcyD expression and microcystin-LR synthesis in Microcystis aeruginosa PCC7806. *Environmental microbiology*, *10*(10), 2476-2483.
[68] Tonk, L., Visser, P. M., Christiansen, G., Dittmann, E., Snelder, E. O., Wiedner, C., ... & Huisman, J. (2005). The microcystin composition of the cyanobacterium Planktothrix agardhii changes toward a more toxic variant with increasing light intensity. *Applied and environmental microbiology*, *71*(9), 5177-5181.
[69] Scherer, P. I., Raeder, U., Geist, J., & Zwirglmaier, K. (2017). Influence of temperature, mixing, and addition of microcystin-LR on microcystin gene expression in Microcystis aeruginosa. *MicrobiologyOpen*, *6*(1), e00393.

[70] Schatz, D., Keren, Y., Vardi, A., Sukenik, A., Carmeli, S., Börner, T., ... & Kaplan, A. (2007). Towards clarification of the biological role of microcystins, a family of cyanobacterial toxins. *Environmental microbiology*, *9*(4), 965-970.
[71] Elliott, J. A. (2010). The seasonal sensitivity of cyanobacteria and other phytoplankton to changes in flushing rate and water temperature. *Global Change Biology*, *16*(2), 864-876.
[72] Reynolds, C. S. (1997). *Vegetation processes in the pelagic: a model for ecosystem theory*. In Kinne, O. (ed.), *Excellence in Ecology*. Vol. 9. International Ecology Institute, Oldendorf/Luhe.
[73] Chu, Z., Jin, X., Iwami, N., & Inamori, Y. (2007). The effect of temperature on growth characteristics and competitions of Microcystis aeruginosa and Oscillatoria mougeotii in a shallow, eutrophic lake simulator system. In *Eutrophication of Shallow Lakes with Special Reference to Lake Taihu, China* (pp. 217-223). Springer, Dordrecht.
[74] Li, M., Nkrumah, P. N., & Xiao, M. (2014). Biochemical composition of Microcystis aeruginosa related to specific growth rate: insight into the effects of abiotic factors. *Inland Waters*, *4*(4), 357-362.
[75] Nicklisch, A., & Kohl, J. G. (1983). Growth kinetics of Microcystis aeruginosa (Kütz) Kütz as a basis for modelling its population dynamics. *Internationale Revue der gesamten Hydrobiologie und Hydrographie*, *68*(3), 317-326.
[76] Watanabe, M. F., & Oishi, S. (1985). Effects of environmental factors on toxicity of a cyanobacterium (Microcystis aeruginosa) under culture conditions. *Applied and Environmental microbiology*, *49*(5), 1342-1344.
[77] Van der Westhuizen, A. J., & Eloff, J. N. (1985). Effect of temperature and light on the toxicity and growth of the blue-green alga Microcystis aeruginosa (UV-006). *Planta*, *163*(1), 55-59.
[78] World Health Organization (1999). *Toxic Cyanobacteria in Water: A guide to their public health consequences, monitoring and management.* World Health Organization.
[79] Kromkamp, J., & Walsby, A. E. (1990). A computer model of buoyancy and vertical migration in cyanobacteria. *Journal of Plankton Research*, *12*(1), 161-183.
[80] Nakamura, T., Adachi, Y., & Suzuki, M. (1993). Flotation and sedimentation of a single Microcystis floc collected from surface bloom. *Water Research*, *27*(6), 979-983.
[81] Howard, A., Irish, A. E., & Reynolds, C. S. (1996). A new simulation of cyanobacterial underwater movement (SCUM'96). *Journal of Plankton Research*, *18*(8), 1375-1385.
[82] Visser, P. M., Passarge, J., & Mur, L. R. (1997). Modelling vertical migration of the cyanobacterium Microcystis. *Hydrobiologia*, *349*(1-3), 99-109.
[83] Guven, B., & Howard, A. (2006). Modelling the growth and movement of cyanobacteria in river systems. *Science of the Total Environment*, *368*(2-3), 898-908.
[84] Guven, B., & Howard, A. (2011). Sensitivity analysis of a cyanobacterial growth and movement model under two different flow regimes. *Environmental Modeling & Assessment*, *16*(6), 577.

[85] Cirés, S., Wörmer, L., Carrasco, D., & Quesada, A. (2013). Sedimentation patterns of toxin-producing Microcystis morphospecies in freshwater reservoirs. *Toxins*, *5*(5), 939-957.
[86] Thomas, R. H., & Walsby, A. E. (1986). The effect of temperature on recovery of buoyancy by Microcystis. *Microbiology*, *132*(6), 1665-1672.
[87] Rowe, M. D., Anderson, E. J., Wynne, T. T., Stumpf, R. P., Fanslow, D. L., Kijanka, K., ... & Davis, T. W. (2016). Vertical distribution of buoyant Microcystis blooms in a Lagrangian particle tracking model for short-term forecasts in Lake Erie. *Journal of Geophysical Research: Oceans*, *121*(7), 5296-5314.
[88] Katz, J., & Sheng, J. (2010). Applications of holography in fluid mechanics and particle dynamics. *Annual Review of Fluid Mechanics*, *42*, 531-555.
[89] Béchet, Q., Shilton, A., Fringer, O. B., Munoz, R., & Guieysse, B. (2010). Mechanistic modeling of broth temperature in outdoor photobioreactors. *Environmental science & technology*, *44*(6), 2197-2203.
[90] Schulte, P. M. (2015). The effects of temperature on aerobic metabolism: towards a mechanistic understanding of the responses of ectotherms to a changing environment. *Journal of Experimental Biology*, *218*(12), 1856-1866.
[91] Lobry, J. R., Rosso, L., & Flandrois, J. P. (1991). A FORTRAN subroutine for the determination of parameter confidence limits in non-linear models. *Binary*, *3*(86-93), 25.
[92] Rosso, L., Lobry, J. R., & Flandrois, J. P. (1993). An unexpected correlation between cardinal temperatures of microbial growth highlighted by a new model. *Journal of Theoretical Biology*, *162*(4), 447-463.
[93] Bernard, O., & Rémond, B. (2012). Validation of a simple model accounting for light and temperature effect on microalgal growth. *Bioresource technology*, *123*, 520-527.
[94] Missaghi, S., Hondzo, M., Sun, C., & Guala, M. (2016). Influence of fluid motion on growth and vertical distribution of cyanobacterium Microcystis aeruginosa. *Aquatic Ecology*, *50*(4), 639-652.
[95] Wilkinson, A., Hondzo, M., & Guala, M. (2016). Effect of small-scale turbulence on the growth and metabolism of Microcystis aeruginosa. *Advances in Microbiology*, *6*(05), 351.
[96] Guillard, R. (1973) Division rates. In Stein, J. R. (ed.), *Handbook of phycological methods*. Vol. 19. Cambridge University Press, pp. 289-311.
[97] Liu, Z., Häder, D. P., & Sommaruga, R. (2004). Occurrence of mycosporine-like amino acids (MAAs) in the bloom-forming cyanobacterium Microcystis aeruginosa. *Journal of Plankton Research*, *26*(8), 963-966.
[98] Hong, J., Talapatra, S., Katz, J., Tester, P. A., Waggett, R. J., & Place, A. R. (2012). Algal toxins alter copepod feeding behavior. *PloS one*, *7*(5), e36845.
[99] Kumar, S. S., Sun, Y., Zou, S., & Hong, J. (2016). 3d holographic observatory for long-term monitoring of complex behaviors in drosophila. *Scientific reports*, *6*, 33001.
[100] Crocker, J. C., & Grier, D. G. (1996). Methods of digital video microscopy for colloidal studies. *Journal of colloid and interface science*, *179*(1), 298-310.

[101] Imai, H., Chang, K. H., Kusaba, M., & Nakano, S. I. (2009). Temperature-dependent dominance of Microcystis (Cyanophyceae) species: M. aeruginosa and M. wesenbergii. *Journal of plankton research*, *31*(2), 171-178.
[102] Le Marc, Y., Huchet, V., Bourgeois, C. M., Guyonnet, J. P., Mafart, P., & Thuault, D. (2002). Modelling the growth kinetics of Listeria as a function of temperature, pH and organic acid concentration. *International journal of food microbiology*, *73*(2-3), 219-237.
[103] Robarts, R. D., & Zohary, T. (1987). Temperature effects on photosynthetic capacity, respiration, and growth rates of bloom-forming cyanobacteria. *New Zealand Journal of Marine and Freshwater Research*, *21*(3), 391-399.
[104] Panton, R. L. (2006). *Incompressible flow*. John Wiley & Sons.
[105] Reynolds, C. S., Oliver, R. L., & Walsby, A. E. (1987). Cyanobacterial dominance: the role of buoyancy regulation in dynamic lake environments. *New Zealand journal of marine and freshwater research*, *21*(3), 379-390.
[106] Okada, M., & Aiba, S. (1983). Simulation of water-bloom in a eutrophic lake—III. Modeling the vertical migration and growth of Microcystis aeruginosa. *Water Research*, *17*(8), 883-893.
[107] Chung, S. W., Imberger, J., Hipsey, M. R., & Lee, H. S. (2014). The influence of physical and physiological processes on the spatial heterogeneity of a Microcystis bloom in a stratified reservoir. *Ecological Modelling*, *289*, 133-149.
[108] Georgianna, D. R., & Mayfield, S. P. (2012). Exploiting diversity and synthetic biology for the production of algal biofuels. *Nature*, *488*(7411), 329–335.
[109] Staples, M. D., Malina, R., & Barrett, S. R. H. (2017). The limits of bioenergy for mitigating global life-cycle greenhouse gas emissions from fossil fuels. *Nature Energy*, *2*, 16202.
[110] Elrayies, G. M. (2018). Microalgae: Prospects for greener future buildings. *Renewable and Sustainable Energy Reviews*, *81*, 1175–1191.
[111] Guschina, I. A., & Harwood, J. L. (2006). Lipids and lipid metabolism in eukaryotic algae. *Progress in Lipid Research*, *45*(2), 160–186.
[112] Scott, S. A., Davey, M. P., Dennis, J. S., Horst, I., Howe, C. J., Lea-Smith, D. J., & Smith, A. G. (2010). Biodiesel from algae: challenges and prospects. *Current Opinion in Biotechnology*, *21*(3), 277–286.
[113] Lardon, L., Hélias, A., Sialve, B., Steyer, J.-P., & Bernard, O. (2009). Life-Cycle Assessment of Biodiesel Production from Microalgae. *Environmental Science and Technology*, *43*(17), 6475–6481.
[114] Mata, T. M., Martins, A. A., & Caetano, N. S. (2010). Microalgae for biodiesel production and other applications: A review. *Renewable and Sustainable Energy Reviews*, *14*(1), 217–232.
[115] Acién, F. G., Fernández, J. M., Magán, J. J., & Molina, E. (2012). Production cost of a real microalgae production plant and strategies to reduce it. *Biotechnology Advances*, *30*(6), 1344–1353.
[116] Slade, R., & Bauen, A. (2013). Micro-algae cultivation for biofuels: Cost, energy balance, environmental impacts and future prospects. *Biomass and Bioenergy*, *53*, 29–38.

[117] Phadwal, K., & Singh, P. . (2003). Effect of nutrient depletion on β-carotene and glycerol accumulation in two strains of Dunaliella sp. *Bioresource Technology*, *90*(1), 55–58.
[118] Wang, D., Lai, Y.-C., L. Karam, A., L. de los Reyes, F., & J. Ducoste, J. (2019). Dynamic Modeling of Microalgae Growth and Lipid Production under Transient Light and Nitrogen Conditions. *Environmental Science and Technology*, *53*(19), 11560–11568.
[119] Chen, W., Zhang, C., Song, L., Sommerfeld, M., & Hu, Q. (2009). A high throughput Nile red method for quantitative measurement of neutral lipids in microalgae. *Journal of Microbiological Methods*, *77*(1), 41–47.
[120] Bligh, E. G., & Dyer, W. J. (1959). A RAPID METHOD OF TOTAL LIPID EXTRACTION AND PURIFICATION. *Canadian Journal of Biochemistry and Physiology*, *37*(1), 911–917.
[121] Alonzo, F., & Mayzaud, P. (1999). Spectrofluorometric quantification of neutral and polar lipids in zooplankton using Nile red. *Marine Chemistry*, *67*(3–4), 289–301.
[122] Yu, X., Hong, J., Liu, C., & Kim, M. K. (2014). Review of digital holographic microscopy for three-dimensional profiling and tracking. *Optical Engineering*, *53*(11), 1–22.
[123] Mallery, K., & Hong, J. (2019). Regularized inverse holographic volume reconstruction for 3D particle tracking. *Opt. Express*, *27*(13), 18069–18084.
[124] Eyden, B. P. (1975). Light and Electron Microscope Study of Dunaliella primolecta Butcher (Volvocida)*. *The Journal of Protozoology*, *22*(3), 336–344.
[125] Sjoblad, R. D., Chet, I., & Mitchell, R. (1978). Chemoreception in the green algaDunaliella tertiolecta. *Current Microbiology*, *1*(5), 305–307.
[126] Adler, J. (1966). Chemotaxis in Bacteria. *Science*, *153*(3737), 708–716.
[127] Lee, E. S., Lewitus, A. J., & Zimmer, R. K. (1999). Chemoreception in a marine cryptophyte: Behavioral plasticity in response to amino acids and nitrate. *Limnology and Oceanography*, *44*(6), 1571–1574.
[128] Cooksey, K. E., Guckert, J. B., Williams, S. A., & Callis, P. R. (1987). Fluorometric determination of the neutral lipid content of microalgal cells using Nile Red. *Journal of Microbiological Methods*, *6*(6), 333–345.
[129] Elsey, D., Jameson, D., Raleigh, B., & Cooney, M. J. (2007). Fluorescent measurement of microalgal neutral lipids. *Journal of Microbiological Methods*, *68*(3), 639–642.
[130] Siaut, M., Cuiné, S., Cagnon, C., Fessler, B., Nguyen, M., Carrier, P., … Peltier, G. (2011). Oil accumulation in the model green alga Chlamydomonas reinhardtii: characterization, variability between common laboratory strains and relationship with starch reserves. *BMC Biotechnology*, *11*(1), 7.
[131] Govender, T., Ramanna, L., Rawat, I., & Bux, F. (2012). BODIPY staining, an alternative to the Nile Red fluorescence method for the evaluation of intracellular lipids in microalgae. *Bioresource Technology*, *114*, 507–511.
[132] Moheimani, N. R., Borowitzka, M. A., Isdepsky, A., & Sing, S. F. (2013). Standard methods for measuring growth of algae and their composition. In *Algae for biofuels and energy* (pp. 265–284). Springer.

[133] Barsanti, L., & Gualtieri, P. (2018). Is exploitation of microalgae economically and energetically sustainable? *Algal Research*, *31*, 107–115.
[134] Ruiz, J., Olivieri, G., de Vree, J., Bosma, R., Willems, P., Reith, J. H., … Barbosa, M. J. (2016). Towards industrial products from microalgae. *Energy & Environmental Science*, *9*(10), 3036–3043.
[135] Gerber, L. N., Tester, J. W., Beal, C. M., Huntley, M. E., & Sills, D. L. (2016). Target Cultivation and Financing Parameters for Sustainable Production of Fuel and Feed from Microalgae. *Environmental Science and Technology*, *50*(7), 3333–3341.
[136] Lee, J., Rai, P. K., Jeon, Y. J., Kim, K. H., & Kwon, E. E. (2017). The role of algae and cyanobacteria in the production and release of odorants in water. *Environmental Pollution*, *227*, 252-262.
[137] Chen, L., Chen, J., Zhang, X., & Xie, P. (2016). A review of reproductive toxicity of microcystins. *Journal of hazardous materials*, *301*, 381-399.
[138] Zamora-Barrios, C. A., Nandini, S., & Sarma, S. S. S. (2019). Bioaccumulation of microcystins in seston, zooplankton and fish: A case study in Lake Zumpango, Mexico. *Environmental pollution*, *249*, 267-276.
[139] Li, Y., Chen, J. A., Zhao, Q., Pu, C., Qiu, Z., Zhang, R., & Shu, W. (2011). A cross-sectional investigation of chronic exposure to microcystin in relationship to childhood liver damage in the Three Gorges Reservoir Region, China. *Environmental health perspectives*, *119*(10), 1483-1488.
[140] Cao, Q., Steinman, A. D., Su, X., & Xie, L. (2017). Effects of microcystins contamination on soil enzyme activities and microbial community in two typical lakeside soils. *Environmental Pollution*, *231*, 134-142.
[141] Wood, S. A., Prentice, M. J., Smith, K., & Hamilton, D. P. (2010). Low dissolved inorganic nitrogen and increased heterocyte frequency: precursors to Anabaena planktonica blooms in a temperate, eutrophic reservoir. *Journal of Plankton Research*, *32*(9), 1315-1325.
[142] Karlson, A. M., Duberg, J., Motwani, N. H., Hogfors, H., Klawonn, I., Ploug, H., ... & Larsson, U. (2015). Nitrogen fixation by cyanobacteria stimulates production in Baltic food webs. *Ambio*, *44*(3), 413-426.
[143] World Health Organization (1998). *Guidelines for drinking-water quality. Vol. 2, Health criteria and other supporting information: addendum* (No. WHO/EOS/98.1). World Health Organization.
[144] You, J., Mallery, K., Hong, J., & Hondzo, M. (2018). Temperature effects on growth and buoyancy of Microcystis aeruginosa. *Journal of Plankton Research*, *40*(1), 16-28.
[145] Paerl, H. W., Xu, H., McCarthy, M. J., Zhu, G., Qin, B., Li, Y., & Gardner, W. S. (2011). Controlling harmful cyanobacterial blooms in a hyper-eutrophic lake (Lake Taihu, China): the need for a dual nutrient (N & P) management strategy. *Water research*, *45*(5), 1973-1983.
[146] Paerl, H. W. (2018). Mitigating toxic planktonic cyanobacterial blooms in aquatic ecosystems facing increasing anthropogenic and climatic pressures. *Toxins*, *10*(2), 76.
[147] Zhang, X., Ji, W., Zhang, H., Zhang, W., & Xie, P. (2011). Studies on the toxic effects of microcystin-LR on the zebrafish (Danio rerio) under different temperatures. *Journal of Applied Toxicology*, *31*(6), 561-567.

[148] Pavagadhi, S., Gong, Z., & Balasubramanian, R. (2013). Toxicological implications of microcystins for zebrafish embryos in the presence of other environmental pollutants. *Environmental toxicology and chemistry*, *32*(7), 1574-1581.
[149] Pimentel, J. S., & Giani, A. (2014). Microcystin production and regulation under nutrient stress conditions in toxic Microcystis strains. *Applied and environmental microbiology*, *80*(18), 5836-5843.
[150] Wagner, C., & Adrian, R. (2009). Cyanobacteria dominance: quantifying the effects of climate change. *Limnology and Oceanography*, *54*(6part2), 2460-2468.
[151] Paerl, H. W., & Paul, V. J. (2012). Climate change: links to global expansion of harmful cyanobacteria. *Water research*, *46*(5), 1349-1363.
[152] Paerl, H. W., & Otten, T. G. (2013). Harmful cyanobacterial blooms: causes, consequences, and controls. *Microbial ecology*, *65*(4), 995-1010.
[153] Havens, K. E., Fukushima, T., Xie, P., Iwakuma, T., James, R. T., Takamura, N., ... & Yamamoto, T. (2001). Nutrient dynamics and the eutrophication of shallow lakes Kasumigaura (Japan), Donghu (PR China), and Okeechobee (USA). *Environmental Pollution*, *111*(2), 263-272.
[154] Rinta-Kanto, J. M., Konopko, E. A., DeBruyn, J. M., Bourbonniere, R. A., Boyer, G. L., & Wilhelm, S. W. (2009). Lake Erie Microcystis: relationship between microcystin production, dynamics of genotypes and environmental parameters in a large lake. *Harmful algae*, *8*(5), 665-673.
[155] Sitoki, L., Kurmayer, R., & Rott, E. (2012). Spatial variation of phytoplankton composition, biovolume, and resulting microcystin concentrations in the Nyanza Gulf (Lake Victoria, Kenya). *Hydrobiologia*, *691*(1), 109-122.
[156] Aparicio Medrano, E., Uittenbogaard, R. E., Pires, L. D., Van De Wiel, B. J. H., & Clercx, H. J. H. (2013). Coupling hydrodynamics and buoyancy regulation in Microcystis aeruginosa for its vertical distribution in lakes. *Ecological Modelling*, *248*, 41-56.
[157] Li, C., Feng, W., Chen, H., Li, X., Song, F., Guo, W., ... & Sun, F. (2019). Temporal variation in zooplankton and phytoplankton community species composition and the affecting factors in Lake Taihu—a large freshwater lake in China. *Environmental Pollution*, *245*, 1050-1057.
[158] Pannard, A., Beisner, B. E., Bird, D. F., Braun, J., Planas, D., & Bormans, M. (2011). Recurrent internal waves in a small lake: Potential ecological consequences for metalimnetic phytoplankton populations. *Limnology and Oceanography: Fluids and Environments*, *1*(1), 91-109.
[159] Planas, D., & Paquet, S. (2016). Importance of climate change-physical forcing on the increase of cyanobacterial blooms in a small, stratified lake. *Journal of Limnology*, *75*.
[160] Wilkinson, A. A., Hondzo, M., & Guala, M. (2019). Investigating abiotic drivers for vertical and temporal heterogeneities of cyanobacteria concentrations in lakes using a seasonal in situ monitoring station. *Water Resources Research*, *55*(2), 954-972.
[161] Wilkinson, A. A., Hondzo, M., & Guala, M. (2020). Vertical heterogeneities of cyanobacteria and microcystin concentrations in lakes using a seasonal in situ monitoring station. *Global Ecology and Conservation*, *21*, e00838.

[162] Kasinak, J. M. E., Holt, B. M., Chislock, M. F., & Wilson, A. E. (2015). Benchtop fluorometry of phycocyanin as a rapid approach for estimating cyanobacterial biovolume. *Journal of Plankton Research*, *37*(1), 248-257.
[163] Canter-Lund, H., & Lund, J. (1995). *Freshwater algae: their microscopic world explored*. Biopress Ltd., Bristol, England.
[164] Bellinger, E. G., & Sigee, D. C. (2015). *Freshwater algae: identification, enumeration and use as bioindicators*. John Wiley & Sons.
[165] Nienaber, M. A., & Steinitz-Kannan, M. (2018). *A Guide to Cyanobacteria: Identification and Impact*. University Press of Kentucky.
[166] Hillebrand, H., Dürselen, C. D., Kirschtel, D., Pollingher, U., & Zohary, T. (1999). Biovolume calculation for pelagic and benthic microalgae. *Journal of phycology*, *35*(2), 403-424.
[167] Napiórkowska-Krzebietke, A., & Kobos, J. (2016). Assessment of the cell biovolume of phytoplankton widespread in coastal and inland water bodies. *Water research*, *104*, 532-546.
[168] Read, J. S., Hamilton, D. P., Jones, I. D., Muraoka, K., Winslow, L. A., Kroiss, R., ... & Gaiser, E. (2011). Derivation of lake mixing and stratification indices from high-resolution lake buoy data. *Environmental Modelling & Software*, *26*(11), 1325-1336.
[169] Eriksson, L., Johansson, E., Kettaneh-Wold, N., Trygg, J., Wikström, C., & Wold, S. (2006). *Multi-and megavariate data analysis* (Vol. 1, p. 1). Umea, Sweden: Umetrics Ab.
[170] Huber, V., Wagner, C., Gerten, D., & Adrian, R. (2012). To bloom or not to bloom: contrasting responses of cyanobacteria to recent heat waves explained by critical thresholds of abiotic drivers. *Oecologia*, *169*(1), 245-256.
[171] Rolland, D. C., Bourget, S., Warren, A., Laurion, I., & Vincent, W. F. (2013). Extreme variability of cyanobacterial blooms in an urban drinking water supply. *Journal of plankton research*, *35*(4), 744-758.
[172] World Health Organization (2003). *Guidelines for safe recreational water environments: Coastal and fresh waters* (Vol. 1). World Health Organization.
[173] Macário, I. P., Castro, B. B., Nunes, M. I., Antunes, S. C., Pizarro, C., Coelho, C., ... & de Figueiredo, D. R. (2015). New insights towards the establishment of phycocyanin concentration thresholds considering species-specific variability of bloom-forming cyanobacteria. *Hydrobiologia*, *757*(1), 155-165.
[174] U.S. EPA (2015). Drinking water health advisory for the cyanobacterial microcystin toxins. United States Environmental Protection Agency.
[175] U.S. EPA (2019). Recommended human health recreational ambient water quality criteria or swimming advisories for microcystins and cylindrospermopsin. United States Environmental Protection Agency.
[176] Christensen, V. G., Maki, R. P., Stelzer, E. A., Norland, J. E., & Khan, E. (2019). Phytoplankton community and algal toxicity at a recurring bloom in Sullivan Bay, Kabetogama Lake, Minnesota, USA. *Scientific reports*, *9*(1), 1-11.
[177] Humphries, S. E., & Lyne, V. D. (1988). Cyanophyte blooms: The role of cell buoyancy. *Limnology and Oceanography*, *33*(1), 79-91.

[178] Hozumi, A., Ostrovsky, I., Sukenik, A., & Gildor, H. (2020). Turbulence regulation of Microcystis surface scum formation and dispersion during a cyanobacteria bloom event. *Inland Waters*, *10*(1), 51-70.
[179] Ren, L., Wang, P., Wang, C., Chen, J., Hou, J., & Qian, J. (2017). Algal growth and utilization of phosphorus studied by combined mono-culture and co-culture experiments. *Environmental Pollution*, *220*, 274-285.
[180] Downing, J. A., & McCauley, E. (1992). The nitrogen: phosphorus relationship in lakes. *Limnology and Oceanography*, *37*(5), 936-945. blooms. *Harmful algae*, *8*(5), 715-725.
[181] Scott, J. T., McCarthy, M. J., & Paerl, H. W. (2019). Nitrogen transformations differentially affect nutrient-limited primary production in lakes of varying trophic state. *Limnology and Oceanography Letters*, *4*(4), 96-104.
[182] Harke, M. J., Steffen, M. M., Gobler, C. J., Otten, T. G., Wilhelm, S. W., Wood, S. A., & Paerl, H. W. (2016). A review of the global ecology, genomics, and biogeography of the toxic cyanobacterium, Microcystis spp. *Harmful Algae*, *54*, 4-20.
[183] Sahoo, G. B., Forrest, A. L., Schladow, S. G., Reuter, J. E., Coats, R., & Dettinger, M. (2016). Climate change impacts on lake thermal dynamics and ecosystem vulnerabilities. *Limnology and Oceanography*, *61*(2), 496-507.
[184] Ibelings, B. W., & Chorus, I. (2007). Accumulation of cyanobacterial toxins in freshwater "seafood" and its consequences for public health: a review. *Environmental pollution*, *150*(1), 177-192.
[185] Olson, N. E., Cooke, M. E., Shi, J. H., Birbeck, J. A., Westrick, J. A., & Ault, A. P. (2020). Harmful Algal Bloom Toxins in Aerosol Generated from Inland Lake Water. *Environmental Science & Technology*, *54*(8), 4769-4780.

Appendix A

Protocols for Chemical Analyses

Phycocyanin Analysis

Sample filtering and storage

1. Vacuum filter the water samples (100 mL) through the GF/F filters (Whatman, Maidstone, UK)
2. Place the filters in centrifuge tubes wrapped with foil and store at – 20 ˚C.

Phycocyanin extraction

1. Phosphate buffer (50 mM): 40 mL of concentrated phosphate buffer (#5807-16/#5808-16 Ricca Chem Co, IN, USA) and 960 mL Milli-Q water (Millipore, MA, USA).
2. Grind the filters in 10 mL phosphate buffer under reduced light using a smooth Teflon Grinder in a 50 mL centrifuge tube for 1 min.
3. Rinse the grinder into the centrifuge tube with another 10 mL aliquot of phosphate buffer, bringing the total volume to 20 mL.
4. Cap the centrifuge tubes, mixed well, store in the dark at 4 ˚C for 2 hours.
5. Place the tubes in a dark laminar flow hood for another 2 hours to warm to room temperature (~ 20˚C).
6. Centrifuge the tubes at 15,000 rpm for 20 min.
7. Filter the supernatant with inline filters (0.45 µm, VWR #28145-485; 0.2 µm, VWR #28145-483) to remove the particulates prior to analyses.

Standard curve

1. The C-Phycocyanin from Spirulina (Sigma-Aldrich #P2172-10MG)
2. Standard concentrations (µg/L): 0, 10, 50, 100, 500, 1000 and 2000.

Phycocyanin measurement

1. Measure the samples by a laboratory benchtop fluorometer (Trilogy, Turner Designs, CA, USA) augmented with an orange module (#7200-044, Turner Designs, CA, USA)
2. Collect 3 mL of samples in the four-sided, clear 10-mm, glass square cuvette, accommodate the cuvette into the module and measure.

3. Read and record the raw fluorescence units (RFU) and converted to phycocyanin concentration (μg/L) with the standard curve.

Nitrate/Nitrite Analysis

Sample filtering and storage

1. Vacuum filter the water samples through the GF/F filters (Whatman, Maidstone, UK).
2. Save duplicate 14 mL filtrate samples in centrifuge tubes wrapped with foil and store at – 20 ˚C.

Reagents and standard solutions

1. Use the LaMotte Nitrate/Nitrite Test Kit (Code #3519-01, LaMotte company, Maryland, USA), which includes the mixed acid solution and the nitrate reducing reagent (containing 7% cadmium powder)
2. Prepare $NaNO_3$ standard solutions (mg/L) in the concentration of 0.25, 0.5, 1, 2, 5, 10.

Preliminary test of trial samples

1. The detection limit of the module is 0.04 – 14 mg N/L.
2. Pre-test some of the samples to determine what dilution factors are needed.

Nitrate/Nitrite measurement

1. Measure the (properly diluted) samples with the Turner Designs Trilogy Nitrate/Nitrite module (PN 7200-074, Turner Designs, CA, USA). Choose the Absorbance module from the Home screen.
2. Mix 2.5 mL sample and 2.5 mL mixed acid solution and wait for at least 2 minutes but no longer than 8 minutes.
3. Add 0.1g (1 scoop provided in the kit) of the nitrate reducing reagent. Invert the test tube approximately 60 times in one minute. Wait for 10 minutes.
4. Collect 3 mL of reacted samples in the four-sided, clear 10-mm, glass square cuvette, accommodate the cuvette into the module and measure.
5. Read and record the absorbance units (AU) and converted to nitrate concentration (mg N/L) with the standard curve.

Notes:

1. A blank sample (DI water) needs to be prepared and measured using the "Nitrate/Nitrite measurement" steps, before the samples can be tested. After inserting the reacted blank sample, press "Calibration" button to calibrate.
2. The mixed acid reagents and the cadmium powder-contained nitrate reducing reagent need to be safely disposed.

Phosphate Analysis

Sample filtering and storage

1. Vacuum filter the water samples through the GF/F filters (Whatman, Maidstone, UK).
2. Save duplicate 14 mL filtrate samples in centrifuge tubes wrapped with foil and store at – 20 ˚C.

Reagents and standard solutions

1. The primary reagents include 30 g/L ammonium molybdate solution, 13.5% sulfuric acid solution, 54 g/L ascorbic acid solution and 1.36 g/L potassium antimonyl-tarte solution. Preparation and storage of these reagents can be found in the user manuals of Trilogy.
2. Mixed together in a dark glass bottle: 100 mL ammonium molybdate solution, 250 mL sulfuric acid solution, 100 mL ascorbic acid solution, and 50 mL potassium antimonyl-tartrate solution. This mixed solution will be stable up to six hours so measurements need to be completed within 6 hours or new mixed reagent need to be prepared.
3. Prepare potassium dihydrogen phosphate standard by dissolving 0.816 g of anhydrous potassium dihydrogen phosphate in 1000 mL DI water, and dilute to solutions (µg/L) in the concentration of 17.81, 35.63, 71.25, 142.5, 285, 570, and 760.

Preliminary test of trial samples

3. The detection limit of the module is 1 – 930 µg PO_4/L.
4. Pre-test some of the samples to determine what dilution factors are needed.

Phosphate measurement

6. Measure the (properly diluted) samples with the Turner Designs Trilogy phosphate absorbance module (PN 7200-020, Turner Designs, CA, USA). Choose the Absorbance module from the Home screen.
7. Mix the sample and mixed reagent with 10:1 ratio and wait for at least 5 minutes but no more than 2 hours.
8. Collect 3 mL of reacted samples in the four-sided, clear 10-mm, glass square cuvette, accommodate the cuvette into the module and measure.
9. Read and record the absorbance units (AU) and converted to phosphate concentration (µg PO_4/L) with the standard curve.

Notes:

1. A blank sample (DI water) needs to be prepared and measured using the "Phosphate measurement" steps, before the samples can be tested. After inserting the reacted blank sample, press "Calibration" button to calibrate.

Appendix B

Supplementary Protocols for *Dunaliella primolecta* Cultivation and Treatments

Growth Medium Preparation

The growth medium for the *Dunaliella primolecta* follows the recipe of the Erdschreiber's medium, which includes the following components:

2.3 mM $NaNO_3$;

0.067 mM $Na_2HPO_4 \cdot 7H_2O$;

2 mM $Na_2EDTA \cdot 2H_2O$;

0.36 mM $FeCl_3 \cdot 6H_2O$;

0.21 mM $MnCl_2 \cdot 4H_2O$;

0.037 mM $ZnCl_2$;

0.0084 mM $CoCl_2 \cdot 6H_2O$;

0.017 mM $Na_2MoO_4 \cdot 2H_2O$;

0.135 mg/L Vitamin B12;

HEPES buffer (pH7.8) 0.012g/L;

Soil water (0.25 tsp/L greenhouse soil with 0.05 mM $CaCO_3$);

Synthetic seawater (RICCA 8363-1, ASTMD 1141 Substitute Ocean Water, RICCA chemical company, USA).

Note: The original recipe and details can be found on the website of UTEX (https://utex.org/products/erdschreibers-medium?variant=30991769862234)

Cell Dry Weight Measurement

1. Wash the GF/F glass microfiber filters (0.7 µm pore size, Whatman, GE Healthcare Life Science, USA) by Milli-Q water (MilliporeSigma, USA). Dry the washed filters in an oven overnight at 104˚C
2. Weigh the dried filters before use.
3. Filter the algal samples through the pre-weighed filters.
4. Dry the filters in the oven at 104˚C overnight and weigh again.
5. Subtract the weight of filters from the weight of filter + sample.

Cell Fixation for Microscopic Observation

1. Collect a sample of certain volume from the algal cultures and transfer into a microcentrifuge tube containing an equal volume of 4% glutaraldehyde solution.
2. After 10 min of fixation, gently centrifuged (2xg) the microcentrifuge tube.
3. Remove the fixing solution and gently resuspend the cells into the growth medium to get to the optimal concentration for imaging.
4. Place an aliquot of 3 µL of sample on a cleaned glass slide and mounted with a cleaned coverslip sealed with the nail polish at the edges.

Note: Properly cut the pipette tips to avoid damaging the fixed cells.

Appendix C

Protocols for Intracellular Neutral Lipid Determination

Nile Red Fluorescence Method

1. Prepare a 5 mM Nile red stock solution (Nile red 72485, Sigma-Aldrich Inc., USA) with DMSO (34869, Sigma-Aldrich Inc., USA) and store at – 20 ˚C for later use.
2. Prepare a diluted solution of 250 µg/mL Nile red from the stock every time before cell staining.
3. Add a 5 µL algal sample of known cell concentration to a microcentrifuge tube. Then add 3 µL of 250 µg/L Nile red dye and 292 µL of 25% DMSO (v/v) solution into the microcentrifuge tube and gently vortex.
4. Transfer the mixed solution to a well of a 96-microwell black polystyrene plate (#137101, Thermo Fisher Scientific Inc., USA).
5. Incubate the plate in dark for 30 minutes.
6. Examine the fluorescence emissions using a BioTek Synergy Neo2 Hybrid multi-mode reader (BioTek Instruments, Inc., USA), with an excitation wavelength of 530 nm and an emission wavelength of 575 nm.

Notes:

1. Trial experiments may be necessary to determine the optimal range of cell concentration, optimal dose of Nile read, and incubation time, when measuring the lipid of different species of algae or algae under different conditions.
2. It is suggested to include several wells of background (e,g., algal samples without staining or growth medium without algae) samples in each test to exclude the background fluorescence readings.

Gravimetric Method

1. Collect a sample from the algal culture and centrifuge three times to obtain a concentrated cell sample.
2. Transfer the concentrated cells into a microcentrifuge tube.
3. Extract the crude lipids (including neutral lipids and other polar lipids) from the cells using a chloroform-methanol-water system. The ratio of these three solvents may vary. The ratio used in this dissertation is chloroform: methanol: water = 2:1:0.625.
4. Store the extracted cell sample with the solvents in a glass tube with cap in the freezer overnight for better extraction.
5. On the next day, centrifuge the sample and transfer the layer with crude lipids (green in color) to a new tube. Add equal amount of chloroform for additional extraction overnight.
6. On the third day, centrifuge the sample and transfer the layer with crude lipids (green in color) to a new tube.
7. Set up a column chromatography, using a column with appropriate diameter and length, according to the volume of samples need to be separated. Fill the silica gel (70-230 mesh, Sigma-Aldrich Inc., USA) into the column to form a stationary phase layer with diameter: height = 1:6.5.
8. Weigh a dry and clean vial to collect the neutral lipids.
9. Transfer the extracted crude lipids into the column and use extra chloroform to drive the crude lipids to pass through the silica stationary phase. The neutral lipids will be separated from the crude lipids and flow through the stationary phase into the pre-weighed vial.
10. Dry the vial containing neutral lipid in a 37˚C water bath under a stream of nitrogen (MULTIVAP nitrogen evaporator, Organomation Association Inc., USA) and weigh the dried vial.

Notes:

1. Trial experiments may be necessary to determine the extraction solvent ratio and the optimal column set up.
2. All processes need to be operated carefully to minimize the loss of lipids during the operations.

Appendix D

Supplementary Methods of Swimming Speed and Trajectories Analyses for *Dunaliella primolecta*

Swimming Speed Measurement by Micro-PTV

The micro-PTV system set up (Figure S1) includes an inverted microscope equipped with an epi-fluorescence filter cube (Nikon Eclipse TE2000-S), a CCD camera (PIVCAM 14-10), a halogen light source, and a PC installed with Insight3G software (TSI Inc.). To perform the velocity measurement of algal cells in the stagnant fluid, samples were collected from each *D. primolecta* culture, and each sample was injected into a fluid channel made with poly-dimethylsiloxane, which was 35 mm in length and had a rectangular cross-section with a depth of 0.45 mm and a width of 3.5 mm. The fluid channel was placed on the holder stage of the microscope and was lighted by a halogen lamp. A 10X objective lens was used, and the dimension of each image recorded was 1376 pixels × 1024 pixels, with the spatial calibration of 0.38 μm/pixel. To avoid the wall effects on the algal swimming, the images were recorded focusing on the center of the channel depth, where the cells were observed moving independently.

At least four samples were collected from each culture group (30%N, 70%N and 100%N) and two image sequences were recorded at a frame rate of 5 Hz (ΔT=200000 μs) to provide at least 100 pairs of frames for each sample. For each sequence, the adjacent two images were paired up as Frame A and Frame B for processing. All the processing procedures were conducted in Insight3G using Direct Imaging Particle Analyzer (DIPA). Several image pairs of each sequence were first inverted to greyscale to find out the intensity threshold for background subtraction. The processing was performed by the DIPA Processor to track the displacement of particles from Frame A to Frame B and generate velocity vectors. To ensure that the movements of cells perpendicular to the imaging plane would not affect the two-dimensional results, a threshold of maximum 10% size change of cells was set, i.e., only the tracks with cell size changes within 10% between frames were counted. Several parameters relevant to particle sizing and particle matching needed to be set, such as the maximum displacement between frames, the

maximum size difference of a tracked particle, and the binarization threshold value. These were adjusted based on the size of *D. primolecta* cells and the intensity of particles recorded in each image.

After the pre-processing and processing, the location coordinates, the horizontal velocities in the *x*- and *y*-direction and diameter of each tracked particle were obtained. The results were double-checked with the original images to remove some noise, e.g., the non-moving cells or residual spots on the background. The two-dimensional swimming speed of algal cells (μm/s) was calculated as $v = \sqrt{U^2 + V^2}$, where U is the *x*-direction velocity (μm/s) and V is the *y*-direction velocity (μm/s).

Swimming Trajectories Tracking by DIH-PTV

The DIH-PTV system (Figure S2) consists of a 532 nm diode laser (Thorlabs CPS532), an optical spatial filter and collimating lens assembly, 5X microscopic objective (Mitutoyo 10X/0.14 NA), and a CCD camera (Flare 2M360-CL). The camera sensor size is 2048 pixels × 1088 pixels with a pixel pitch of 5 μm. The holograms were recorded at a framerate of 100 Hz with an exposure time of 50 μs and cropped to a 1024 pixels × 1024 pixels window for processing. Measurements of the 30%N cultures were performed at the lag, exponential, and early stationary phases. For imaging, samples were pipetted into a glass cuvette with a height of 30 mm, a width of 10 mm, and a depth of 1 mm. The recorded volume is 1 × 1 × 1 mm^3 (1 μL). Each sample was recorded for 20 seconds (2000 frames) with the exception of the lag stage samples which were recorded for 60 seconds in order to increase the total number of cells recorded at the lowest concentration. Two replicate cultures were measured at each stage and five recordings were made of each culture.

The 3D positions of each cell in the recorded hologram were extracted using the Regularized Inverse Holographic Volume Reconstruction (RIHVR) method. Briefly, RIHVR iteratively finds a 3D object field that would produce the recorded image, using regularization to ensure that the volume is sparsely populated with smooth objects. This volume is then automatically thresholded and segmented to get the centroids of the algal cells. At the highest concentrations, an additional step to reduce over-segmentation showed improved results. This step merges any objects that overlap by more than 10% in the lateral (image) plane. The cell positions were tracked in time to produce trajectories illustrating the swimming pattern of each cell.